Titre: Title:	Design and Analysis of a 35 GHz Rectenna System for Wireless Power Transfer to an Unmanned Aerial Vehicle
Auteur: Author:	Muttahid Ull Hoque
Date:	2021
Type:	Mémoire ou thèse / Dissertation or Thesis
Référence: Citation:	Hoque, M. U. (2021). Design and Analysis of a 35 GHz Rectenna System for Wireless Power Transfer to an Unmanned Aerial Vehicle [Mémoire de maîtrise, Polytechnique Montréal]. PolyPublie. https://publications.polymtl.ca/10001/

URL de PolyPublie: PolyPublie URL:	https://publications.polymtl.ca/10001/
Directeurs de recherche: Advisors:	Yves Audet, Yvon Savaria, & Deepak Kumar
Programme: Program:	Génie électrique

POLYTECHNIQUE MONTRÉAL

affiliée à l'Université de Montréal

Design and analysis of a 35 GHz rectenna system for wireless power transfer to an unmanned aerial vehicle

MUTTAHID ULL HOQUE

Département de génie électrique

Mémoire présenté en vue de l'obtention du diplôme de *Maîtrise ès sciences appliquées*

Génie électrique

Décembre 2021

POLYTECHNIQUE MONTRÉAL

affiliée à l'Université de Montréal

Ce mémoire intitulé :

Design and analysis of a 35 GHz rectenna system for wireless power transfer to an unmanned aerial vehicle

présenté par **Muttahid Ull HOQUE**

en vue de l'obtention du diplôme de *Maîtrise ès sciences appliquées*

a été dûment accepté par le jury d'examen constitué de :

Jean-Jacques LAURIN, président

Yves AUDET, membre et directeur de recherche

Yvon SAVARIA, membre et codirecteur de recherche

Deepak KUMAR, membre et codirecteur de recherche

Mohammad S. SHARAWI, membre

DEDICATION

To my family

For their endless love, support, and encouragement

ACKNOWLEDGEMENTS

Firstly, I would like to express my sincere gratitude to my supervisors Prof. Yves Audet, and Prof. Yvon Savaria for their continuous support of my master's program and related research, for their motivation, patience, and immense knowledge. Their wise guidance enlightened my first glance of research and helped me throughout my studies. I could not have imagined having better advisers and mentors for my program.

I must thank my co-supervisor, Dr. Deepak Kumar for his advice and feedback during my research work and providing continued support throughout my entire program. Without his profound knowledge in RF energy harvesting and renewable energy, as well as his great patience throughout the program, the present work would not have been possible. Our productive discussions helped me to elevate the quality of my research work.

I sincerely acknowledge MITACS Scholarship Council, for offering me a partial scholarship to continue my studies in Canada

Finally, I would like to thank and express my deepest gratitude to my family and friends for their continuous support.

RÉSUMÉ

Dans cet article, la conception et l'optimisation d'une antenne (émetteur) et d'un système rectenna (récepteur) sont présentées pour traiter le transfert de puissance micro-ondes sans fil pour alimenter un véhicule aérien sans pilote en mouvement de 22 kW. La fréquence d'émission de la puissance micro-ondes de 35 GHz est sélectionnée afin d'obtenir une architecture de système compacte à faible coût. Pour ce faire, tout d'abord, la taille de l'antenne d'émission et de réception a été calculée en utilisant l'équation de transmission de puissance Friis pour une distance de 10 km. La distance de transmission de puissance peut être modifiée en fonction de la demande. Par conséquent, un réseau d'antennes patch micro-ruban rectangulaires de 4x2 à haut gain et haute efficacité a été conçu et simulé à l'aide de l'outil de conception électromagnétique CST. Et puis, un simple système de redressement (rectenna) a été conçu et optimisé par le logiciel Advanced Design System (ADS). Une diode GaAs Schottky MA4E1317 est choisie pour le système de redressement. La fréquence de résonance du réseau d'antenne patch et de la rectenna est de 35 GHz. Le gain et l'efficacité des antennes patch micro-ruban 4x2 proposées sont respectivement de 13,4 dBi et 85%. De plus, l'efficacité de conversion RF en DC de la tension de sortie rectenna proposée atteint respectivement 80% et 3,5 V pour une puissance d'entrée de 10 dBm contre une charge résistive de 1500 Ω. Le système d'antenne et de rectenna proposé démontre les possibilités detransfert de puissance micro-ondes sans fil sur une longue distance avec efficacité et ce pour des diamètres d'antenne respectables.

ABSTRACT

In this article, the design and optimization of an antenna (transmitter) and a rectenna (receiver) system is presented to process the wireless microwave power transfer to feed a 22-kW moving unmanned air vehicle. The microwave power transmitting frequency of 35 GHz is selected in order to obtain a low-cost compact system architecture. To do so, first, the size of the transmitting and receiving antenna has been calculated using Friis' power transmission equation for a distance of 10 km. The power transmitting distance can be varied according to the demand. Therefore, an array of high gain and high efficiency of 4x2 rectangular microstrip patch antenna has been designed and simulated with the electromagnetic design tool CST. Then a rectifying system (rectenna) is designed and optimized by the advanced design system (ADS) software. A GaAs Schottky diode MA4E1317 is selected for the rectifying system. The resonating frequency for the patch antenna array and rectenna is 35 GHz. The gain and efficiency of the proposed 4x2 microstrip patch antennas achieved 13.4 dBi and 85% respectively. Moreover, RF to DC conversion efficiency of the proposed rectenna and DC output voltage reaches 80% and 3.5V respectively for a 10 dBm input power against a 1500 Ω resistive load. The proposed 35 GHz antenna and rectenna system have a high potential for wireless microwave power transfer on a long-distance with higher efficiency.

TABLE OF CONTENTS

LIST OF TABLES

LIST OF FIGURES

LIST OF SYMBOLS AND ABBREVIATIONS

ADS	Agilent advanced design system
UAV	Unmanned aerial vehicle
WPT	Wireless power transmission
MPT	Microwave power transfer
MMW	Millimeter wave
Tx	Transmitting antenna
Rx	Receiving antenna
VSWR	Voltage standing wave ratio
RF	Radio frequency
DC	Direct current
HB	Harmonic Balance
AE	Analytical Equation

LIST OF APPENDICES

CHAPTER 1 INTRODUCTION

1.1 Background

Unmanned areal vehicles (UAV) have great potential for their versatility in several fields of applicability where continuous surveillance monitoring of areas affected by disaster is required such as floods, and bushfire without endangering human life. In addition, flying UAVs could be deployed as a platform for terrestrial telecommunication, TV broadcasting, or internet supplying service to remote areas. Moreover, UAVs could be used for crime prevention observation, radiation observation, and metrological concentration i.e., CO_2, SO_2, and NO_2 monitoring platforms in various locations around the world [1].

Electric aircraft has drawn attention as a possible candidate for UAV applications. It has several advantages over the conventional gasoline-based airplane. An electric aircraft used an electric motor that can be 95% efficient instead of the 18% to 23% efficiency of regular combustion engines [2]. It is more reliable, light in weight, safe, low cost, and less noisy. Finally, it has zero carbon emissions.

Most of the currently available commercial electric aircraft have a major disadvantage; it has limited flight duration because an electric aircraft runs only on its battery power. As a result, compared to gasoline-powered flights, it has a much shorter flying time [3]. To enhance their flight time and extend their roaming range, an electric aircraft needs to be powered remotely. Therefore, there is a necessity for an external power source that can feed power to the aircraft during flight time. To accomplish this task, a microwave power transmission (MPT) system could be used to power the flight. The benefit of an MPT system is the capability of contactless long-distance power transmission with lower power transmission loss. Mainly, the MPT system consists of two sections: a transmitting antenna (Tx), and a receiving antenna or rectifying antenna (Rx). In Tx, DC power is converted to microwave power by a microwave oscillator i.e., magnetron, klystron, and radiates it to the free space towards the Rx. Rx receives microwave power and reverts it back to DC power [3-4].

Previous studies on MPT to UAVs mainly focused on systems working at 2.45 GHz and 5.8 GHz. However, for the lower frequency band, the size of the transmitting and receiving system will be large for a long-distance RF power transfer. Therefore, to obtain a compact transmitting and receiving system, the choice of a higher frequency band is better. Hence, 35 GHz, 61 GHz, and 94 GHz frequency bands can be utilized. Among them, 35 GHz frequency is selected because its atmospheric attenuation is lower. Therefore, the millimeter-wave rectenna operating at 35 GHz has motivated this work. We are proposing a transmitting and receiving system for MPT to a moving airplane at a distance of 10 km. This 35 GHz frequency reduced the size of the Tx antenna and Rx rectenna significantly which is crucial for limited antenna area, especially on the receiver side. In this thesis, a 35 GHz 4x2 microstrip patch antenna array and a rectenna system have been designed and optimized to process the wireless microwave power transfer to feed a 22-kW moving unmanned air vehicle.

1.2 Objectives of the Project

To transfer uninterrupted microwave energy to a high-altitude airplane, it is essential to have a compact size of transmitting and receiving system. The main objective of the project can be divided into the following subsections:

1. Literature review of the MPT history and its improvement in past decades.
2. Investigation of the UAVs applications, benefits, and limitations.
3. Examine a suitable frequency in millimetre wave (MMW) frequency for MPT.
4. Determine the specifications of the antenna array in order to satisfy MPT conditions.
5. Design of microstrip antenna array by CST Studio suite software.
6. Investigate the various rectifier circuit configuration and come up with a simple architecture in order to obtain a higher RF to DC conversion efficiency at MMW.
7. Figure out the optimized designed parameters of a high-power rectenna system in MMW using ADS software.
8. Design and optimize an MMW high-efficiency rectifier system.
9. Design an impedance matching network to improve the rectenna efficiency.

1.3 Contributions of the Thesis

1. This work proposes a microwave power transfer to an electric-powered unmanned aerial vehicle for charging wirelessly at a maximum distance of 10 km.
2. Design of a high gain and high directivity 4x2 microstrip patch antenna array at 35 GHz for point-to-point MPT.
3. Design and optimize a high-power rectifier system at 35 GHz.

1.4 Structure of the thesis

This thesis presents a 22-kW microwave power transfer to a UAV flying at a distance of 10 km where the key technologies are analyzed, estimated, and designed. The remaining of this paper is organized as follows: Chapter 2 describes the state of the art and theoretical background of the project. Design, simulation, and optimization of the transmitting and receiving systems are analyzed in Chapter 3 and Chapter 4 respectively. Chapter 5 covers a paper submitted to the MDPI Energies journal, where the description of efficient system architecture based on MPT working at 35 GHz. Transmission analysis, Tx, Rx, and a 4x2 rectangular patch antenna array are reviewed. The efficient rectifying system is conceived using the Agilent advanced design system (ADS). The conclusion is presented in Chapter 6.

CHAPTER 2 LITERATURE REVIEW

2.1 State of the art - wireless power transmission technology

The concept of the wireless power transmission (WPT) system was first introduced and demonstrated by Nicola Tesla in 1899. In his experiment, he successfully received 100 KV at the receiver side, and with this power, he could light 200 lamps 26 miles apart from the transmitter [4]-[5]. Later on, in the 1960s W.C. Brown started microwave power transmission (MPT) research and made significant progress in MPT technology. In 1963 he conducted an experiment where he could capture 100 W of RF power with an efficiency of 26% at 2.45 GHz from a distance of 5.48 m. In this experiment, an ellipsoidal reflector and a diagonal horn antenna of 3 m and 2 m were utilized as a transmitting and receiving antenna respectively. A 400 W magnetron was adopted in order to feed RF energy to the transmitting antenna [6]. He then investigated the possibility of feeding wireless power to a flying helicopter. Thereafter, W.C Brown and his team developed a 55% efficient rectifying antenna, successfully demonstrating the first microwave-powered helicopter at an altitude of 50 feet.

Figure 2.1 First microwave-powered helicopter built by W. C. Brown in 1964 [7]

In this demonstration, a magnetron oscillator providing an output power of 3 to 5 kW at a frequency of 2.45 GHz was used as a power source for a 3 m ellipsoidal reflector. And a 4 m^2 rectenna with an output power of 270 W was used to feed the 78 W helicopter engine [7]. W.C Browns developed helicopter and MPT system is shown in Figure 2.1 and Figure 2.2 respectively.

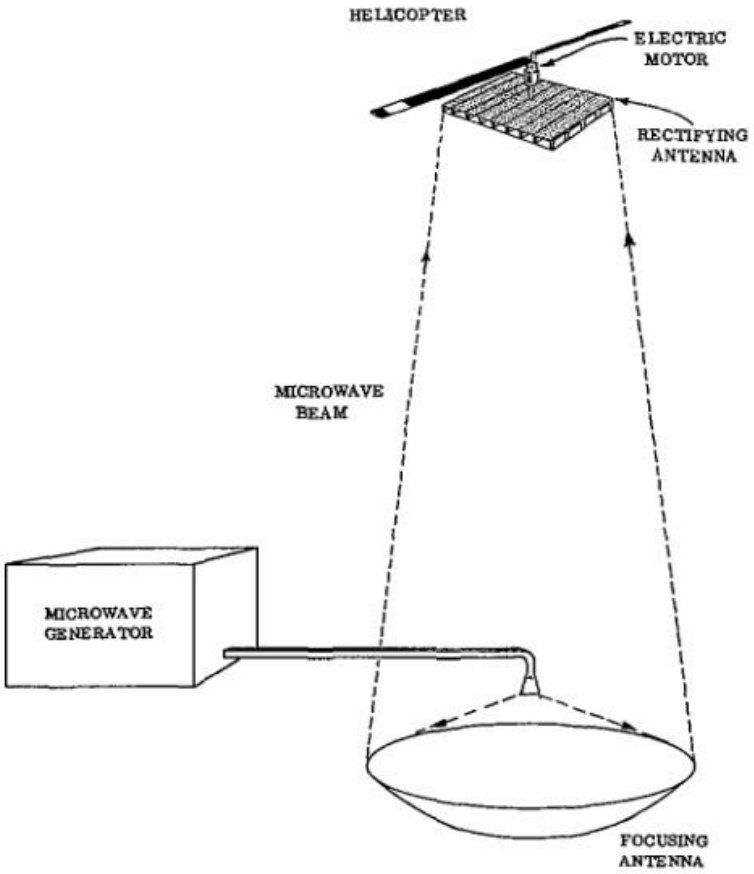

Figure 2.2 MPT system for helicopter system by W.C Brown [7]

By 1975 W.C Brown and his team working on a NASA project built the largest MPT made of a 26 m diameter parabolic antenna transmitting to a rectenna array size of 3.4 m x 7.2 m. The distance between the Tx antenna and Rx rectenna was one mile and could receive 30 kW of DC power at the receiver end with an efficiency of 82.5% at 2.45 GHz [8]. Ground to ground MPT system of the NASA project is shown in Figure 2.3. In 1987 SHARP Canada conducted an MPT project for a fuel-free model airplane. They transmitted a 10-kW microwave signal to the airplane at 2.45 GHz at a flying altitude of 150 m. The length of the plane was 2.9 m with a wingspan of 4.5 m [9]. Sharp experimental details are shown in Figure 2.4.

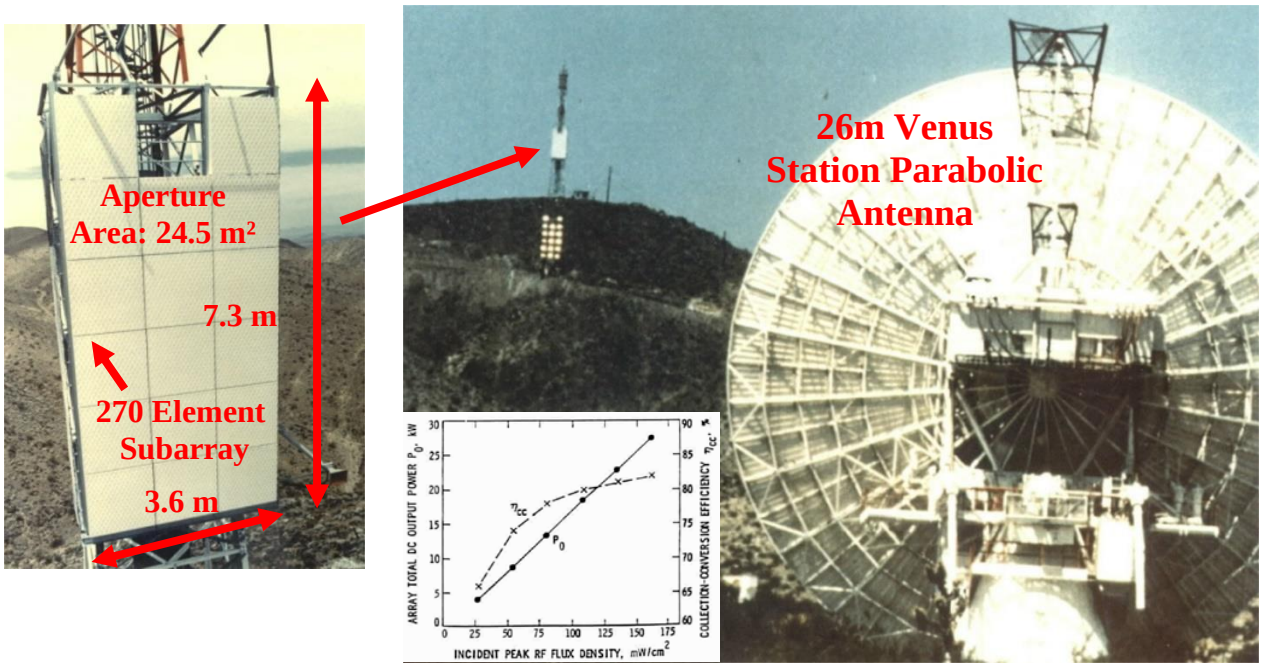

Figure 2.3 Ground-to-Ground MPT Experiment in 1975 by NASA. 34 kW collected from a rectenna located 1 mile (1.54 km) from a 320-kW transmitter [8]

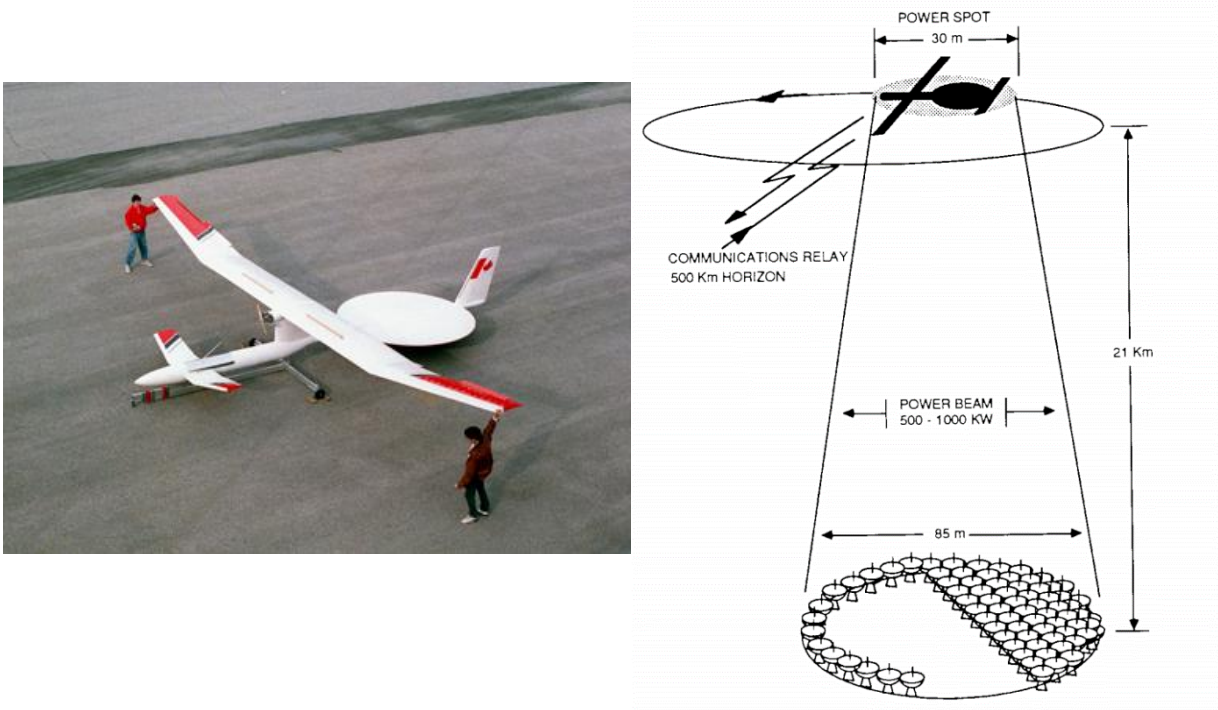

Figure 2.4 SHARP MPT configuration [9]

Many Japanese researchers have investigated and carried out fuel-free airplane MPT research in the 1980s at 2.45 GHz [10]-[13]. They made significant progress in MPT technologies. Experiments MINIX and ISY-METS were executed by Hiroshi Matsumoto's team in 1983 and 1993, respectively. In MINIX and ISY-METS a magnetron microwave transmitter generating an output power of 800 W was used at 2.45 GHz [10]. Project ISY-METS and MINIX experimental demonstration are shown in Figure 2.5 (a) and Figure 2.5 (b).

(a) **(b)**

Figure 2.5 Microwave power transmission experiments a) Project ISY-METS airplane experiment, b) Project MINIX rocket experiment [10]

Later on, Kansai Electronic Co. Ltd; took an initiative with Kyoto and Kobe University on an MPT project in 1994. In this project, they used a parabolic antenna diameter of 3 m as a transmitter and a square shape 3.2 m x 3.5 m rectenna array as a receiving antenna at the frequency of 2.45 GHz.

The distance between the transmitter and the receiver was 42 m and could receive 0.75 kW of DC power at a transmitted power of 5 kW [14]. The experimental detail is shown in Figure 2.6.

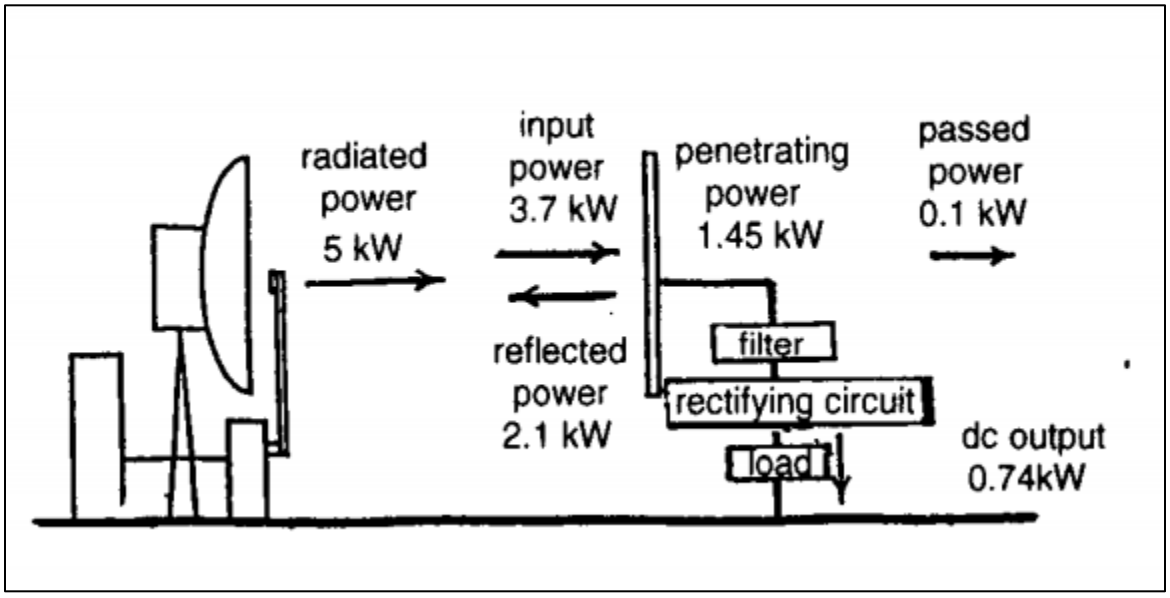

Figure 2.6 MPT experiment conducted by Kaisai Electronics [14]

In 2001, JAXA Japan analyzed an MPT from space to the ground at a distance of 36000 km. The required diameter of the transmitting and receiving systems are 1 km and 3.4 km respectively, in order to harvest 1 GW of power [15]. Still, now many researchers are working on MPT projects for various fields of application.

2.2 Frequency selection for MPT

For wireless microwave power transmission industrial, scientific, and medical, ISM frequency bands 2.45 GHz, 5.8 GHz, and 24.5 GHz are recommended [16]-[17]. Various researchers work on different frequency bands for MPT. For example, NASA recommended 2.45 GHz, on the other hand, Japanese scientists prefer 5.8 GHz [15]. Each frequency bands have their own advantages. So, the selection of the frequency is completely dependent on the type of application. The size of the transmitting and receiving antenna varies as a function of the distance. For the short distance of MPT, a lower frequency band works nicely with a compact transmitting and receiving system. However, in the case of long-distance power transmission, the sizes of the transmitting and the receiving system will be larger at a lower frequency band. Therefore, a higher frequency band is

needed to achieve a more compact MPT system. In this work we are proposing an MPT to power a high-altitude UVA, therefore the choice of a high frequency is mandatory in order to get compact MPT antennas.

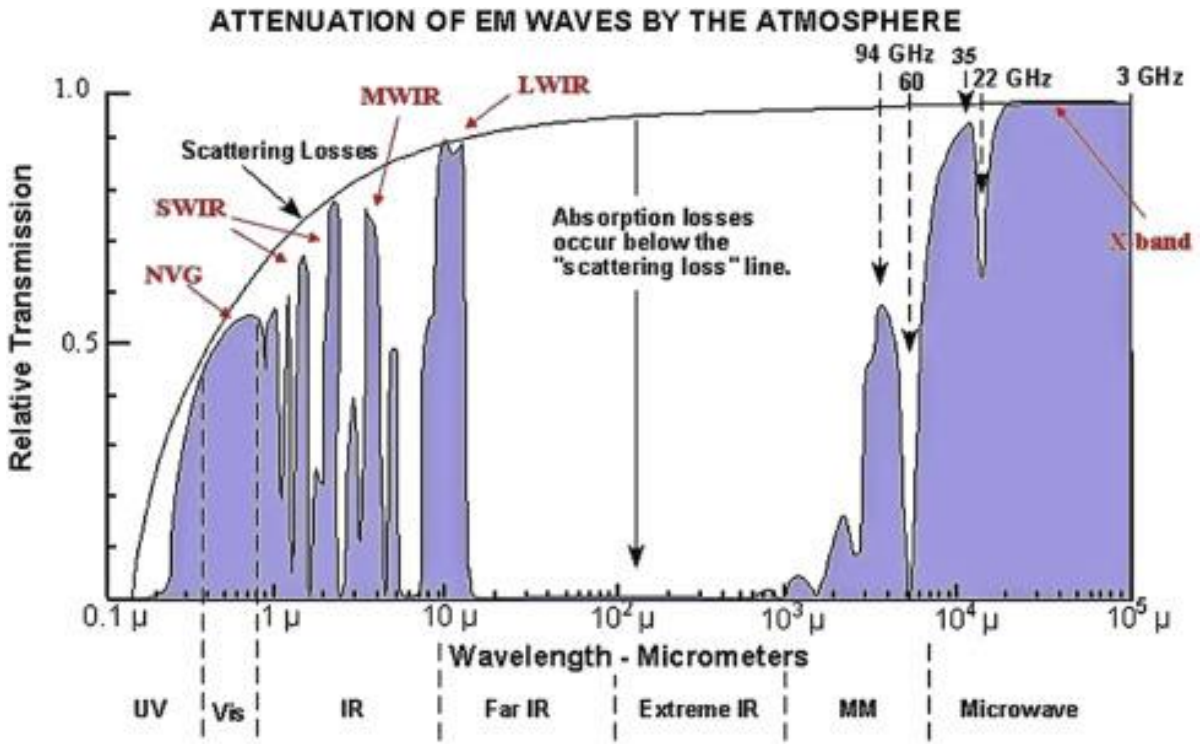

Figure 2.7 Atmospheric attenuation in the electromagnetic spectrum [58]

Figure 2.7 shows the effect of atmospheric attenuation on the electromagnetic spectrum. In X-band, nearly 100% transmission is possible, and at a higher frequency transmission is decreasing. However, at 35 GHz nearly 93% transmission is possible. Hence, in this project, the 35 GHz frequency band is selected which not only decreases the transmitter and receiver size but also offers reasonable power transmission through the atmosphere**.**

2.3 Rectenna topologies for wireless power transmission

Rectenna is one of the most important parts of the wireless power transmission system. It is a combination of rectifying circuit and antenna. A rectenna can have a different topology such as series, shunt, voltage doubler, and bridge rectifier. Figure 2.8 (a) and Figure 2.8 (b) are the simplest structure of a rectifier circuit where a Schottky diode is placed at the circuit. This type of rectifier is known as half-wave. A half-wave rectifier that allows the only half cycle (positive or negative half cycle) of the input signal and blocks the other half. The design and simulation of series and shunt rectennas are simple and easier. These rectennas are suitable for low-power applications [18].

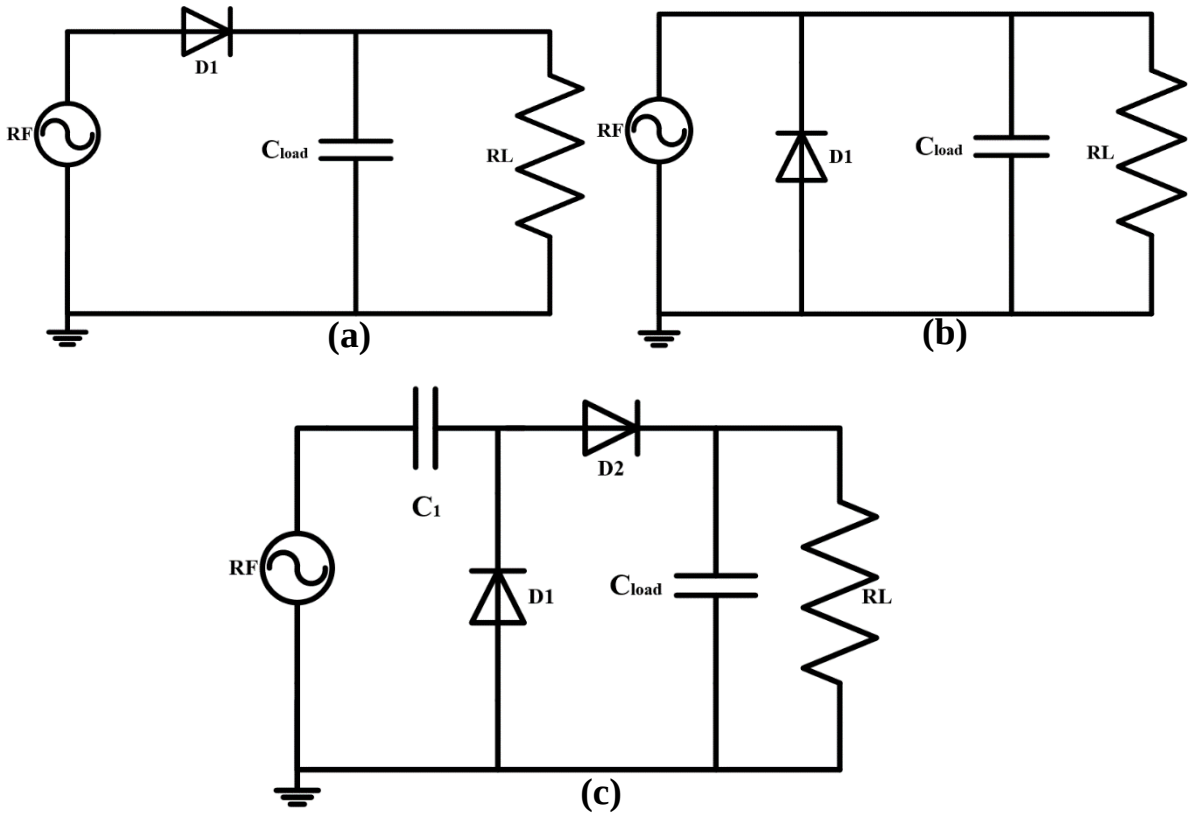

Figure 2.8 Typical rectifier topologies a) Series rectenna, b) Shunt rectenna, and c) Voltage doubler rectenna

A voltage doubler rectenna is a combination of series and shunt rectenna. It has two diodes placed in series and parallel positions of the circuit as shown in Figure 2.8. (c). One diode rectifies the

negative half whereas another diode rectifies the positive half. This rectenna topology is suitable for high-power applications. A study and comparison of different rectennas were done in [16].

Different types of antennas can be used in rectenna system for example, dipole antenna [4], [19], monopole antenna [20], coplanar patch [21], microstrip patch [22], [23], Yagi-Uda antenna [24]-[25], spiral [26] and parabolic [27]. RF to DC conversion efficiency mainly depends on the input RF power and the load resistance. Typical rectenna efficiency behavior is plotted in Figure 2.9. The efficiency of the rectenna will be significant if the power and the load are matched and this can be determined by the diode characteristics. The diode junction voltage and the breakdown voltage are two important parameters in order to improve the RF to DC conversion efficiency of the rectenna. For example, the diode will not rectify if its input voltage is smaller than the junction voltage or its input voltage is greater than the breakdown. Therefore, RF to DC conversion efficiency will fluctuate.

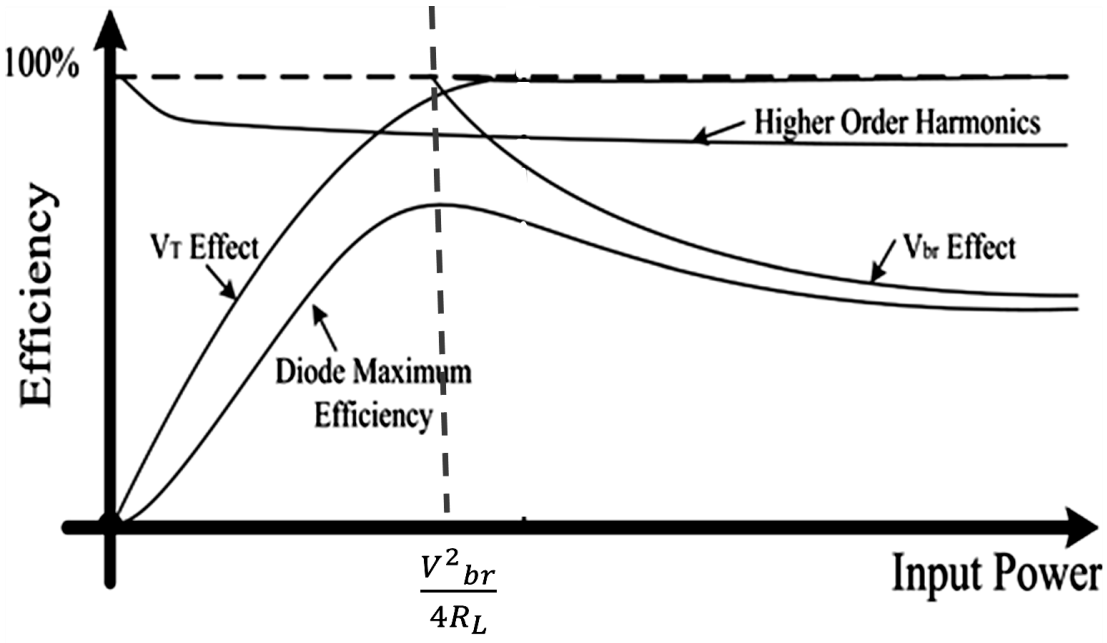

Figure 2.9 Typical RF-DC conversion efficiency characteristic of a rectenna [28]-[31]

2.4 Theoretical background of Friis' power transmission formula

Using Friis' formula, we can estimate the available transmitted and radiated power. Depicted in Figure 2.10, the transmitting and receiving antennas are connected to their respective circuit. The transmitter and receiver are separated by a distance d.

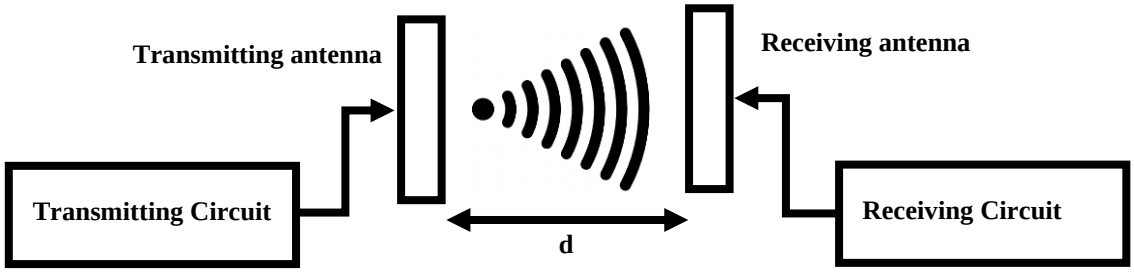

Figure 2.10 Trans-receiver system

If we consider a transmitting antenna as an isotropic source, then it will radiate equally in all directions and when it reaches the receiving antenna, the power density will be

$$S_T = \frac{P_T}{A_t} = \frac{P_T}{4\pi d^2} \qquad (1)$$

where, S_T is the power density, P_T is the transmitted power, A_t is the area of the transmitting antenna and *d* is the distance between the transmitting and the receiving antenna.

If the gain of the transmitting antenna is G_T then the power density becomes:

$$S_T = \frac{P_T}{A_t} = \frac{P_T G_T}{4\pi d^2} \qquad (2)$$

Under ideal conditions, if the impedance of the receiving antenna is matched with the transmitting antenna and its effective aperture becomes A_{eR}, then the received power P_R will be,

$$P_R = S_T A_{eR} = \left(\frac{P_T G_T}{4\pi d^2}\right) A_{eR} \ . \qquad (3)$$

If the gain of the transmitting antenna is $G_T = \frac{4\pi A_{eT}}{\lambda^2}$, then from equation (3),

$$P_R = S_T A_{eR} = P_T \left(\frac{\frac{4\pi A_{eT}}{\lambda^2}}{4\pi d^2} \right) A_{eR} \quad . \tag{4}$$

A_{eT} is the effective aperture of transmitting antenna.

Similarly, If the gain of the receiving antenna is

$$G_R = \frac{4\pi A_{eR}}{\lambda^2} . \tag{5}$$

then from equations (4) and (5), Friis' power transmission formula will be

$$P_R = P_T G_T \left(\frac{\lambda}{4\pi d}\right)^2 G_R \tag{6}$$

From equation (6), it is possible to calculate the transmission path loss.

The Friis' power transmission formula (6) is taken in decibel,

$$10 \log \left(\frac{P_R}{P_T}\right) = 10 \log \left(\frac{G_T G_R}{\left(\frac{4\pi d}{\lambda}\right)^2} \right)$$

$$or, 10\ log\ P_R - 10\ log\ P_T = 10\ log\ G_T + 10\ log\ G_R + 20\ log\ \left(\frac{\lambda}{4\pi d}\right)$$

$Let, -L(s) = 20\ log\ \left(\frac{\lambda}{4\pi d}\right)$ where L(s) is the free space path loss and, $\lambda = \frac{c}{f} = \frac{3x10^8}{f}$, then,

$$10\ log\ P_R - 10\ log\ P_T = 10\ log\ G_T + 10\ log\ G_R - L(s) \tag{7}$$

$$and, -L(s) = 20\ log\ \left(\frac{3x10^8}{4\pi f d}\right).$$

If we consider the frequency, *f*, in GHz and the distance d, in km then *L(S)* becomes,

$$L(s) = 92.44 + 20 \log d + 20\ log\ f_{GHz} \quad . \tag{8}$$

It is seen from the equations shown above that the received power will be very low. This is because Friis' power formula works only for the far-field condition and then only full dispersion occurs [16].

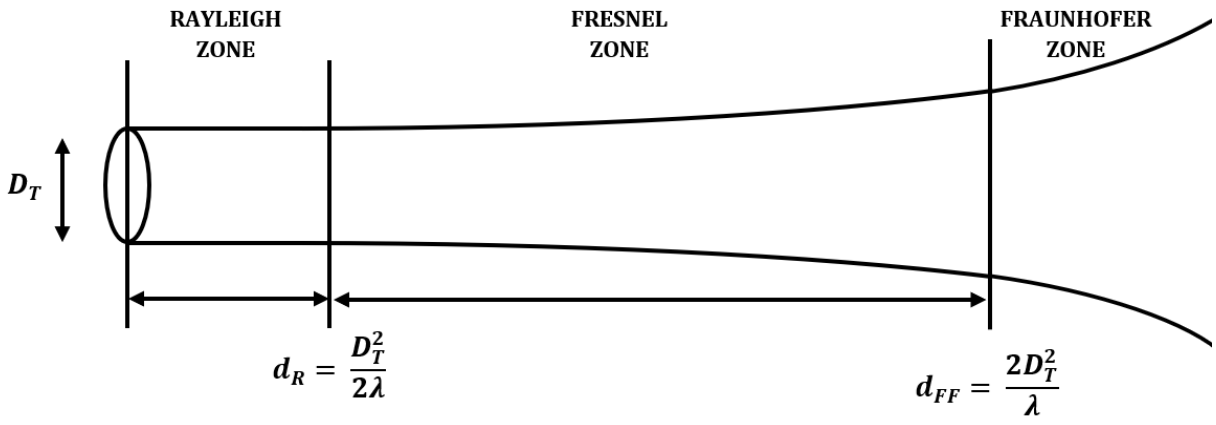

Figure 2.11 The dispersion effects of a microwave beam transmitted by an aperture antenna of diameter D_T [16]

As depicted in Figure 2.11, the beam diameter from an antenna aperture of dimension, D_T, remains constant when the transmitted distance is within the near field Rayleigh zone, d_R. Whereas in the near field Fresnel zone it slightly disperses up to a distance of d_{FF}. However, in the far-field Fraunhofer zone, full dispersion occurs. As a result, higher power loss happens. For point-to-point power transfer, the near-field condition needs to be considered. Hence, G. Goubau and W.C. Brown shows the relationship between wireless beam power transfer efficiency and beam power transmission parameter for near field condition in equation (10) and (11), [28]-[32].

The Friis transmission formula can be written as,

$$P_R = P_T G_T \left(\frac{\lambda}{4\pi d}\right)^2 G_R = \frac{A_t A_r}{\lambda^2 d^2} P_T \qquad (9)$$

Since the Friis transmission equation assumes spherical wave at the far-field condition and it is plane wave at near field condition where the MPT is used. Then, it is not possible to utilize equation (9) for receiving power calculation at a distance of the near field because of high power loss. However, in this work, we are aiming for MPT transfer up to a distance of 10 km. Therefore, bringing this long-distance in the near-field zone is a challenging task, but it is possible with the help of modern technologies. A Gaussian beamforming technique would be suitable for effective

energy transmission in the near field [28]-[29]. An amplitude tapering phased antenna array could be useful for Gaussian beam forming. It generates planner wavefronts up to the long-distance, so it would be useful for MPT [15]. Therefore, to achieve efficient power at the near field zone, equation (9) needs to be converted for near field condition.

The power transmission is given by the ratio of the integral of the product of the transmitted field and the receiver response to the product of the integrals of the power over the transmitting and receiving apertures [28]-[29]. Therefore, the near field power transmission formula can be written as,

$$\frac{P_R}{P_T} = \frac{\left| \int_A E_r \cdot E_t \, ds \right|^2}{\left\{ \mathrm{Re} \int_{A_r} |E_r|^2 \, ds \right\} \left\{ \mathrm{Re} \int_{A_t} |E_t|^2 \, ds \right\}} \tag{10}$$

Here, P_R, E_r, power and electric field at receiving station respectively; P_T, E_t, power and electric field at transmitting station respectively, A_t, is the effective surface area of Tx, and A_r, the effective surface area of Rx.

For the fundamental Gaussian mode [28]-[29], the equation (10) integration result is,

$$\frac{P_R}{P_T} = \frac{A_t A_r}{\left(\frac{A_t + A_r}{2}\right)^2 + \lambda^2 d^2} \tag{11}$$

Here λ is the operating wavelength and d is the distance between Tx and Rx antenna. For the large values of d, the equation (11) becomes,

$$\frac{P_R}{P_T} \simeq \frac{A_t A_r}{(\lambda^2 d^2)} = \tau^2 \tag{12}$$

where τ is beam transmission parameter.

Equation (12) is also referred to the beam transmission efficiency, $\eta_{\text{beam}} = \frac{P_R}{P_T}$. The equation (12) does not depend on power. Therefore, it is possible to transmit the high power of kWs, MWs via microwaves.

The relationship between the beam transmission efficiency (η_{beam}) and beam transmission parameter (τ) for the near field zone can be calculated by the Fresnel Kirchhoff diffraction theory using paraxial equation of Gaussian beam in the form of the Helmholtz equation under the assumptions that amplitude and phase distributions in the beam are optimized for maximum transmission efficiency [28]-[32]. From equation (12), the beam transmission efficiency for the near field zone is given by [32],

$$\eta_{\text{beam}} = 1 - e^{-\tau^2} \quad . \tag{13}$$

The equation number (12) and (13) are used for the near field conditions.

Conclusion:

In summary, some earlier MPT works have been discussed in this chapter and it is established that for MPT we need a transmitting and a receiving system. The size of the transmitting and the receiving system depends on the frequency. Therefore, we made a choice of suitable frequency in MMW where it would be possible to achieve an efficient and compact transmitting and receiving system. The different rectenna topologies are investigated in order to obtain a suitable rectifier circuit with higher RF to DC conversion efficiency. For long-distance MPT it is found that the receiving system should be kept within a near field zone. Therefore, a Gaussian beamforming technique is proposed for transmission. This technique is useful for MPT because creates a planner wavefront and it is feasible for more than 10 km distance. In the next chapter, we will discuss the design and analysis of the microstrip patch antenna array as a transmitting and receiving system.

CHAPTER 3 MICROSTRIP PATCH ANTENNA

3.1 Introduction

In the previous chapter, the key issue of the MPT has been discussed. The MPT consists of a transmission and a receiving system. An onboard rectenna is required to receive microwave power to a flying aircraft. Hence, for the transmitting and receiving system, a microstrip patch antenna design was selected for the antenna array. Microstrip patch antenna typically consists of a patch, a ground plane, a dielectric substrate, and a transmission line. The patch and the ground plane act as a conducting layer which is separated by the dielectric substrate as shown in Figure 3.1. It is one of the most widely used antennas in RF applications because of its ease of fabrication, lower cost, small size, light weight, and lower profile. Therefore, microstrip patch antennas are suitable for aircraft, spacecraft, satellite, and missile applications. These patch antennas are easily compatible with the planar and non-planar surfaces. It is possible to design a particular shape and mode [33].

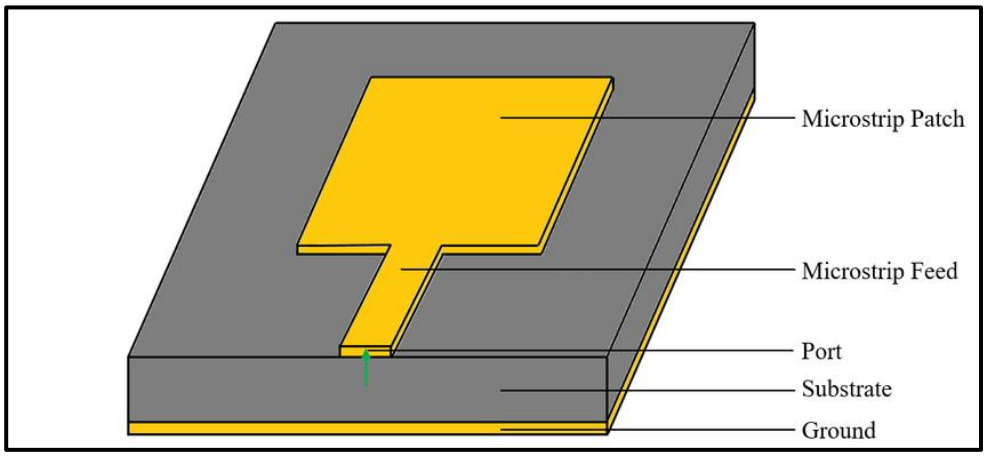

Figure 3.1 Typical structure of patch antenna

The main limitations of the microstrip patch antenna are poor power capability, low gain, and high loss [33]-[34]. To solve this problem, a proper substrate material needs to be selected. If the dielectric constant of the material is high, the bandwidth will decrease, and the gain will increase.

On the other hand, if the thickness of the substrate material is low then it will decrease the efficiency of the antenna and increase the bandwidth.

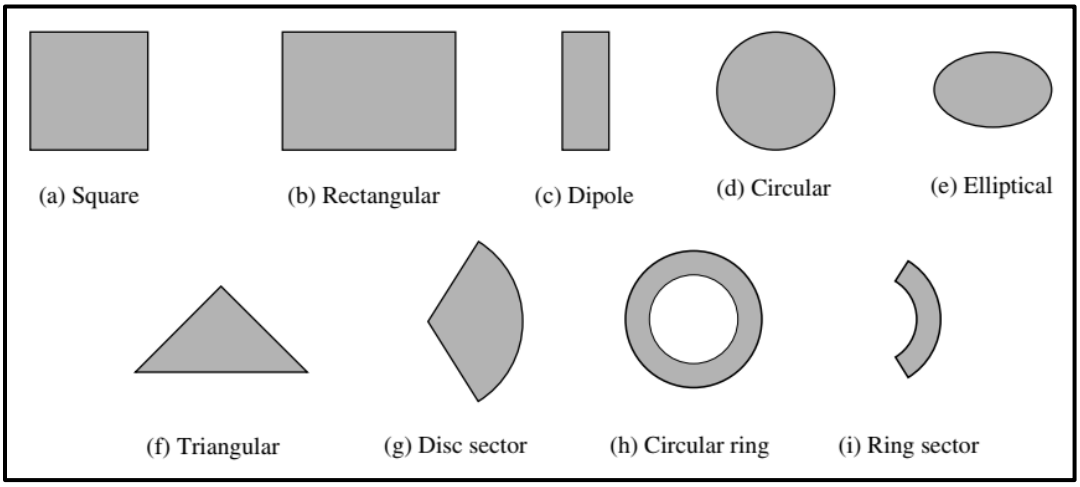

Figure 3.2 Shape of the patch antenna

The microstrip patch antenna can have various shapes as shown in Figure 3.2. The square, rectangular, and circular patches are examples of common patches for millimetre wave applications. After the selection of the patch, it is important to select the proper feeding and analysis methods. The widely used feeding methods are microstrip, coaxial probe (coplanar feed), proximity coupling, and aperture coupling. Microstrip patch antenna can be analyzed in many ways, some popular methods employed are: - transmission line, cavity, and full-wave.

3.2 Design and simulation of a single microstrip patch antenna

Since we have selected a 35 GHz frequency to design a compact transmitting and receiving system. An RT DUROID 5880 material is selected to fabricate our microstrip patch antenna. The properties of the selected material are: a dielectric constant of 2.2, a loss tangent of 0.0004-0.0009, and a thickness of 0.254 mm. Copper is selected as the conducting material because of its low cost and high conductivity. The copper thickness is 0.0035 mm. The rectangular shape is adopted for the simulation because of its simple design and easy fabrication. The transmission line method is

chosen to analyze the antenna parameter. This method offers decent physical insight and less complexity compared to the cavity method. A typical shape of the microstrip patch antenna is shown in Figure 3.3, where $\boldsymbol{W_P}$, $\boldsymbol{L_P}$, $\boldsymbol{d}$, $\boldsymbol{L_f}$, $\boldsymbol{W_f}$ and $\boldsymbol{Gpf}$ are the width, length, insert distance of the patch, length, and width of the feed line, and gaps between patches and feedlines. These antenna parameters can be calculated [33]. All necessary information about the antenna parameter calculation will be presented in Appendix A.

Hence, using the above-mentioned equations the calculated values of the antenna parameter are: - $\boldsymbol{W_P}$ - 3.4 mm, $\boldsymbol{L_P}$ - 2.7 mm, $\boldsymbol{W_f}$ - 0.8 mm, $\boldsymbol{L_f}$ - 1.6 mm, $\boldsymbol{d}$ - 1.07 mm, and $\boldsymbol{Gpf}$ -0.1mm. The simulation of the microstrip patch antenna is carried out using an EM simulation tool, CST.

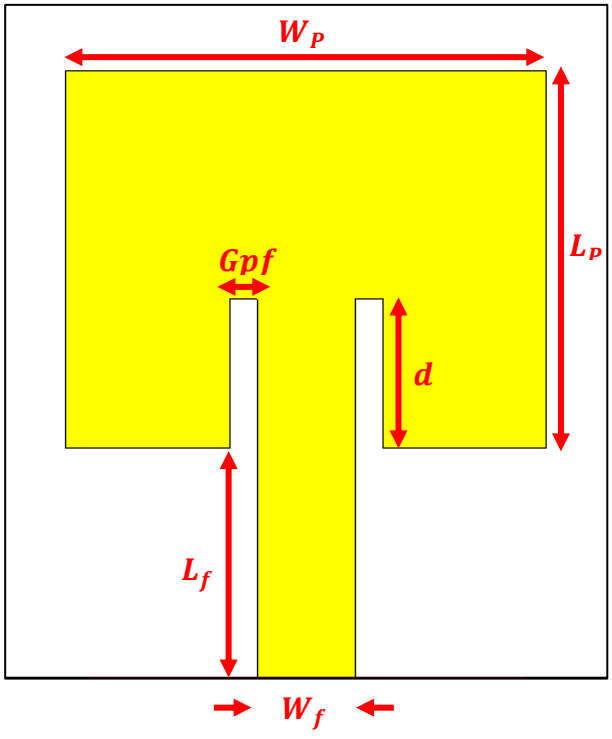

Figure 3.3 Design of a microstrip patch antenna

3.3 Single patch antenna simulation results

The surface current flow of a single microstrip patch antenna is shown in Figure 3.4 at 35 GHz. It can be seen that the maximum surface current is oriented in the Y- direction and it originates from the feed point. The maximum current intensity is observed on the middle of the patch and the minimum on the edge. It satisfied the patch antenna current distribution theory [33]. The surface current flow reverses its direction for reverse polarity, so, the designed antenna is linearly polarised.

The single microstrip patch antenna is designed and optimized with the software tool CST Studio Suite. The S11 of the designed patch antenna is shown in Figure 3.5. This antenna resonates at the desired 35 GHz center frequency with a reflection coefficient value of around -50 dB when the port impedance is 50 ohm. Hence, the outcome is excellent. The S11 is below -10dB and this value is recognized as the acceptable minimum, and it is enough for many RF applications. The bandwidth of the antenna at -10 dB is 0.7 GHz.

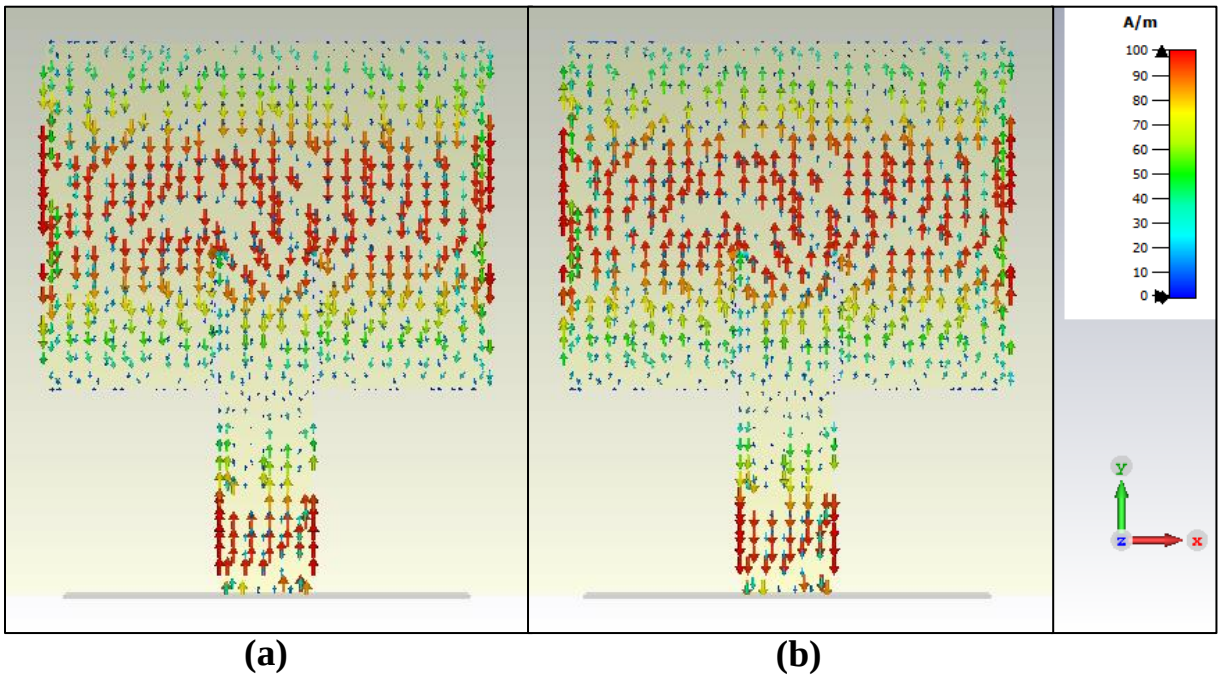

Figure 3.4 Surface currents plot of the single patch antenna at 35 GHz a) 0-degree, b) 180-degree

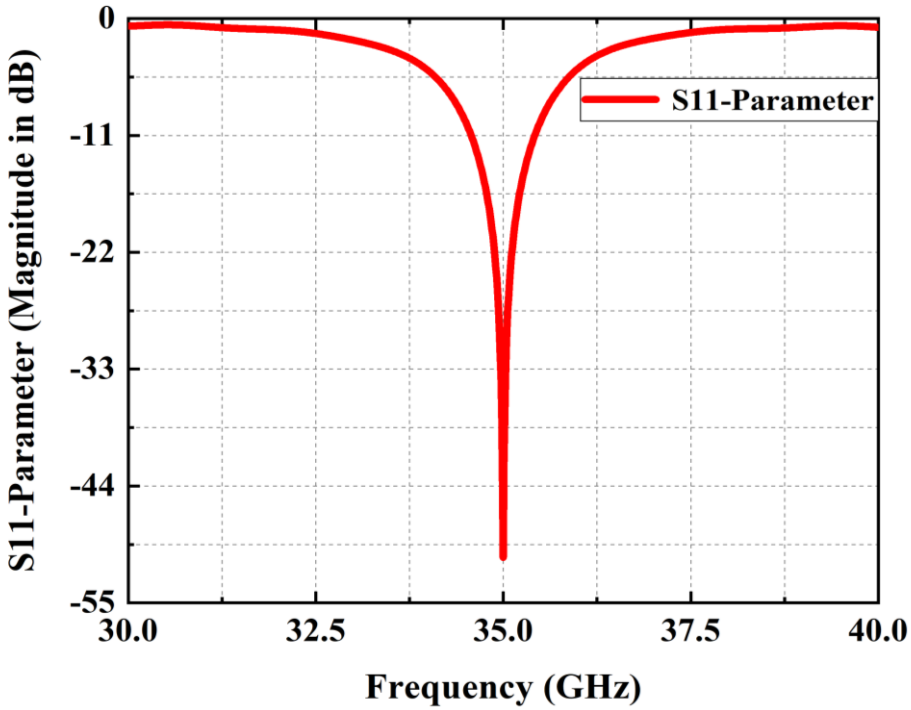

Figure 3.5 S11 of a single patch antenna

The term VSWR stands for voltage standing wave ratio. If the impedance of the antenna and the feedline are different, then part of the feeding signal gets reflected back. The reflected signal adds up with the feeding signal into a single wave called a standing wave. The ratio of the maximum and the minimum standing wave is called VSWR. Ideally VSWR is 1.0 which means that the impedance of the antenna and the cable impedance is equal, there is no mismatch. A ratio greater than 1,0 indicates a mismatch and some input signal gets reflected back. Therefore, more power can be delivered to the antenna. Figure 3.6 shows a VSWR at the center frequency 35 GHz of 1.03, which means an excellent matching between the antenna and the feedline. Hence, the designed single microstrip patch antenna can transfer high power.

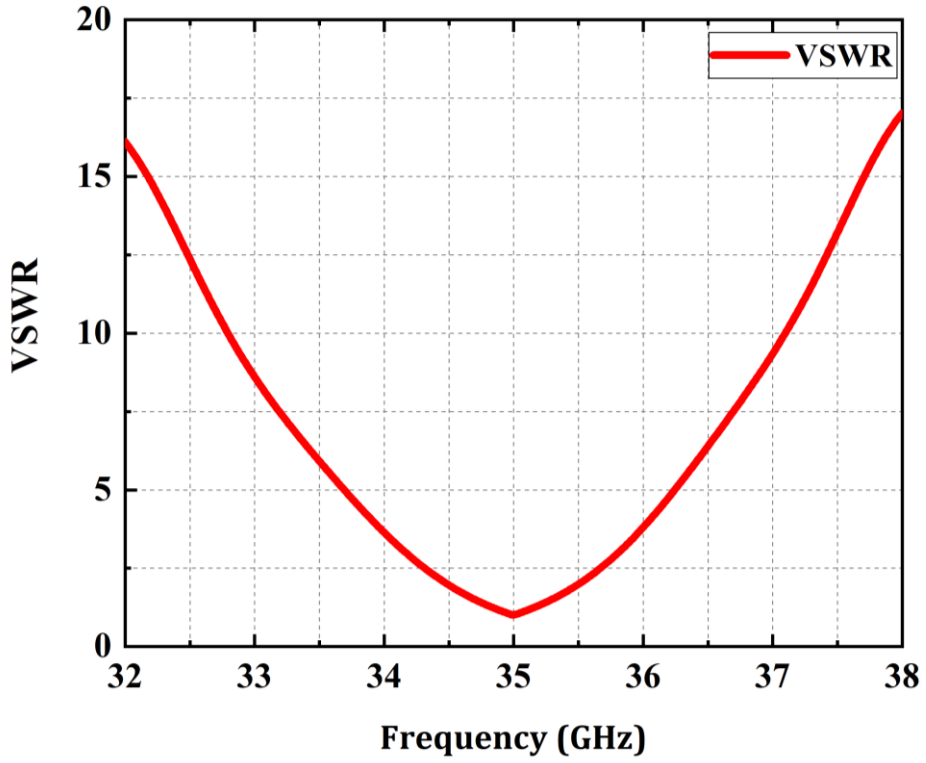

Figure 3.6 Voltage standing wave ratio of a single patch antenna

The 3D radiation diagram of an antenna is the one showing the most important antenna characteristics. The radiation diagram of an antenna describes how strongly an antenna radiates in any direction and the shape of the radiation pattern determines the application of the antenna.

Figure 3.7 shows the radiation pattern of the single patch antenna. The directivity of the single patch antenna is 8.15 dBi.

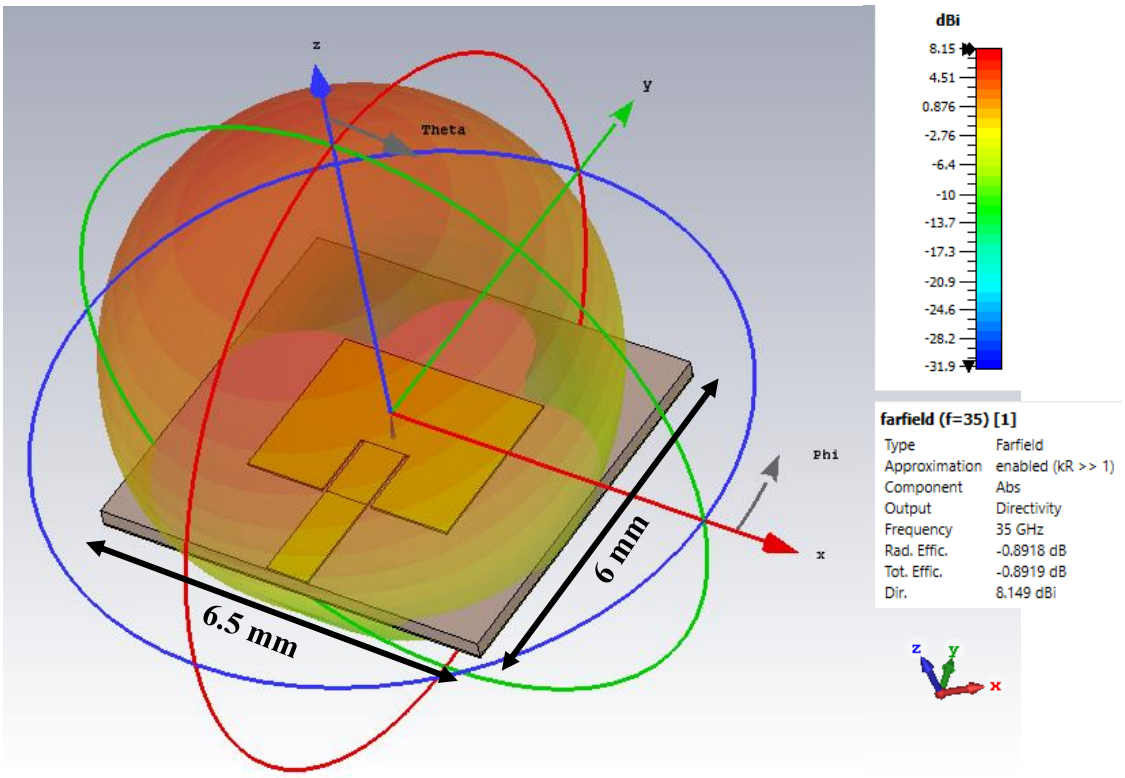

Figure 3.7 3D far-field radiation pattern of a single patch antenna

Directivity and gain are the main parameters of an antenna. Directivity is the measurement of the antenna radiation pattern in a particular direction and the gain says how strongly the antenna radiates in any direction in free space. Its unit of measure is dBi (decibel relative to isotropic). It is the ratio between the gain of the antenna compared to the gain of the theoretical antenna which is known as an isotropic antenna. Figure 3.8 shows the 2D polar plot of the radiation in the E-plane and H-plane. It shows the angular direction around the outer circle and the measured antenna gain and directivity at every angle. The inner-circle represents the axis of the antenna gain and directivity. The gain and the directivity of the single patch antenna are 7.6 dBi and 8.15 dBi respectively.

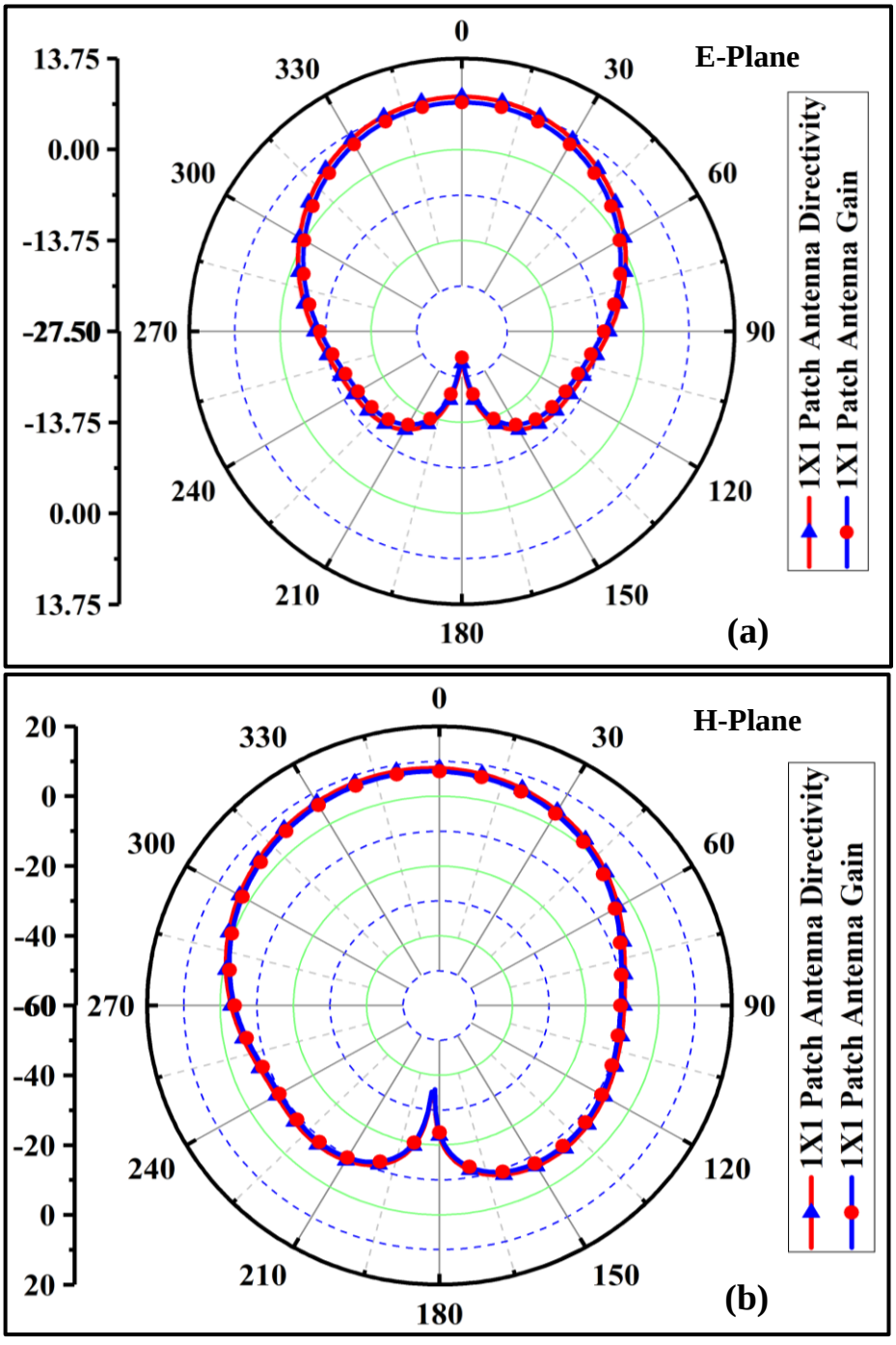

Figure 3.8 2D radiation pattern of a single microstrip patch antenna in dBi a) Gain & Directivity in E-Plane, b) Gain & Directivity in H-Plane

The antenna efficiency is a measure of how well an antenna converts power from the source into radiating electromagnetic power. It is the ratio of the power radiated by the antenna to the input power provided to the antenna. Radiation Efficiency = Radiated Power/Input Power, where the Input Power = Incident Power - Reflected Power. Here, the reflected power is due to impedance mismatch. Figure 3.9 shows the efficiency of the single microstrip patch antenna being 82%. On the contrary, Total Efficiency is the ratio of Radiated Power to Incident Power. Therefore, the Total Efficiency is lower or equal to the Radiation Efficiency.

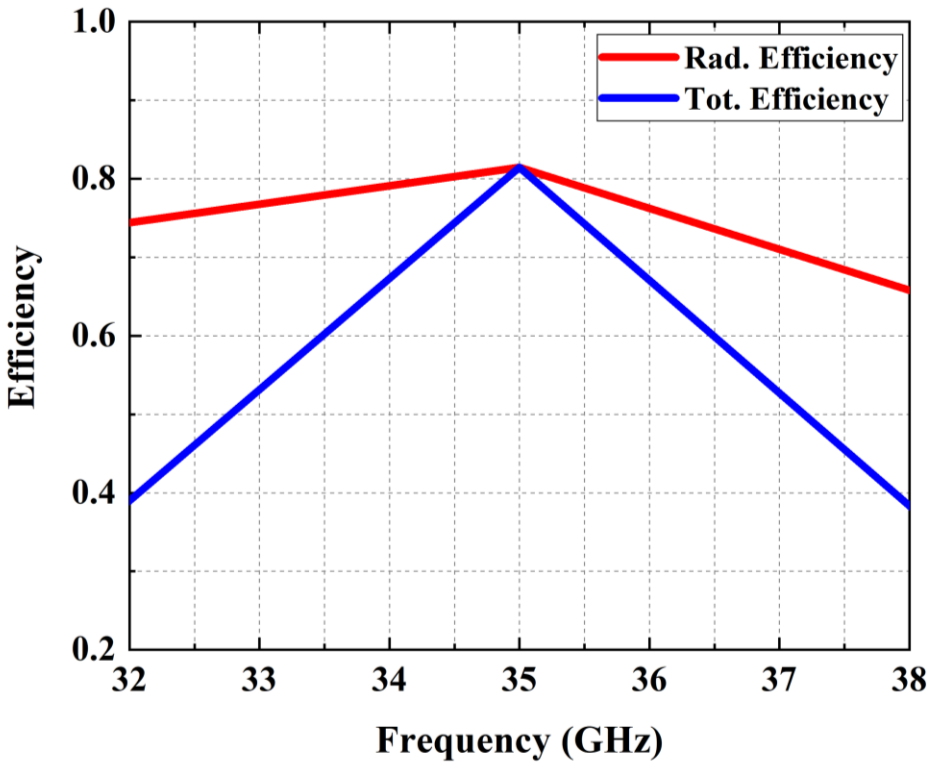

Figure 3.9 Efficiency of a single microstrip patch antenna

For wireless microwave power transfer, higher gain and higher directivity antennas are required. Hence, only an array of patches can satisfy the microwave power transfer requirements [33].

3.4 Design and simulation of microstrip patch antenna array

Microstrip antenna array plays an important role to increase the gain and the directivity and obtaining a controlled radiation pattern with the lower side lobe of the antenna. To make an antenna array, many small patch antennas need to be connected. Therefore, a proper feeding network needs to be selected. The most popular method to connect those patches uses series and corporate feeding networks. In corporate feeding, all patches are fed in parallel. Here, a 2x2 patch array is combined to obtain a common feeding point. Similarly, a 4x2 array is combined through a feeding point in the center of the array. This is the binary feeding method so the array can be increased in a controlled manner according to the demand. The length and the width of all the patches should be the same in order to obtain an efficient radiation pattern. The corporate feeding network offers wide bandwidth and equal power distribution to each patch element. As a result, the feeding network becomes symmetric and is ultimately balancing the mutual coupling effect. The greatest advantage of a corporate feeding network is that it is not dependent on the frequency because all the lengths are equal. Also, it offers higher gain with lower loss. However, the design of a corporate feeding network is a complex process. On the other hand, in the series feeding network, all patches are connected in series. Consequently, it reduces the feed length and narrows the bandwidth. The maximum radiation of the series feeding network is not stable because feedlines attenuate the patch elements. As a result, the gain of the antenna is poor compared to the one of the corporate feeding network and loss is increased. The design of the series feed network is however simpler [34].

The design and simulation of the microstrip patch antenna array are carried out using the corporate feed network since the incident power can be distributed equally to each antenna element from a single power port. Three different transmission lines are used to design the feeding network for the antenna array. The widths of 50 Ω (W_{50}), 70.71 Ω ($W_{70.71}$), and 100 Ω (W_{100}) transmission lines are 0.8 mm, 0.45 mm, and 0.25 mm, respectively. Spacing between each antenna element is optimized to 0.8λ as shown in Figure 3.10.

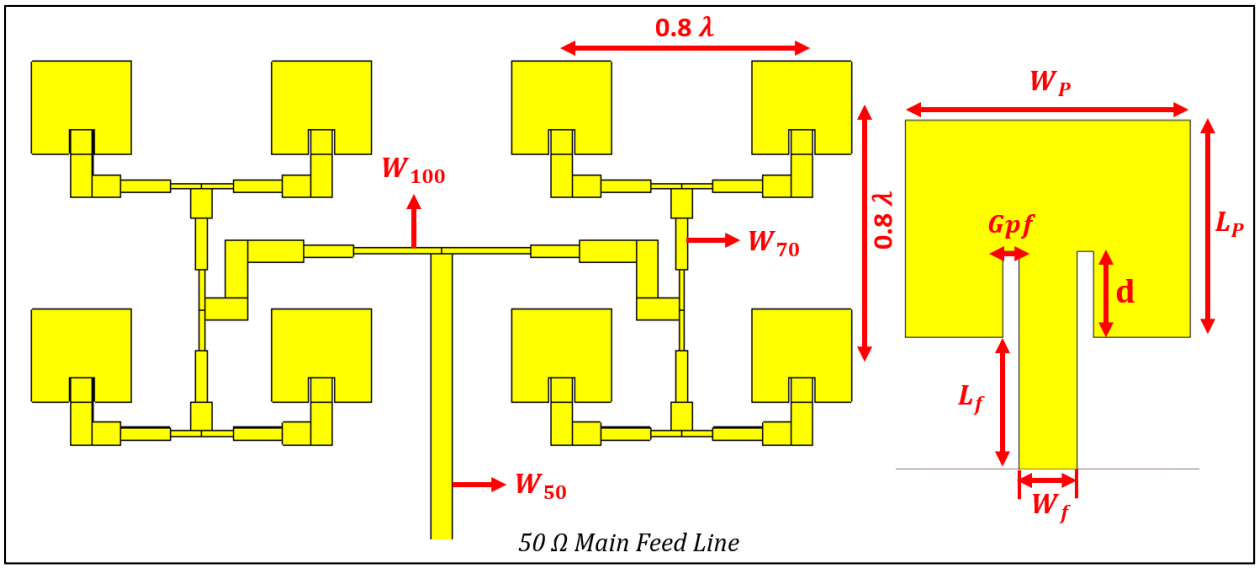

Figure 3.10 The proposed 4x2 microstrip patch antenna array

3.5 4x2 Patch antenna array simulation results

The surface current flow of the 4x2 microstrip patch antenna array is shown in Figure 3.11. Similarly, the maximum surface current towards the Y-direction and the maximum current intensity is observed in the middle of the patches and the minimum at the edge. We observed that the surface current flow reverses its direction for reverse polarity. So, it can be said that the designed 4x2 antenna array is linearly polarised. In addition, the simulation software CST automatically simulates the antenna for 0.5 W of power. Therefore, each antenna element is expected to have 0.0625 W of power. However, due to the power loss in each splitting section of the network the total power received by 1/8 element is 0.0525 W.

The S11 of the 4x2 microstrip patch antenna array is shown in Figure 3.12. The antenna array presents reflection coefficient values close to -33 dB, and it resonates at a desired 35 GHz center frequency.

The VSWR is shown in Figure 3.13. At 35 GHz frequency VSWR is 1.06. Lower VSWR indicates that antenna impedance and transmission lines are matched. Therefore, it can be claimed that the designed 4x2 antenna array is suitable for transferring high power.

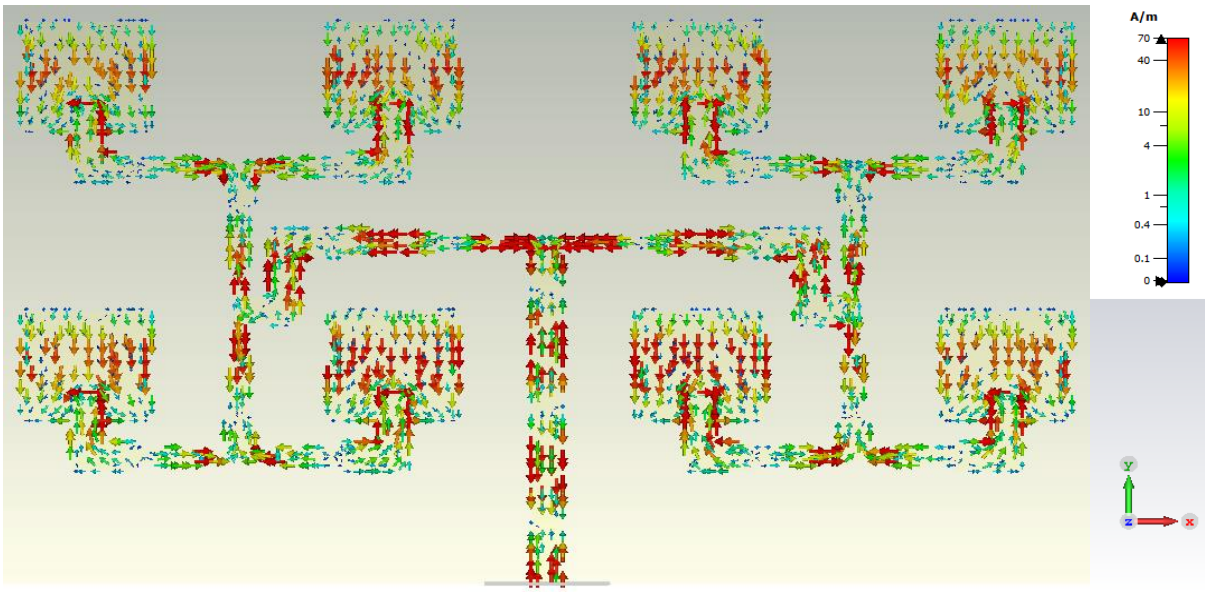

Figure 3.11 Surface current flow of 4x2 antenna array

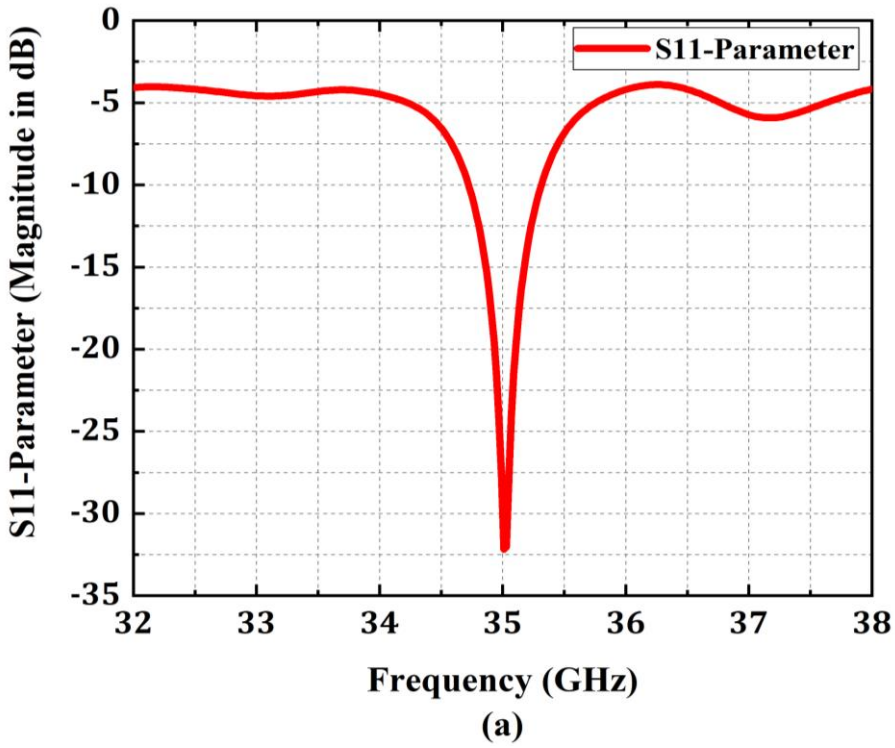

Figure 3.12 S11 of a 4x2 patch antenna array

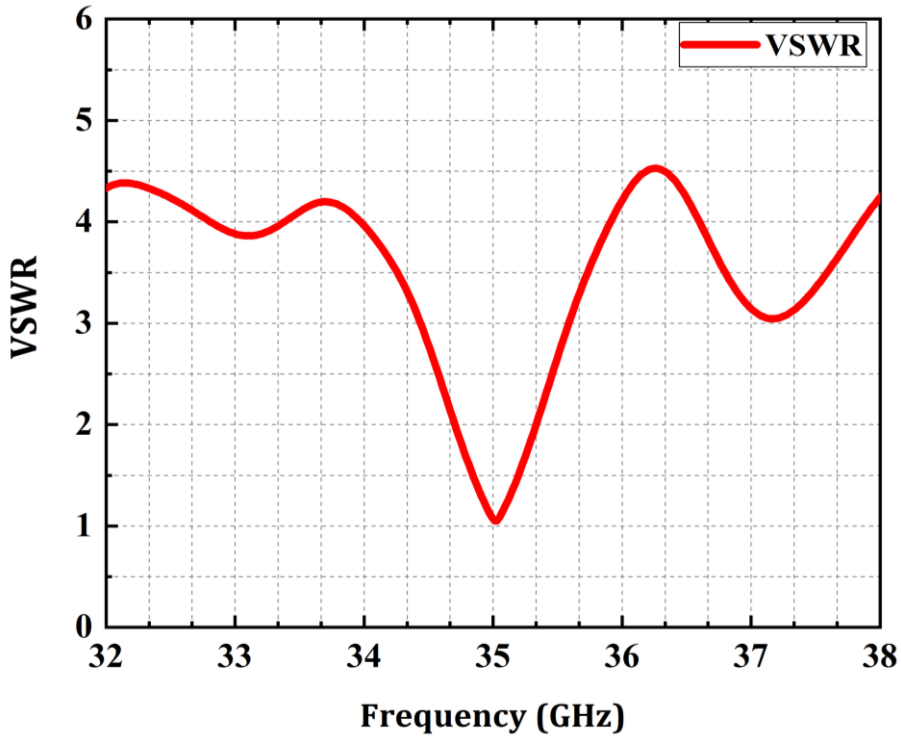

Figure 3.13 VSWR of the 4x2 antenna array

In this project, point-to-point microwave power transfer is used. Therefore, a highly directive, and the higher gain antenna is required for wireless power transmission with lower side lobes. With a directional antenna, the axis of the maximum gain and directivity is known as boresight. The 4x2 patch antenna array radiation pattern is shown in Figure 3.14. The intensity of the color corresponds to the energy level. The maximum energy is passing through the main lobe, and it has the highest gain and directivity. The antenna must have only one main lobe. Other lobes are considered side lobes. The size of the side lobes of the antenna for MPT must be smaller to reduce the side transmission which increases the noise level and affect the efficiency.

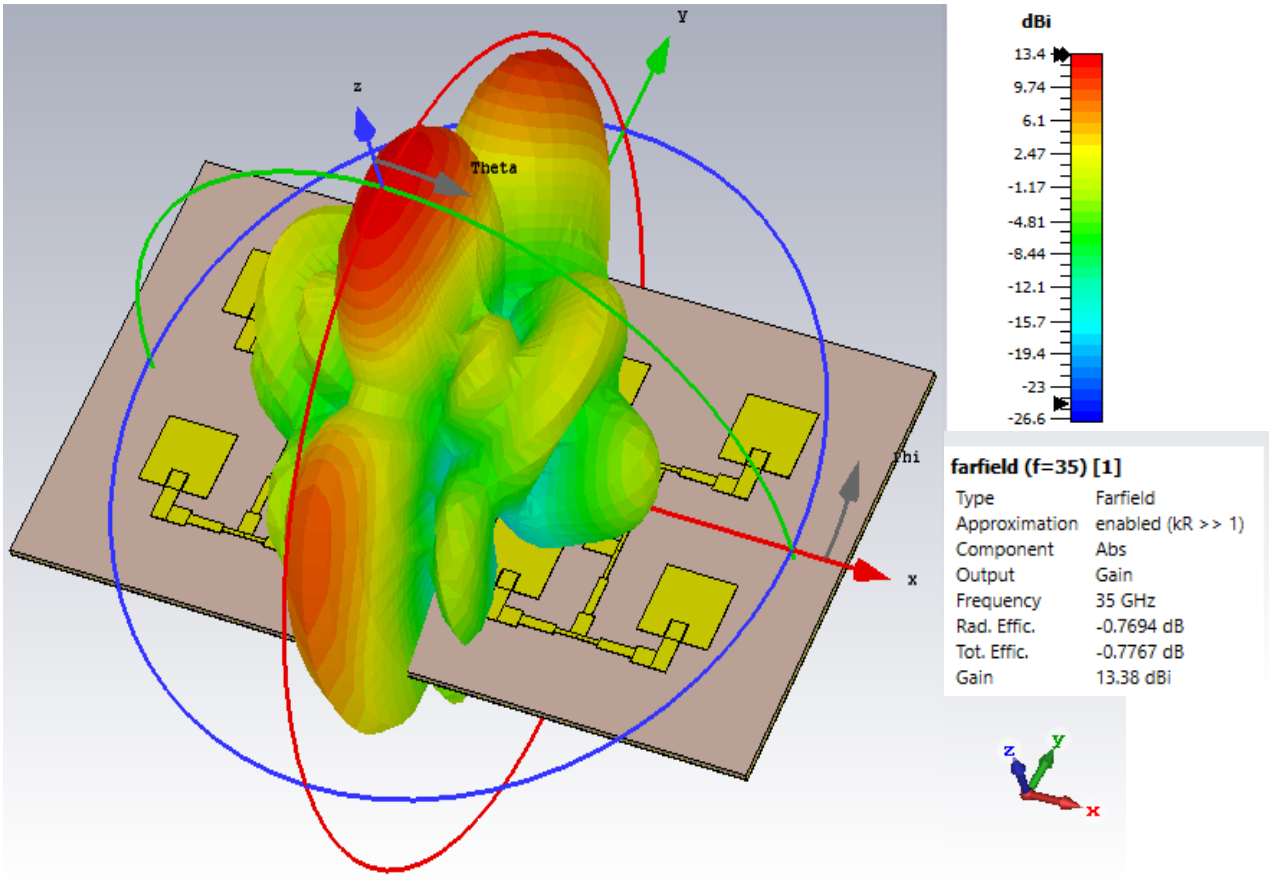

Figure 3.14 3D far-field radiation pattern of a 4x2 patch antenna array

The gain and directivity in E-Plane and H-Plane of the 4x2 patch antenna array are shown in Figure 3.15. The gain and directivity of the antenna array are 13.4 dBi and 14 dBi respectively. Since the side lobes are less than -11 dBi, we can claim that the designed 4x2 antenna array has satisfied the requirements for MPT.

The efficiency of the 4x2 patch antenna array is shown in Figure 3.16. It has an efficiency of more than 85%.

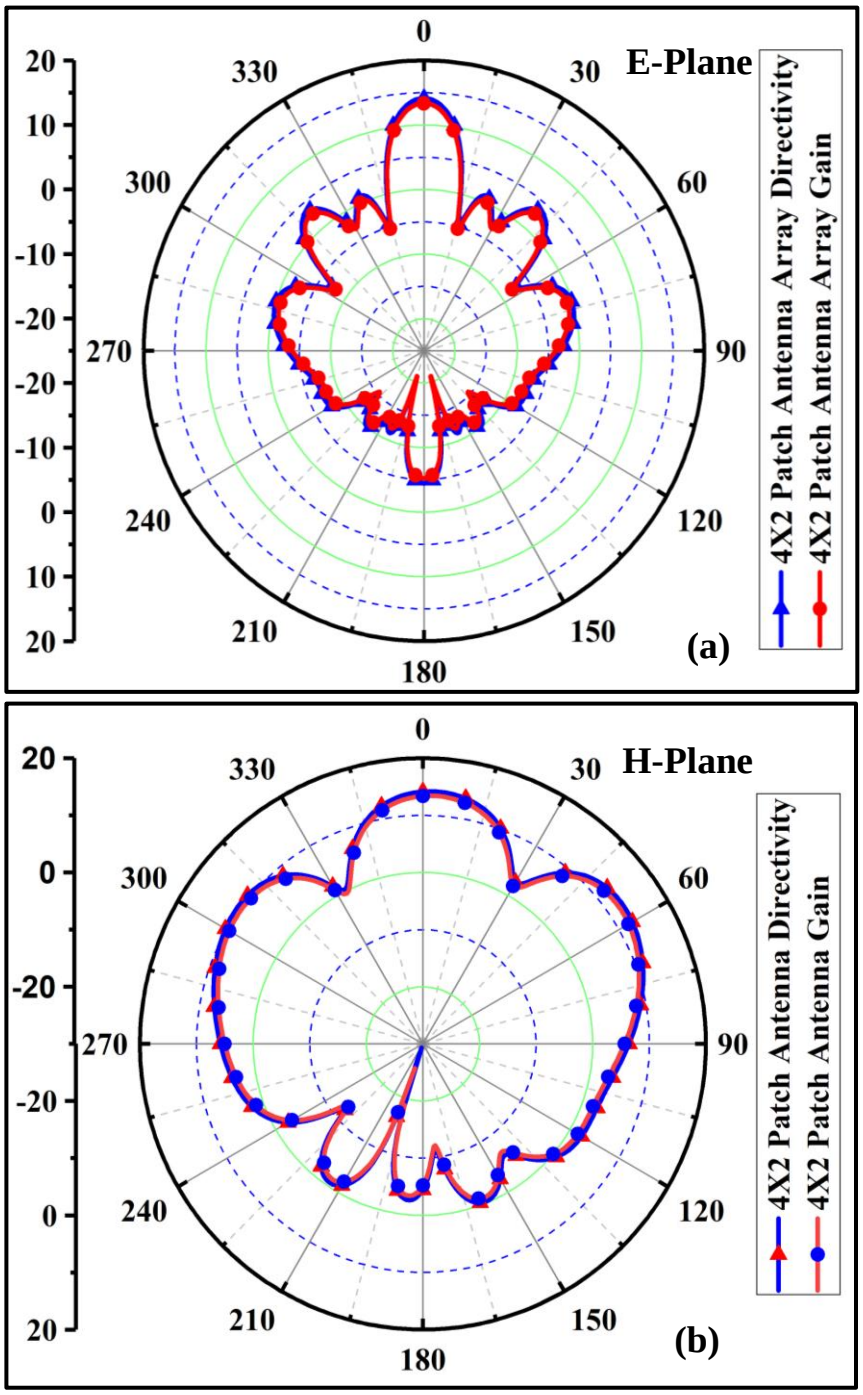

Figure 3.15 2D radiation pattern of 4x2 microstrip patch antenna array in dBi a) gain and directivity in E-Plane, b) gain and directivity in H-Plane

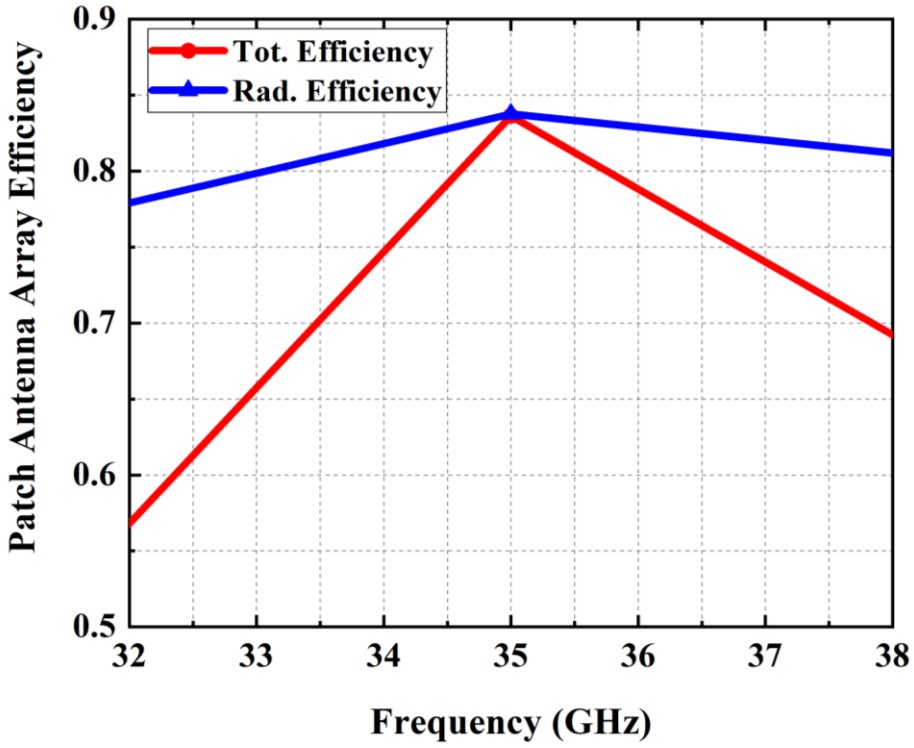

Figure 3.16 Efficiency of a 4x2 patch array

Conclusion:

A microstrip patch antenna has been selected as a transmitting device because of its radiation characteristics, ease of design, and low fabrication cost. In this chapter, we have presented the design and simulation of a single microstrip patch antenna and a patch antenna array. The simulation result of a single microstrip patch antenna shows a gain of 7.6 dBi and directivity of 8.15 dBi, which is suitable for MPT. However, for long-distance MPT the gain and the directivity need to be increased. Consequently, an array of the antenna can be implemented in order to improve the gain and the directivity of the patch antenna. Simulation results of a 4x2 patch antenna array show that it has a gain of 13.4 dBi and directivity of 14 dBi which is higher than the single antenna. The return loss of -33 dBi is also within an acceptable range. To sum up, for MPT array of an antenna can be utilized to make the transmitting system more directive towards the receiving system. More details of the 4x2 antenna array for MPT are presented in chapter 5. The design and optimization of the receiving system will be discussed in chapter 4.

CHAPTER 4 DESIGN AND OPTIMISATION OF A RECTIFIER CIRCUIT

In the UAV segment, a large rectenna array is required to collect the RF energy to convert it to usable DC power to feed the UAV engine. The rectenna is the combination of an antenna, a diode, a matching circuit, and a resistive load (R_L). A rectifier can have different topologies such as series, shunt, voltage doubler, and bridge rectifier. In this work, the selected frequency is 35 GHz, therefore a suitable Schottky diode is essential to design and optimize a high-efficiency rectifier. The Schottky diode is working as a rectifying component in the circuit. A commercial Schottky diode MA4E1317 is chosen for this project. This diode has a series resistance, Rs, of 4 Ω, a junction capacitance, $C_{j0,}$ of 0.02 pF, a breakdown voltage, V_{br} of 7 V, and diode turn-on voltage, V_f of 0.6 V. According to diode I-V characteristics, 1 mA of current is required to turn the diode on. An ideal diode has low Rs and C_{j0} with high $V_{br.}$

4.1 Design and optimization of series rectenna

A series rectenna contain a Schottky diode, a capacitor, and load resistance. The selected diode parameters are used to design, simulate, and optimize the series rectenna at 35 GHz in order to maximize the RF to DC conversion efficiency using the tool Advance Design System (ADS). A typical series rectenna topology is shown in Figure 2.8 (a). Harmonics balance (HB) simulator was used for the nonlinear circuit simulation because of its high accuracy. A 10 dBm input RF power was considered for the simulation. In the rectifier circuit, capacitor, C_1, acts as an output DC pass filter. The initial values of the capacitor and load resistance were assumed to be 100 pF and 50 Ω for the simulation.

RF to DC conversion efficiency (η) of the rectenna can be determined using the following equation:

$$P_{out} = \frac{V_{out}^2}{R_L} \tag{14}$$

$$\eta = \frac{V_{out}^2}{P_{in}\, R_L}\, x\, 100\% \tag{15}$$

where, P_{out} is the output DC power, V_{out} is the output DC voltage, R_L is the load resistance, and P_{in} is the input RF power.

4.2 Series rectenna simulation result

Figure 4.1 shows the Output DC voltage of the series rectenna. At 10 dBm input power, the output voltage of 0.26 V is achieved at 35 GHz across a 50 Ω load resistance.

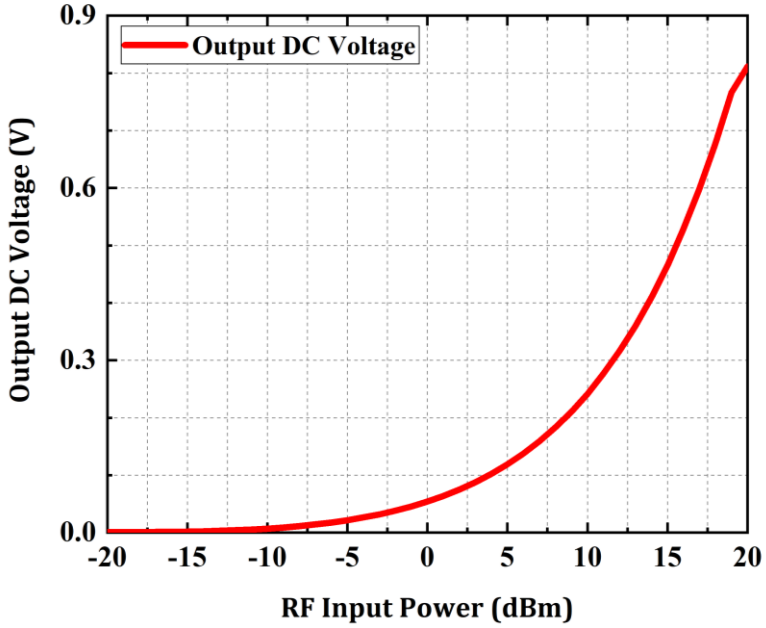

Figure 4.1 Output DC voltage of series rectenna

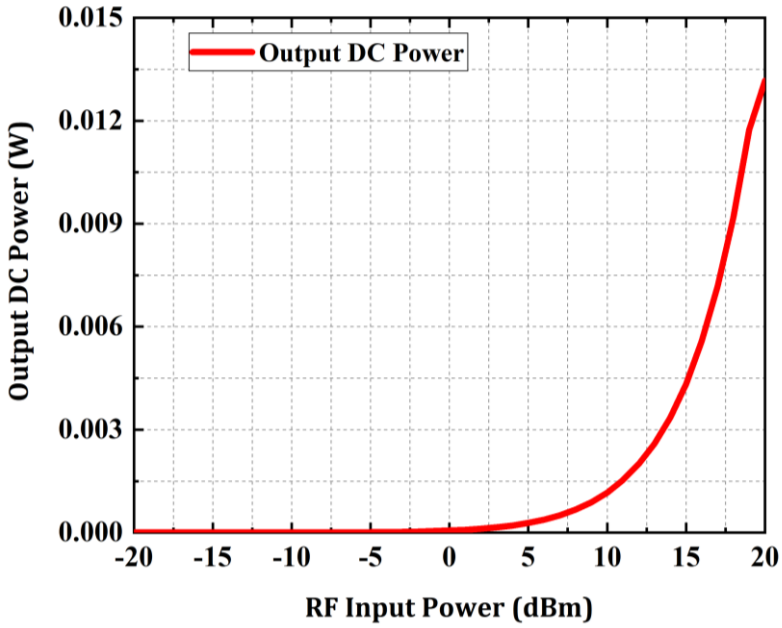

Figure 4.2 Output DC power of series rectenna

Figure 4.2 and Figure 4.3 plot the output DC power and the conversion efficiency of the series rectenna. At 10 dBm, the output power of 0.0014 W and an efficiency of 14 % are obtained. Also, at 18 dBm input power, the efficiency hits a maximum of 18 %. It is seen that at 20 dBm input power the efficiency of the rectenna dropped sharply. The reason behind this behavior is that the selected diode MA4E1317 has reached its reverse breakdown voltage.

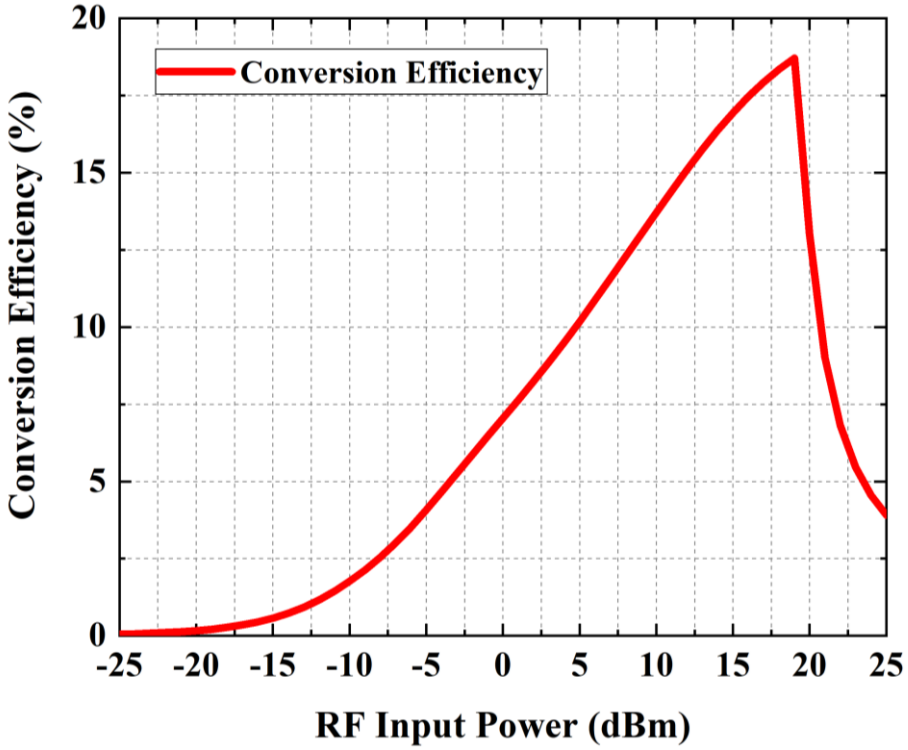

Figure 4.3 Efficiency of series rectenna

It is observed from the above simulation result that the rectenna exhibits poor performance. To improve the performance, the rectenna parameters need to be optimized. A feature offered by ADS called parametric tuning was adopted to get optimum values of the rectenna component. The parametric tuning process is shown in Figure 4.4, where the load resistance (R_L) can be tuned to get the highest performance of the rectenna at the desired input power. Figure 4.5 shows the maximum output power obtained for a 650 Ω load resistance. The optimized values of the load resistor and capacitor are 650 Ω and 100 pF, respectively. After parametric tuning, the optimized value of R_L is inserted in the ADS rectenna circuit for further simulations.

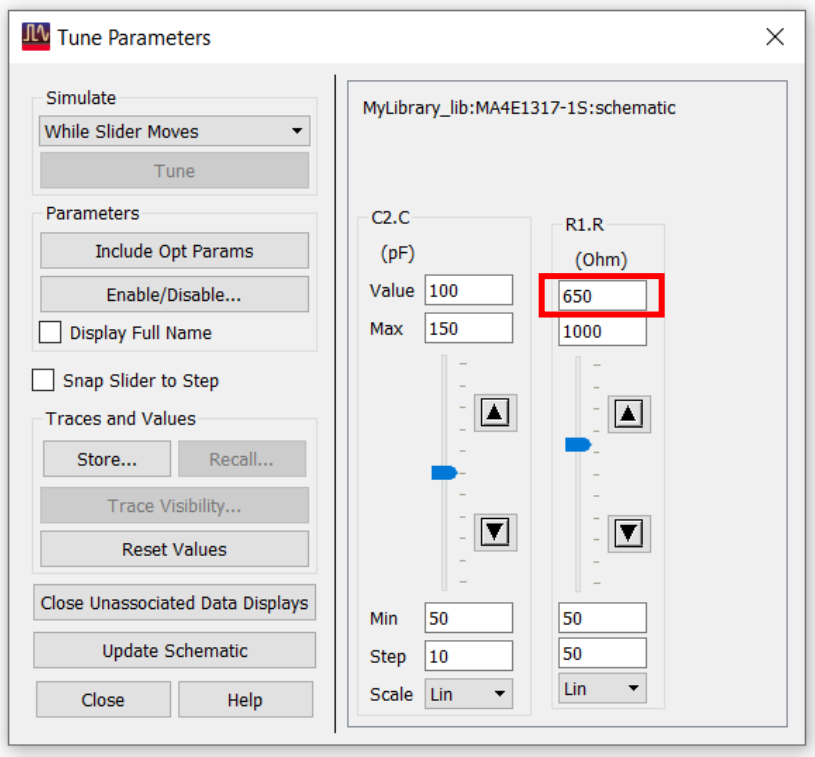

Figure 4.4 ADS Parametric tuning process

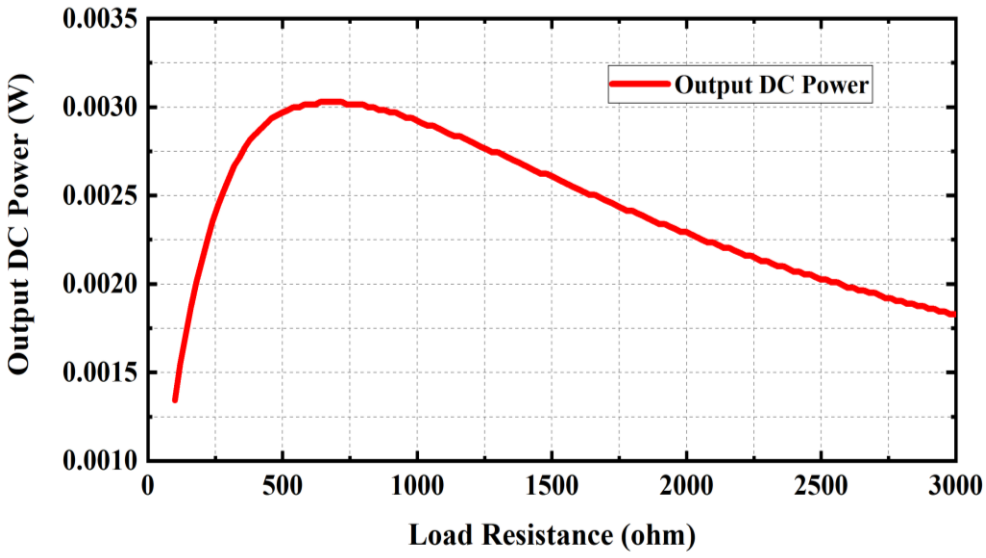

Figure 4.5 Output power variation with different load resistance for series rectenna when the input power is 10 dBm (10 mW)

Figure 4.6 shows the improved result of the output voltage after parametric tuning. Note that the simultation does not inlcude the effect of impedance matching between the input source and the diode. An output voltage of 1.39 V is achieved at 10 dBm of input power when the load resistance is 650 Ω.

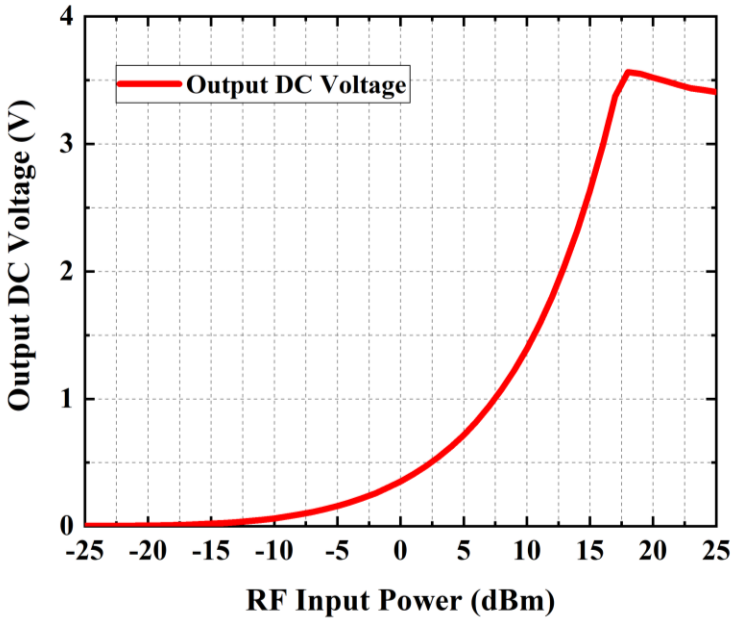

Figure 4.6 Output voltage of series rectenna after R_L tuning

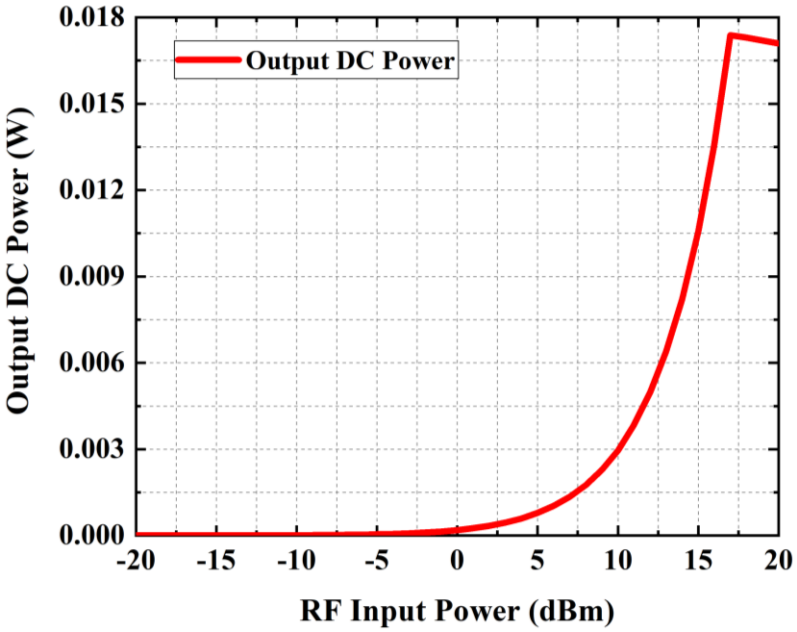

Figure 4.7 Output power of series rectenna after R_L tuning

Figure 4.7 shows the output power of 0.003 W achieved after parametric tuning. Figure 4.8 presents the comparison of the efficiency with and without R_L tuning. The efficiency of the series rectenna is improved sharply up to 30 % at 10 dBm input power, whereas the maximum efficiency of 35 % is obtained at 17 dBm input power.

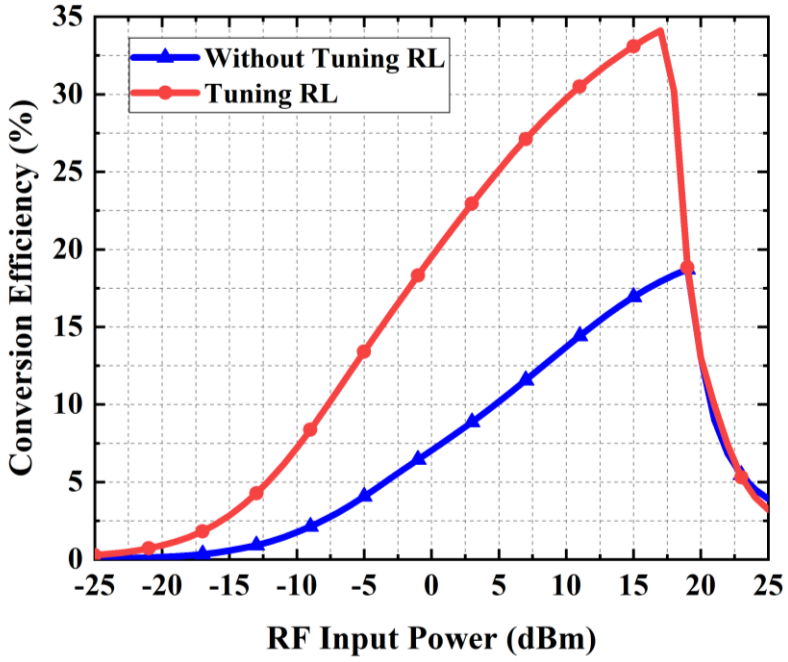

Figure 4.8 Efficiency of series rectenna with and without tuning RL

4.2 Design of Voltage doubler rectenna and discussion of simulation results

The voltage doubler (VD) rectenna consists of two diodes and two capacitors. A typical VD rectenna configuration is shown in Figure 2.8. (c). The simulation of the VD rectenna is done similarly to the simulation of the series rectenna. In a series rectenna, one diode and one capacitor were used. On the other hand, for the VD rectenna, we use two diodes and two capacitors in the circuit. The other parameters were left the same. A simulation with the load resistor as a parametric variable yields a maximum output power for a load resistor of 1500 Ω at 10 dBm input power.

The output voltage and the output power of the VD rectenna are shown in Figure 4.9 and Figure 4.10 respectively, as a function of the RF input power. An output voltage of 3.1 V and an output power of 0.0066 W are obtained for a load resistor of 1500 Ω.

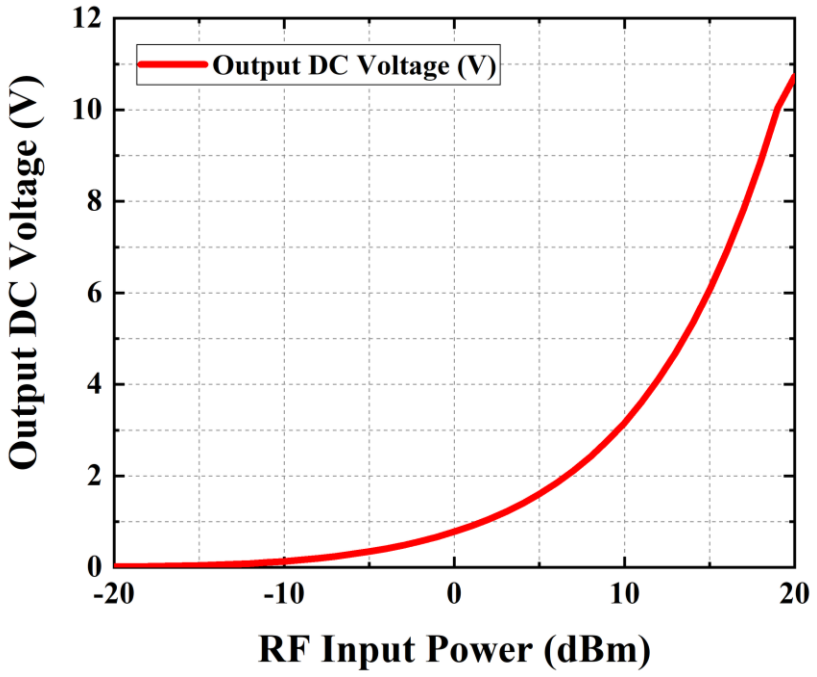

Figure 4.9 Output voltage of VD rectenna

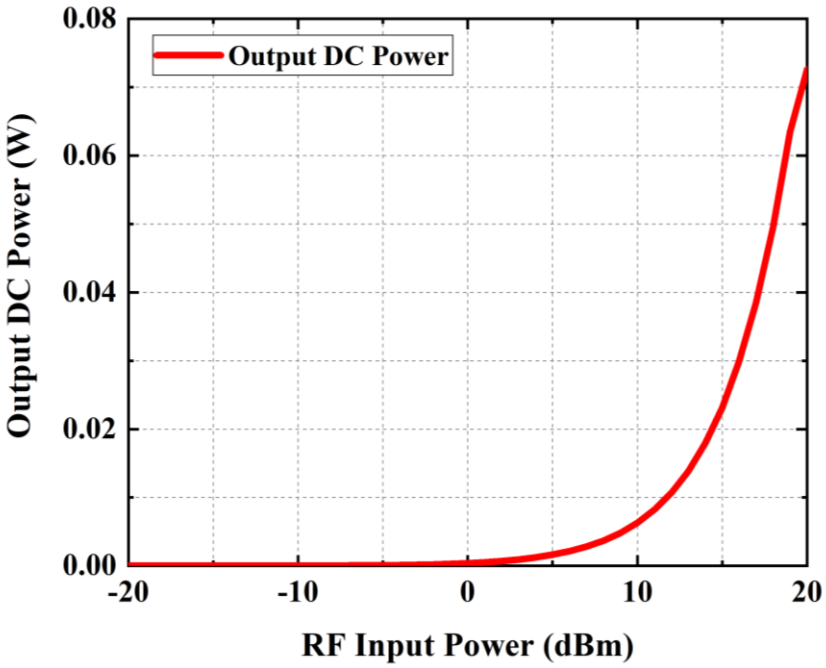

Figure 4.10 Output power of VD rectenna

The efficiency comparison of series and VD rectenna is shown in Figure 4.11. At the desired 10 dBm input power, the efficiency of series and VD rectenna are 30 % and 66 % respectively. The maximum efficiency of both rectennas is obtained at 17 dBm and 19 dBm RF input power, respectively. From this comparison, it is clearly visible that the VD rectenna shows higher efficiency than the series rectenna.

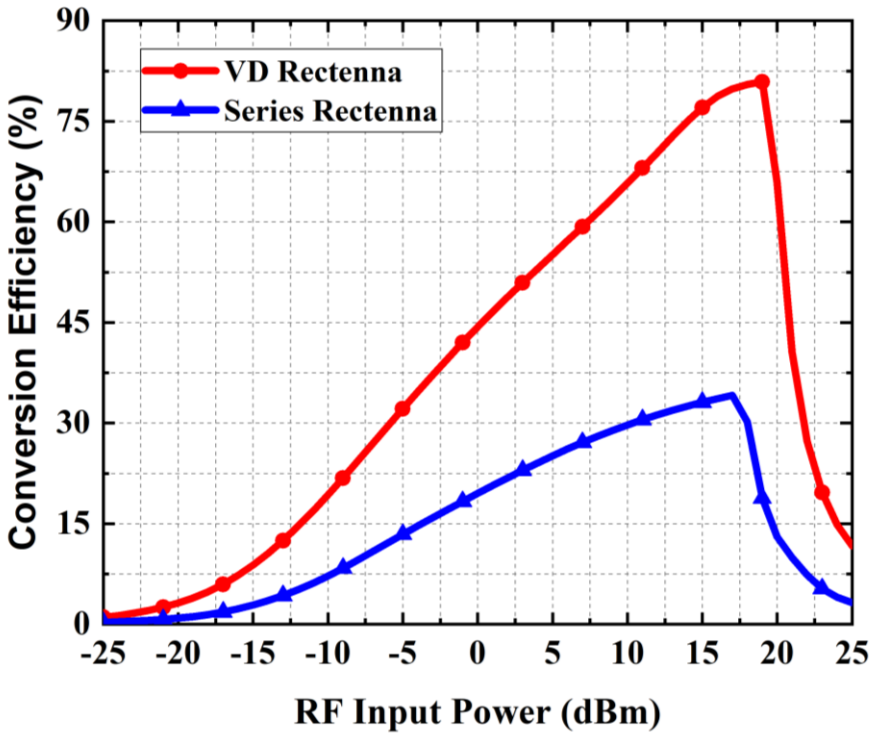

Figure 4.11 Efficiency comparison of series and VD rectenna

Conclusion:

A simple rectenna system is designed and optimized to convert the RF energy to the usable DC power to feed the UAVs electrical motor. The series, shunt, and voltage doubler rectenna are an example of some rectennas. In this work, we have simulated and optimized the series and voltage doubler rectenna. To improve the rectenna efficiency, parametric tuning of R_L is applied. Hence, the variation of R_L improves the rectenna performance significantly. The VD rectenna shows a higher performance than the series rectenna, therefore, it is employed for this project. In the next chapter, we will present the whole concept of the project.

CHAPTER 5 DESIGN AND ANALYSIS OF A 35 GHZ RECTENNA SYSTEM FOR WIRELESS POWER TRANSFER TO AN UNMANNED AERIAL VEHICLE

5.1 Abstract

In this article, the concept of a 22-kW microwave-powered unmanned aerial vehicle is presented. Its system architecture is analyzed and modeled for wirelessly transferring microwave power to the flying UAVs. The microwave system transmitting power at a 35 GHz frequency is found suitable for low-cost and compact architectures. The size of the transmitting and receiving systems are optimized to 108 m^2, and 90 m^2, respectively. A linearly polarized 4x2 rectangular microstrip patch antenna array has been designed and simulated to obtain a high gain, a high directivity, and a high efficiency in order to satisfy the power transfer requirements. The numerically simulated gain, directivity, and efficiency of the proposed patch antenna array are 13.4 dBi, 14 dBi, and 85%, respectively. Finally, a rectifying system (rectenna) is optimized using the Agilent advanced design system (ADS) software as a microwave power receiving system. The proposed rectenna at the core of the system has an efficiency profile of more than 80% for an RF input power range of 9 to 18 dBm. Moreover, RF to DC conversion efficiency and DC output voltage of the proposed rectenna are 80% and 3.5 V respectively, for a 10 dBm input power at 35 GHz with a load of 1500 Ω.

5.2 Introduction

Unmanned aircraft and drones are employed for applications related to intelligence, surveillance, and reconnaissance (ISR) gathering that are not putting human life in danger [35]-[37]. Unmanned air vehicles (UAVs) using advanced technologies such as Global Positioning System (GPS) and wireless communications offer new business opportunities [38]. Nowadays, UAVs are widely used in fields such as providing coverage, search and rescue missions, scientific research, disaster monitoring, crime prevention, radiation observation, and so on. They can act as a platform for telecommunication services, i.e., mobile radio or TV broadcasting in rural locations at the regional level [39]-[42].

Electric aircraft has drawn attention as a possible candidate for UAVs applications. They have several advantages over the conventional gasoline-based airplane. An electric aircraft can use an electric motor that can be 95% efficient instead of the 18%-23% efficiency of regular combustion engines. It is more reliable, light in weight, safe, low-cost, and quitter. Finally, it has zero carbon emissions, which makes them environmentally friendly.

The concept of wireless power transmission (WPT) via microwave is not a new research project are conducted worldwide for cost-effective and highly efficient system design, which has multiple applications in different areas. In the 1960s W.C Brown [43]-[44] initiated a microwave power transmission (MPT) research program where significant progress was made [4]-[5], [30]. These previous attempts report on an MPT system consisting of two sections: - A Transmitting antenna (Tx), and a receiving antenna or rectifying antenna (Rx). In the Tx section, DC power is converted to microwave power by a microwave oscillator i.e., magnetron, klystron. The microwave power radiates to the free space towards the Rx. The Rx section receives microwave power and reverts it back to DC voltage. In 1963 W.C. Brown conducted an experiment where he could capture 100 W of RF power with an output efficiency of 26% at 2.45 GHz from a distance of 5.48 m [6], [30]. He then investigated the possibility of feeding wireless power to a flying helicopter. Shortly after, he and his team developed a 55% efficient rectifying antenna, and consequently, his team successfully demonstrated the first microwave-powered helicopter that reaches an altitude of fifty feet [7]. By 1975, W.C Brown and his team, while working on a NASA project, built the largest WPT made of a 26 m diameter parabolic antenna transmitting to a rectenna array size of 3.4 m x 7.2 m. The distance between the Tx antenna and Rx rectenna was 1 mile and The Rx side receive 30 kW of DC power with an efficiency of 82.5% [8]. In 1987, SHARP Canada conducted an MPT project that aimed at demonstrating a fuel-free airplane. They transmitted a 10-kW microwave signal at 2.45 GHz to an aircraft at a flying altitude of 150 m. [9]. Many Japanese researchers have investigated and carried out fuel-free airplane MPT research in the 1980s using 2.45 GHz RF carrier [10]-[13]. Some significant experiments including MINIX [10] and ISY-METS [11] were executed by Hiroshi Matsumoto's team in 1983 and 1993, respectively. In MINIX and ISY-METS, a magnetron microwave transmitter generating an 800 W output at 2.45 GHz was used.

Many researchers reported different antennas employed in the design of rectennas such as microstrip patch, co-planer patch, dipole, spiral antennas, and so on [45]-[49]. To receive more power at the rectenna side, a high gain antenna is preferable for WPT applications. A single antenna element is not compatible with WPT applications because it has low gain. To overcome this problem, using an array of micro-antennas is an interesting solution since it can supply more RF power [48]. Many high-frequency rectenna arrays have been reported, specifically below 10 GHz i.e., 2.45 GHz and 5.8 GHz [50]-[51]. On the other hand, only a few millimeter-wave (24 GHz, 35 GHz, and 94 GHz) rectenna designs have been reported so far [52]-[56]. Most of them focused on wireless energy harvesting which is suitable for low-power applications.

The obvious advantages of millimeter-wave rectennas over microwave rectennas are compact antenna size and higher overall system efficiency for long-distance transmission [48]. Very limited attention has been given to millimeter-wave frequencies WPT to UAVs systems. The potential offered by the importance of a millimeter-wave rectenna operating at 35 GHz has motivated the present work.

This paper presents a 22-kW microwave power transfer to a UAV flying at a distance of 10 km. The key technologies that comprise this system are analyzed, estimated, and designed. All the results presented in this work are numerically simulated. The remaining of this paper is organized as follows: Section II describes an efficient overall system architecture based on MPT working at 35 GHz suitable for a compact system that could be implemented at a low cost. The MPT system's key components, i.e., Tx, Rx, and beam efficiency parameters, are optimized in Section III and Section IV, respectively. Section V describes a 4x2 rectangular patch antenna array considering a low cost and a high production capacity. In Section VI, an efficient rectifying system is conceived using the Agilent advanced design system (ADS). Conclusions drawn from this work are presented in Section VII.

5.3 Remotely Powered Unmanned Air Vehicles

A key problem with conventional UAV is the limited amount of energy that can be stored onboard [57]-[58]. In order to increase the mission roaming range, the amount of energy stored needs to be increased at the expense of increased battery weight. One way to counter this problem is by supplying power remotely during the flight enabling recharge during the mission. Also, using microwave energy transmission allows the transfer over several kilometers and extends at the same time the roaming range. The most significant advantage of microwave power transmission technology is the capability for long-distance non-contact power transmission [30]. Wireless power transfer using microwaves is now a mature technology, and it can be utilized for efficient remotely powered UAV systems.

5.3.1 Proposed System Architecture

Pioneer works in that field was initiated many years ago by SHARP [9] where high altitude microwave powered airplane was considered as platforms for relaying telecommunication signals. The idea includes a large ground antenna transferring microwave power to fuel-free airplanes at an altitude of 21 km [6]-[13]. This microwave power captured by the rectenna which is mounted under the airplane is converted into usable DC power to run the electric motor. Sharp has done both theoretical and experimental analysis in this project and the ISM frequency of 2.45 GHz was used [9]. Here, we proposed a microwave-powered UAV; at a transmitting distance of 10 km from the ground station. The transmitting distance can be varied according to the power demand.

The proposed system architecture is shown in Figure 5.1. In this project, the MGM Compro electric propulsion system is adopted using a brushless DC motor with an embedded controller. It has maximum ratings in continuous power, voltage, torque, and revolution of 22 kW, 120 V, 100 Nm, and 8000 RPM, respectively. The UAVs can fly to the surveillance or monitoring area beyond the WPT range using its installed battery power of 120 V and 200 Ah. When the battery power goes down below a certain threshold, the UAV flies back within the WPT range (rechargeable area) for recharging. Several UAVs could use the same WPT ground station [34].

The ground station Tx antenna transmits power to the Rx rectenna mounted under the UAV while flying in the recharging area.

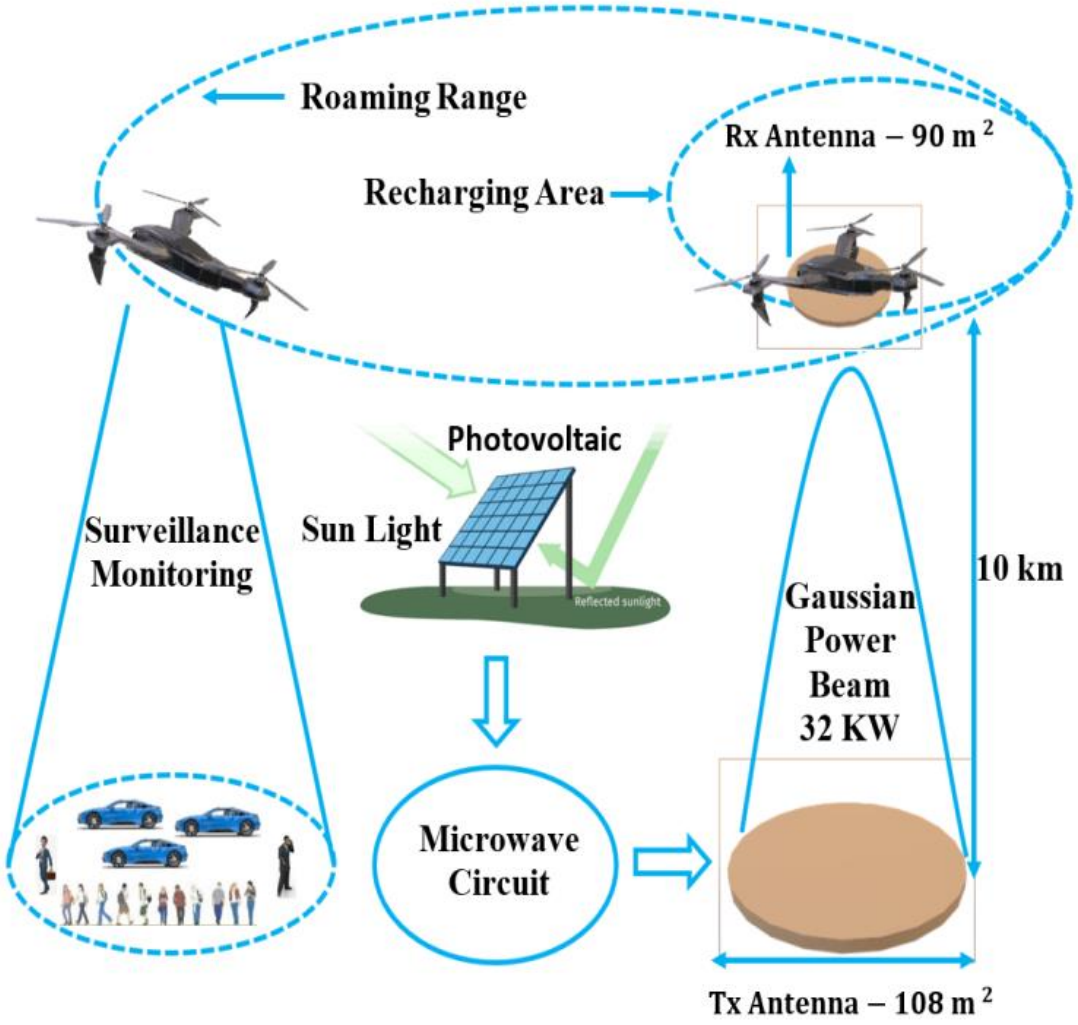

Figure 5.1 Proposed system architecture

The beam direction of the transmitted signal is determined by a pilot signal tracking method [59]. A large Tx and Rx antenna system is required with higher transmission efficiency for the successful MPT. Therefore, phase synchronization becomes an important issue among the unit. Hence, beam steering can be applied in each unit to solve the phase error. When the UAV changes its direction then the direction of the main lobe of the radiation pattern is changed in the Tx system in order to follow the UAV. The wingspan and length of the UAV are 10 m and 9 m, respectively. Therefore,

the maximum antenna area on the UAV is 90 m^2. Given this antenna size, a maximum power, P_T, of 27 kW can be transmitted according to the equation,

$$P_T = P_d * A_{eff} \quad , \qquad (16)$$

where P_d is the beam power density safety limit for microwave on earth atmosphere set to 300 W/m^2 [15], and A_{eff} is the antenna effective area. The impact of the Rx antenna on the UAV's aerodynamics is not considered here as it is beyond the scope of this paper. However, a major redesign of the aircraft could be required.

5.3.2 Selection of the 35 GHz Transmission Frequency

In point-to-point microwave power transfer, the first step is selecting a suitable frequency in the microwave band. Hence**,** industrial, scientific, and medical (ISM) frequency bands 2.45 GHz, 5.8 GHz, 24.5 GHz are recommended for MPTs [16] - [17]. On the other hand, the Tx antenna and Rx rectenna dimension increase with the distance. As a result, for long-distance power transmission, the dimensions of the transmitter and the receiver would be very large and costly for the ISM frequency bands. To decrease the antenna dimensions and to lower the cost, higher frequencies, i.e., 35 GHz, 61 GHz, and 94 GHz, are preferable. Among them, the 35 GHz frequency is chosen for MPT in this research. This frequency window decreases the Tx antenna and the Rx rectenna dimension while keeping a transmission efficiency in the order of more than 90%. [60]. Atmospheric absorption loss is also low at this frequency window [61].

5.4 Microwave Wireless Power Transmission

There are many key issues for deploying microwave-powered UAV. Wireless power transfer for a distance of more than 10 km is a challenging task; Gaussian beam forming technique must be used for efficient transmission [28] - [29]. A 32-kW microwave UAV power flow diagram is shown in Figure 5.2. In this proposed system, photovoltaic arrays transform solar power into electrical power

(DC). The high voltage DC power is then supplied to a microwave generator, i.e., a magnetron that delivers the transferred microwave power [14]. The beam formation is achievable using a phased array antenna [62] - [63]. The receiving microwave antenna connected with the rectifier changes the high-frequency microwave power back to electrical DC power [64].

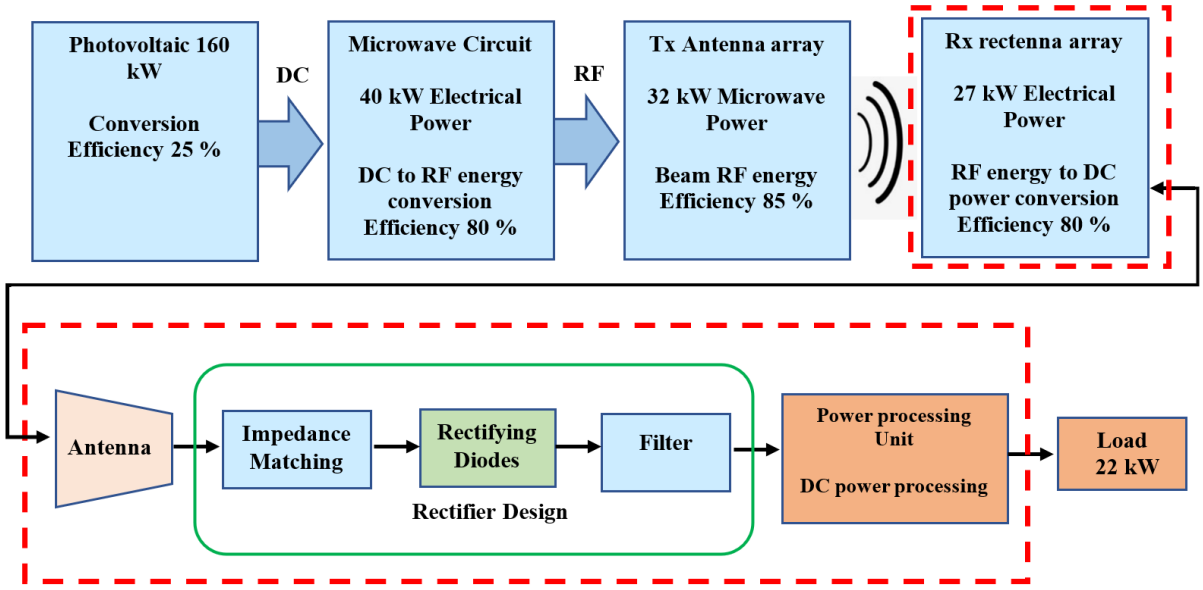

Figure 5.2 Microwave power transmission system block diagram

In this model, a solar array is required for collecting 160 kW of solar insolation at a power density of 1000 W/m^2 and produces 40 kW DC power (25% conversion efficiency). Considering a DC to the microwave conversion efficiency of 80% [65]-[66], 32 kW microwave power would be transmitted from the ground Tx antenna. Here, our target is to design a suitable rectenna to power the 22-kW electrical propeller onboard the UAV.

5.4.1 Microwave Wireless Power Transmission Equations

Equation (9) shows the Friis relationship for transmitted signal within the far-field Fraunhofer zone,

$$P_R = P_T G_T \left(\frac{\lambda}{4\pi D}\right)^2 G_R = \frac{A_t A_r}{\lambda^2 D^2} P_T \quad , \qquad (9)$$

where P_T and P_R are transmitted and received power, G_T and G_R are the gain and, A_t and A_r are the effective surface area of the Tx antenna and Rx rectenna, respectively. D is the separation between the Tx antenna and the Rx rectenna and λ is the transmitted wavelength. This transmission equation is not applicable for long-distance, point-to-point power transfer because, in the Fraunhofer zone, the beam power density decreases as the square of the distance between the Tx and the Rx antennas. As a consequence, full dispersion occurs [16]. In order to obtain efficient power at the receiving antenna, a near field zone needs to be considered, where the beam power density remains constant with respect to distance, and the dispersion is also negligible [16], [30]. G. Goubau and W.C. Brown showed the relationship between wireless beam power transfer efficiency and beam power transmission parameter for near field condition in equations (12) and (13), [30]- [31],

$$\frac{A_t A_r}{\lambda^2 D^2} = \tau^2 \quad , \qquad (12)$$

where, τ is the beam transmission parameter.

Then, the beam transmission efficiency is given by:

$$\eta_{beam} = 1 - e^{-\tau^2} \quad . \qquad (13)$$

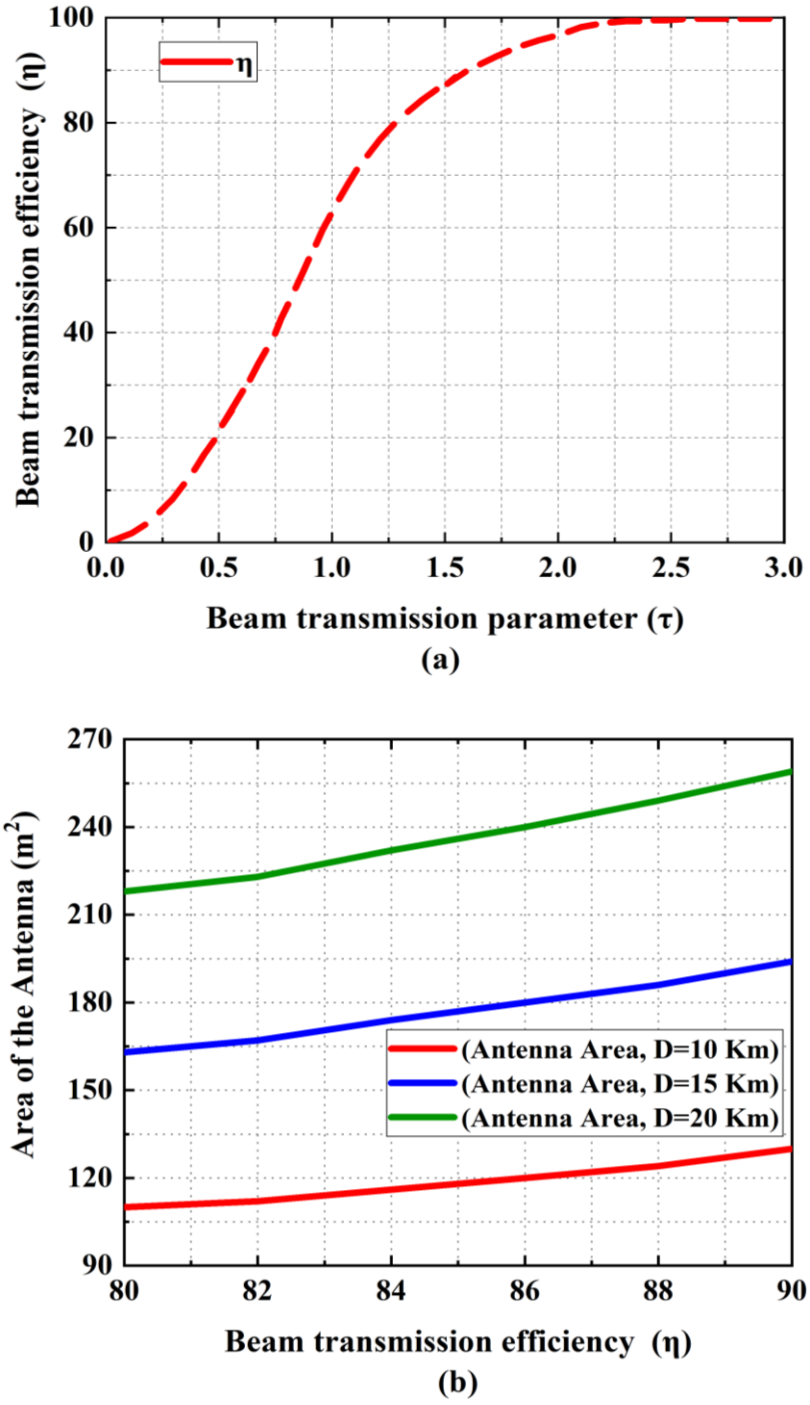

Figure 5.3 Variation of beam transmission efficiency (η) and beam transmission parameter (τ) across the transmitting antenna's aperture a) η as a function of the τ [16], [30], b) Tx antenna aperture variation as a function of η

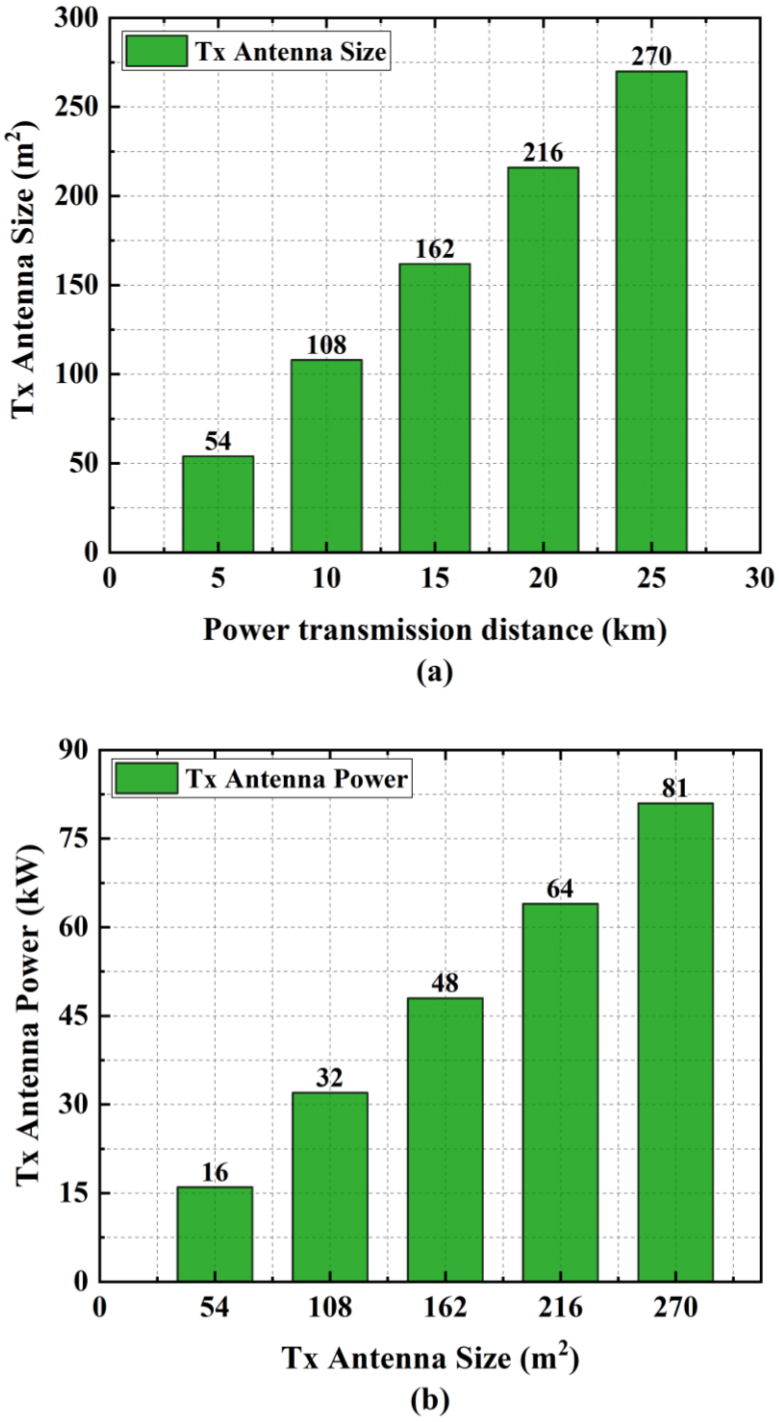

Figure 5.4 Tx area calculation considering a beam transmission efficiency of 80% a) Area of the Tx antenna with different power transmission distances, b) Maximum Power Transmission Capacity of the Tx antenna with respect to the area considering an Tx antenna

Figure 5.3 (a) shows the beam transmission efficiency as a function of the beam transmission parameter. According to Figure 5.3 (a), a theoretical 100% beam transmission efficiency is achievable at a transmission parameter of 2.5 [16], [28-32]. Figure 5.3 (b) shows the Tx antenna aperture variation as a function of the beam efficiency and the transmission distance, as obtained from equations 12 and 13. As expected, a larger antenna area is required, for long-distance power transmission and higher beam transfer efficiency assuming $A_r \cong A_t$.

5.5 Tx Antenna Area Calculation for Different Power Level

Knowing the Rx antenna dimension, it is then possible to calculate the power transmission capacity of the Tx antenna and the power receiving capacity of the Rx rectenna using equation (16). The first area of the Tx antenna needs to be calculated using equations (12) and (13) and considering a 10 km transmission distance at 35 GHz signal frequency. In that case, if we consider a reasonable beam transmission efficiency of 80%, we obtain $\tau = 1.26$ which allows us to extract the required antennas' area ($A_r \cong A_t$). Using the same calculation method as the one used of the Tx antenna size, different power transmission distances are shown in Figure 5.4 (a). For the desired 10 km power transmission distance $A_r \cong A_t = 108\, m^2$ is found, which is the minimum size required to maintain near-field conditions. Tx antenna power capacity variation with the size is given in Figure 5.4 (b); it can be noticed here that an antenna size of $108\, m^2$ is able to transmit 32 kW of power according to equation (16).

Now using equation (16), it is possible to calculate the maximum power transmission capacity of the Tx antenna. For instance, when the Tx antenna area is 108 m^2 and the beam power density is 300 W/m^2 [15], given the safety and security limits then the maximum power transmission capacity of the Tx antenna is 32 kW. If the area of the antenna increases, then it can transmit more power and more distance as well, as shown in Figure 5.4 (b). The area of the selected UAV is 90 m^2 and a rectenna of the same size can receive 27 kW RF power and convert it to usable DC power to feed the electric motor of the propeller.

A comparison with previous MPT work is presented in Table 5.1. With the advancement in microwave technology, the operating frequency can be increased for a cost-effective and highly efficient MPT system.

Table 5.1 Comparison of the previous MPT for various frequencies

Source- agency	Frequency (GHz)	Tx / Rx diameter (m)		Transmission power (kW)	Transmission distance (m)	Received power (kW)
Raytheon's Spencer Laboratory-1964 [7]	2.45	3	0.65	3-5	15	0.28
NASA-1975 [8]	2.45	26	5.6	320	1550	34
SHARP-1987 [9]	2.45	85	30	500-1000	21000	35
SHARP-1987 [9]	2.45	4.5	1	10	150	1
Kansai Electric Power co., 1994 [14]	2.45	3	3.8	5	42	0.75
NICT-1995 [57]	2.45	3	3.4	5	1.9	3
JAXA-2001 [15]	5.8	1000	3400	1.3×10^6	36×10^6	1.1×10^6
IHI Aerospace Co., 2015 [58]	5.8	2	0.8	10	58	1
KAIST 2018 [88]	2.45	1	0.5	0.25	1	0.0125
Sichuan University 2019 [89]	5.8	1	1	0.5	10	0.041
This Work	**35**	**11.7**	**10.7**	**32**	**10000**	**27**

5.6 Design & Simulation of Microstrip Patch Antenna Array

A high gain and high directivity antenna is required for MPT applications. Moreover, an array of antennas has more gain and directivity compared to a single antenna. Therefore, an array of patch antennas is selected for the project. Patch antennas have excellent radiation characteristics and are easier to design and fabricate. In addition, they are light in weight, compact, have a low fabrication cost, and have small dimensions.

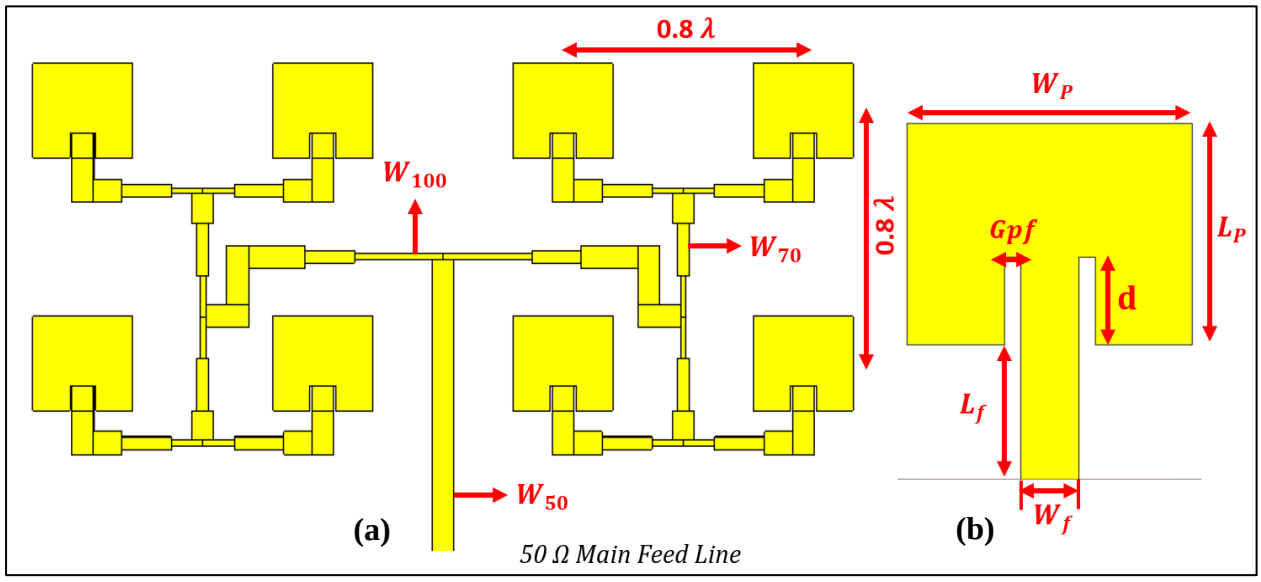

Figure 5.5 Illustration of antenna elements a) with 0.8 λ horizontal and 0.8 λ vertical spacing in a 4x2 patch antenna array with corporate feed, b) Unit element antenna parameters

5.6.1 4x2 Patch Antenna Array Design

The geometry of the proposed 4x2 patch antenna array is shown in Figure 5.5. The proposed antenna is designed on an RT-Duroid substrate having a thickness of 0.254 mm, a dielectric constant of 2.2, and a loss tangent of 0.0004 to 0.0009. Copper is selected as the top and bottom conductor layers because of its low cost and high conductivity. The copper thickness is 0.0035 mm. The bottom conductor can work either as an RF ground or a reflection plane. The widths of 50 Ω (W_{50}), 70.71 Ω ($W_{70.71}$) and 100 Ω (W_{100}) transmission lines are 0.8 mm, 0.45 mm, and 0.25 mm,

respectively. And the single element antenna parameters are, $W_P - 3.4\,mm$, $L_P - 2.7\,mm$, $W_f - 0.8\,mm$, $L_f - 1.6\,mm$, $d - 1.07\,mm$ and $Gpf - 0.1\,mm$.

The design and simulation of the microstrip patch antenna array are carried out using the corporate feed network since the incident power can be distributed equally to each antenna element from a single power port. The 4x2 microstrip patch antenna arrays are designed and optimized with the software tool CST Studio Suite.

5.6.2 Results & Discussion

At 35 GHz, the surface current flow of a 4x2 patch antenna array is shown in Figure 5.6. The designed antenna is linearly polarized and found suitable for point-to-point power transfer. The return loss of the designed patch antenna array is shown in Figure 5.7 (a). This antenna resonates well at a desired 35 GHz center frequency with a reflection coefficient value of -33 dB. The bandwidth of the antenna at -10 dB is 0.6 GHz. The ratio of maximum and a minimum standing wave is called VSWR. Figure 5.7 (b) shows a VSWR of 1.06 at the center frequency of 35 GHz. Hence, the designed 4x2 patch antenna array can transfer high power.

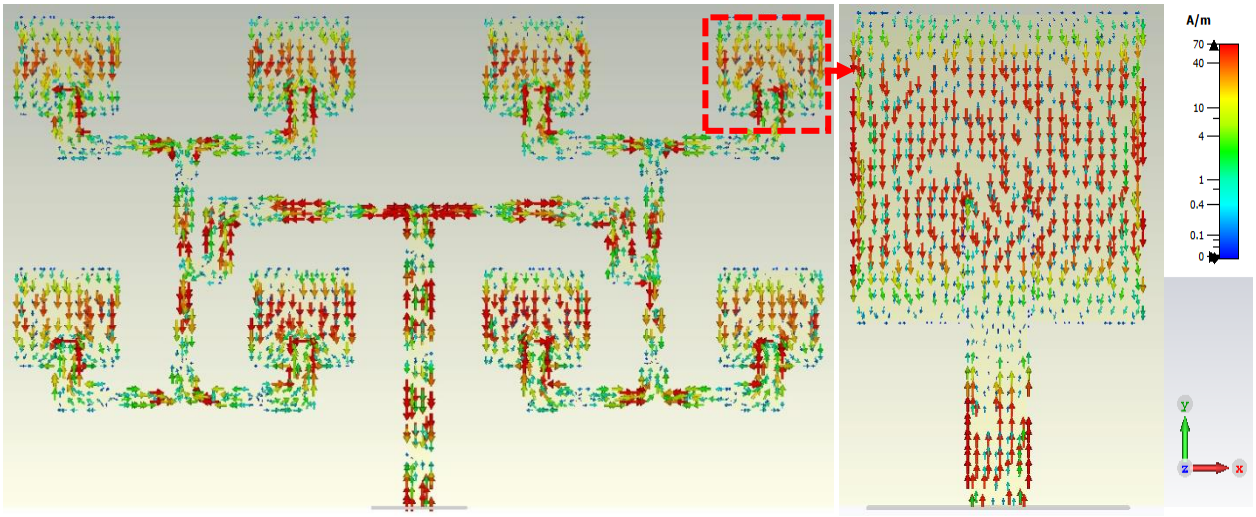

Figure 5.6 Surface currents plot of the 4x2 patch antenna array at 35 GHz

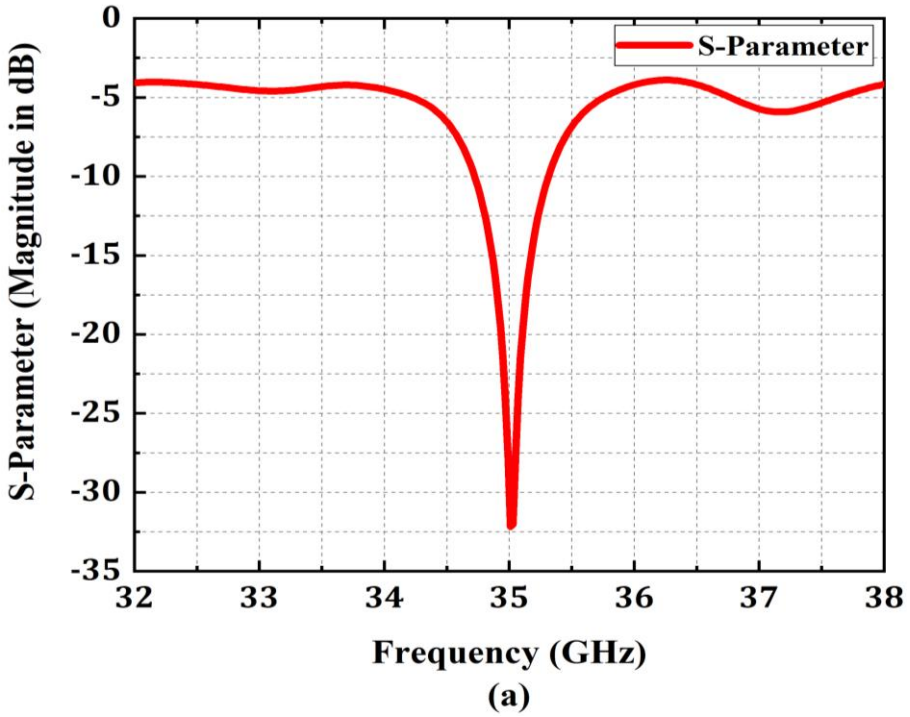

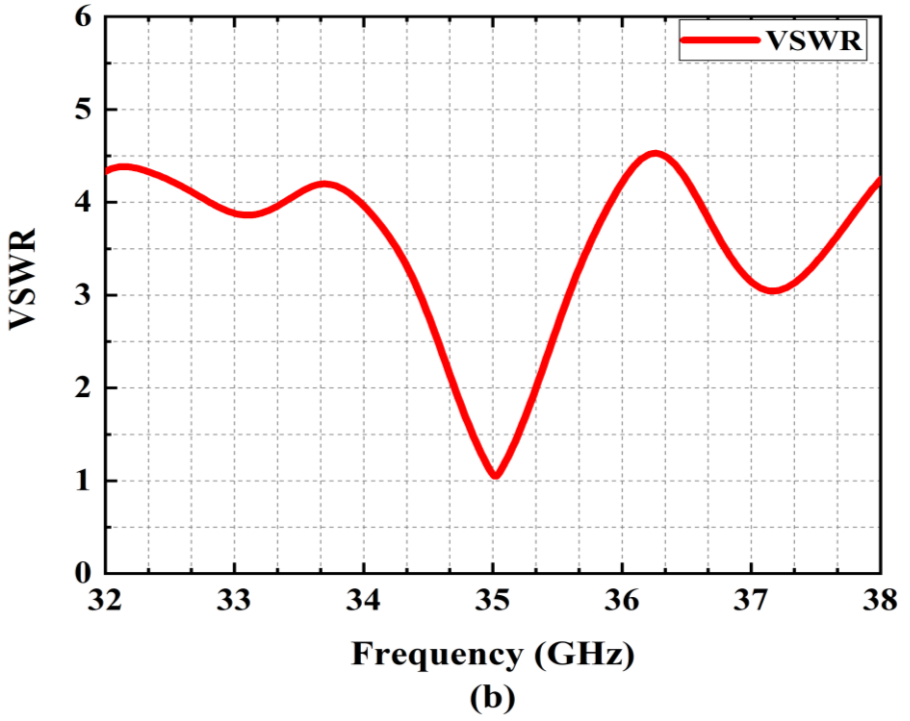

Figure 5.7 Analysis of antenna parameter a) Return loss of a 4x2 patch antenna array, b) voltage standing wave ratio (VSWR) of a 4x2 patch antenna array

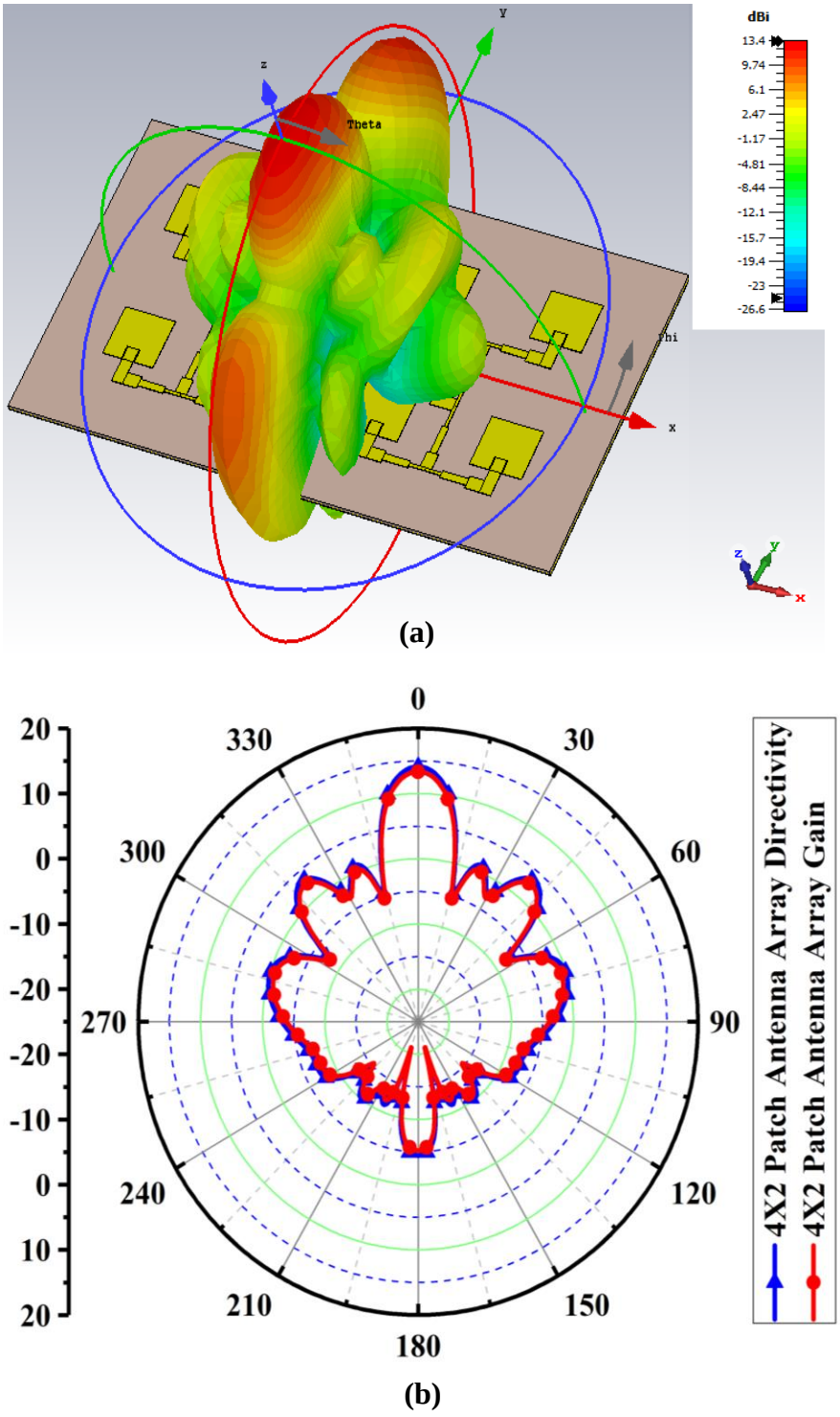

Figure 5.8 Radiation pattern of the proposed patch antenna array a) 3D view of a 4X2 array, b) 2D polar view of a 4X2 array

Figure 5.8. (a) shows the radiation pattern of the 4x2 antenna array. The intensity of the color corresponds to the energy level. The maximum energy is passing through the main lobe, and it has the highest gain and directivity. Figure 5.8. (b) shows the 2D polar plot of the radiation diagram. The gain and directivity at 0 degrees of the 4x2 antenna are 13.4 dBi and 14 dBi respectively, whereas the side lobes are less than -11 dBi. The designed 4x2 microstrip patch antenna array has an efficiency of more than 85%, as shown in Figure 5.9.

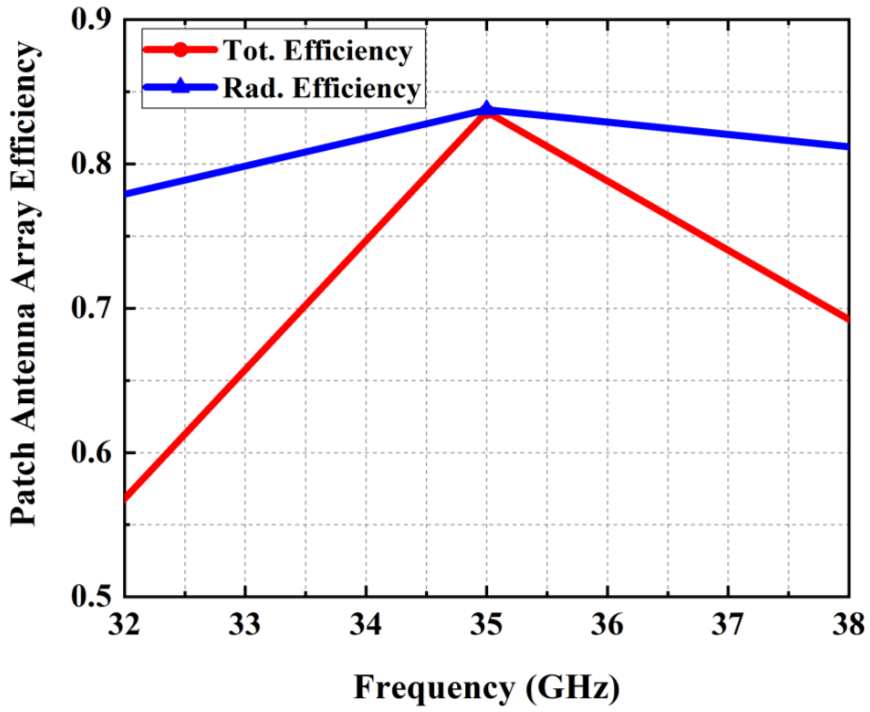

Figure 5.9 Efficiency of 4X2 patch antenna array

5.7 Design and Optimization of Rectifying Circuit

Rectennas typically consist of an antenna, a diode, a matching circuit, and a resistive load (R_L) connected to the end of the circuit to collect the DC power as shown in Figure 5.10. It has various topologies based on the diode orientation such as series [45], [67]-[68], shunt [69]-[70], voltage doubler and bridge rectifier [71]-[72]. A voltage doubler rectifier topology is selected for this project in order to achieve a higher RF to DC conversion efficiency.

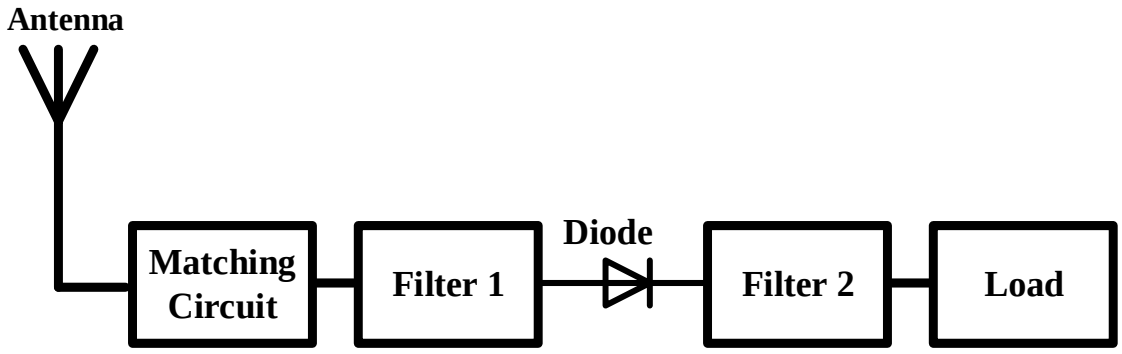

Figure 5.10 Block Diagram of conventional rectenna

5.7.1 Equivalent Circuit Model of A Schottky Diode

The Schottky diode is a nonlinear device, as proved analytically in [73]-[75] and verified in [76]-[77]. The circuit analysis presented in [76] is a standard technique that is quick, precise, and reliable for calculating the input impedance of the packaged Schottky diode as a function of the operating frequency and input power levels. The Schottky diode equivalent circuit model is shown in Figure 5.11. Here, Cj is the junction capacitance, and Cp and Lp are the parasitic packaging capacitance and inductance, respectively. D is the ideal diode, Va is an RF voltage source, and Ra is the internal resistance of the source and series resistance Rs.

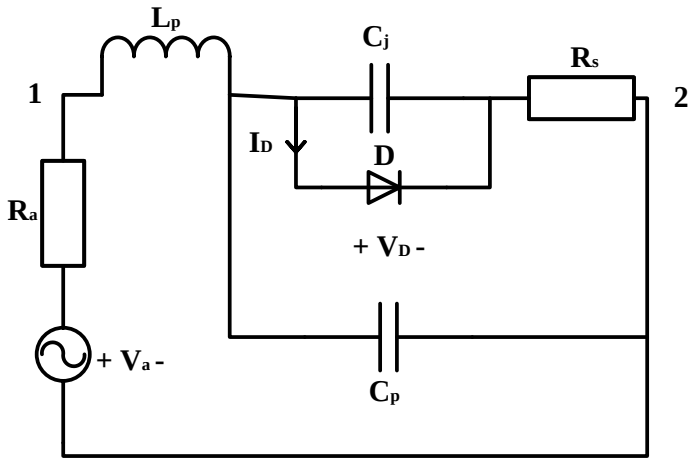

Figure 5.11 Simplified circuit model of a diode [73]-[78]

In Figure 5.11, Kirchhoff's current and voltage laws are used to determine the voltage V_D and current I_D across the diode D. These found values are further used to determine the impedance of

the rectifier. A voltage source with a single frequency f_0 as input, $V_a = |V_a| \cos(2\tau r f_0 t)$, is used as shown in Figure 5.11. The electrical behavior of this circuit can be described with the following expressions, found by applying Kirchhoff's relations:

$$V_a = I_a R_a + L_p \frac{\partial I_a}{\partial t} + V_{C_P} \quad (17)$$

$$V_{C_P} = V_D + V_{R_S} \quad (18)$$

$$V_{R_S} = R_s \left(I_{C_j} + I_D \right) \quad (19)$$

$$I_{C_j} = Cj \frac{\partial V_D}{\partial t} \quad (20)$$

$$I_D = I_s(e^{\alpha V_D} - 1) \quad (21)$$

So that $$\frac{\partial V_D}{\partial t} = \frac{1}{R_s C_j} \left\{ \psi \left(\frac{\partial I_a}{\partial t} \right) - R_s I_s (e^{\alpha V_D} - 1) \right\} \quad (22)$$

Where $$\psi \left(\frac{\partial I_a}{\partial t} \right) = V_a - R_a I_a - V_D - L_p \frac{\partial I_a}{\partial t}, \alpha = \frac{q}{nKT}$$

$\frac{q}{KT}$ is the thermal voltage and n is the ideality factor. The above differential Equation (22) has been solved with the fourth-order Runge–Kutta method and the voltage V_D across the diode, D, is calculated. Furthermore, Equation (21) is used to determine the current I_D flowing through the diode. After the evaluation of V_D and I_D, the input impedance of the diode D is found using Ohm's law:

$$Z_D = \frac{V_D}{I_D} \quad (23)$$

Harmonic Balance (HB) Simulation Validation

The Spice model parameters of the MA4E1317 diode are found in [74]-[78], where the ideality factor N = 1.5, the grading coefficient M = 0.5, the saturation current Is = 100 nA, the series resistance Rs = 4 Ω, the junction capacitance Cjo = 0.02 pF, the parasitic capacitance Cp = 0.025 pF, parasitic inductance Lp = 0.05 nH , the reverse breakdown voltage V_{br} = 7 V, and the forward

voltage V_f = 0.6 V, at forward current I_f =1 mA. Using the values of Spice parameters, the input impedance of the Schottky diode Z_{in} including its series resistance and packaging, parasitics are calculated. To verify the accuracy of the equivalent circuit model, the Schottky diode MA4E1317 ADS harmonic balance simulation model will be compared. The input impedance versus frequency for different power levels is calculated with the aid of the equivalent circuit model and is compared with harmonic balance simulation results.

Figure 5.12 (a) and Figure 5.12 (b) shows the impedance of the rectifier as calculated by using ADS harmonic balance simulations and the presented analytical expressions (AE). For a maximum available power level of 10 dBm calculated using the AE and HB simulations. Ra = 50 Ω. Figure 12 also shows the real and imaginary parts of the input impedance versus frequency at an input power level of 10 dBm.

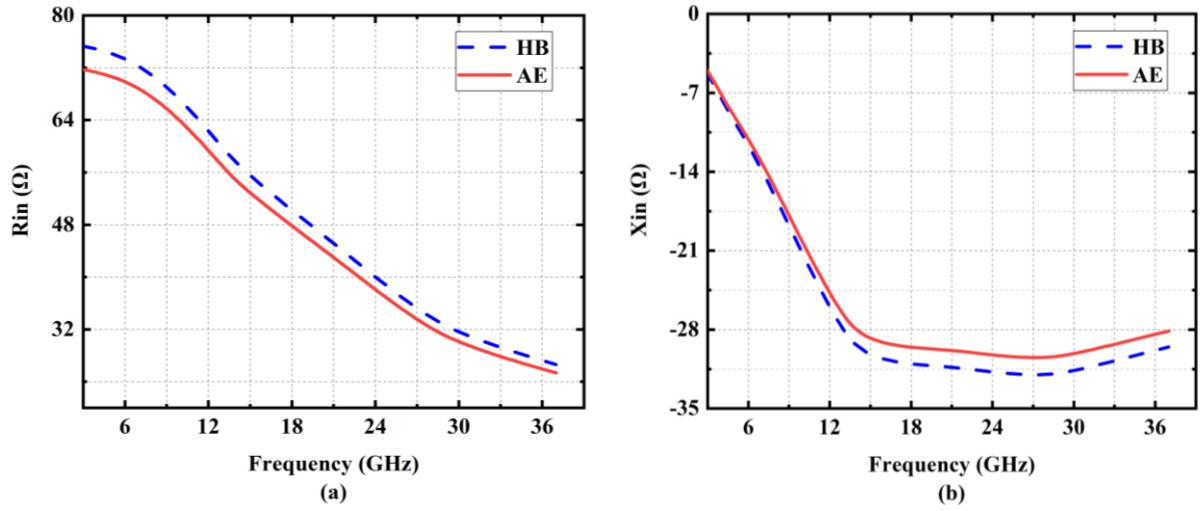

Figure 5.12 Real and imaginary parts of the input impedance of the Schottky diode MA4E1317 versus frequency a) Real impedance as a function of frequency, b) Imaginary impedance as a function of frequency

It is shown in Figure 5.12 that the equivalent circuit model can predict the impedance of the rectifier with a relative difference of less than 10% for the real and imaginary parts of the input impedance. The input impedance is again calculated using ADS harmonic balance simulations and the

equivalent circuit model. It is shown in the figures that the results of the analytical equations are matching the results obtained using harmonic balance simulations.

5.7.2 Rectifying Circuit Configuration

The geometrical structure of the proposed rectifying circuit with impedance matching operating at 35 GHz is shown in Figure 5.13. The rectifying circuit is designed on RT-Duroid substrate thickness of 0.254 mm, a relative dielectric constant of 2.2, and a loss tangent of 0.0004 to 0.0009.

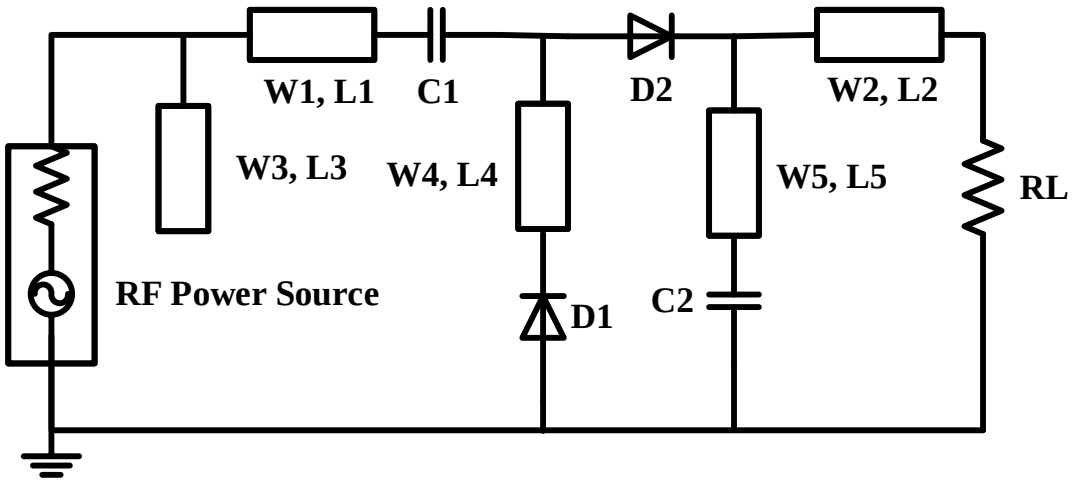

Figure 5.13 Circuit configuration of the proposed rectenna

The rectifying nonlinear circuit simulation is performed in the Advance Design System (ADS) Harmonics Balance (HB) simulator. A 10 dBm input RF power was considered for the simulation. The circuit parameters are first calculated, and then the software ADS optim toolbox with optimization-type genetic and iteration 500 can be utilized to optimize those parameters. After optimization, the parameters found are, L1 = L2 = 1.57 mm, L3 = 0.97 mm, L4 = 0.37 mm, L5 = 0.34 mm, W1 = W2 = W3 = 0.776 mm, W4 = 0.3 mm, W5 = 0.28 mm, C1 = C2 = 100 pF, and RL = 1500 Ω.

5.7.3 Results and Discussion

Output DC power changing across the different load resistors is shown in Figure 5.14. The maximum output DC power is obtained at 1500 Ω. Figure 5.15 exhibits the DC output power (a)

and voltage (b) as a function of the input RF power with different load resistances (R_L). At the desired input power of 10 dBm, a maximum 0.0065 W DC power and 3.1 V are achieved with an operating frequency of 35 GHz across the 1500 Ω load resistance.

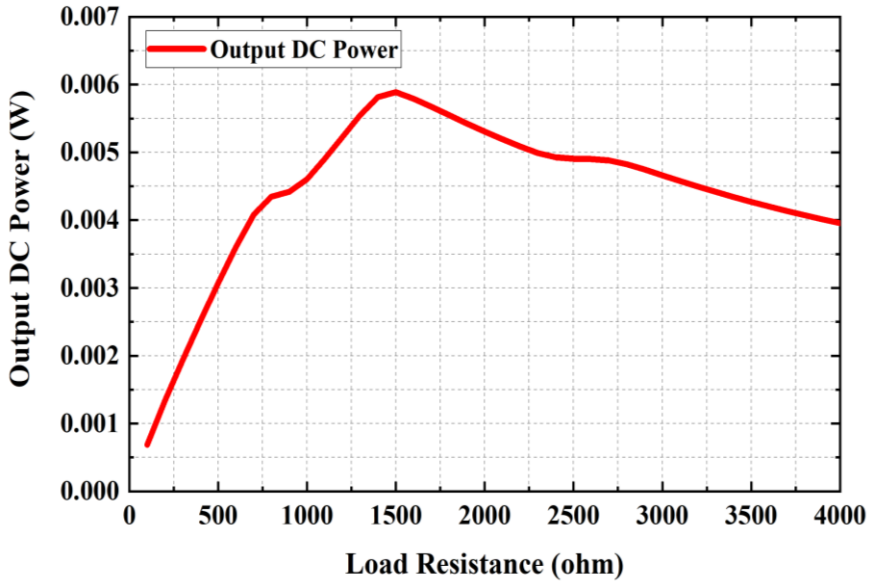

Figure 5.14 Output power variation with different values of load resistance

Figure 5.17 shows the RF to DC conversion efficiency with various load resistance and different RF input power level at the selected 35 GHz frequency. The figure depicted that the maximum efficiency of 82% is observed at 19 dBm input power with a 1500 Ω load resistance whereas, at our desired power level of 10 dBm, an efficiency of 65% is achieved. However, the maximum efficiency was expected to be at 10 dBm input power, the reason for this undesired behavior might be the impedance mismatch between the source power and the rectifier circuit. RF to DC conversion efficiency of the rectenna can be determined using the following equation,

$$\eta = \frac{V_{out}^2}{P_{in}\, R_L}\, x\, 100\% \qquad (15)$$

where, V_{out} is the output DC voltage, R_L is the load resistance, and P_{in} is the input RF power.

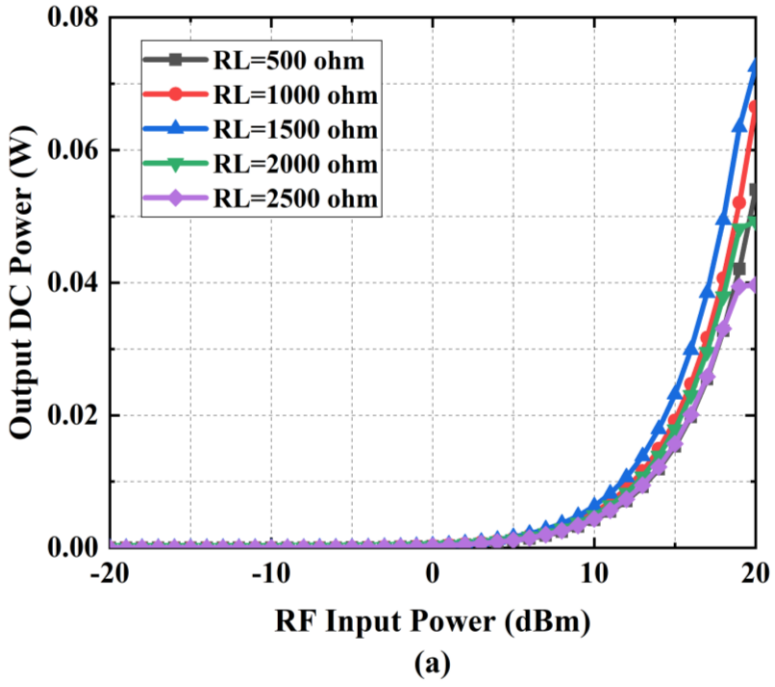

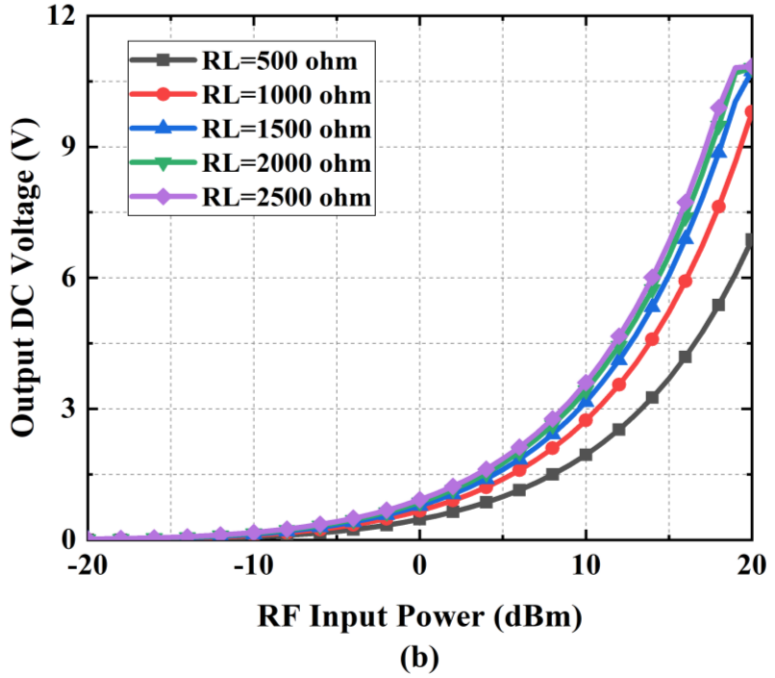

Figure 5.15 Output power and output voltage with different input power level a) Output DC power and, b) Output DC voltage

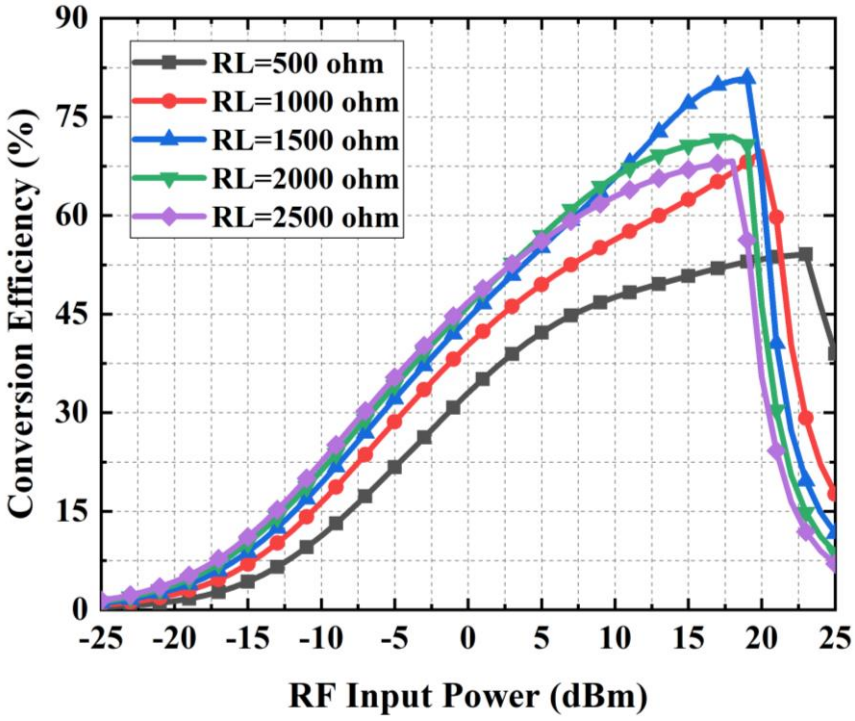

Figure 5.16 Efficiency of the designed rectenna with different input power level

The ADS Smith chart tool is then utilized to match the impedance at 35 GHz frequency with 10 dBm input power. The source power impedance is 50 Ω and the rectifier impedance can be determined by the commercial software ADS [79]-[81]. Rectifier input impedance's real and imaginary value variation with frequency (GHz) and input power (dBm) are provided in Figure 5.17 (a), and Figure 5.17 (b), respectively. The impedance is matched to a 50 Ω load at the selected 35 GHz frequency.

After impedance matching (IM), the output DC power and voltage are improved, consequently, RF to DC conversion efficiency is also improved. A comparison between the proposed rectenna with and without impedance matching is presented in Figure 5.18. The rectenna without IM has a maximum efficiency of 82 % at 19 dBm. The proposed rectenna has a plateau in the efficiency curve at an RF input power range of 9 to 18 dBm, and the average efficiency is greater than 80 % in that range. Table 5.2., compares the efficiency of the proposed rectenna with related works. The reported 80% is higher than all other identified prior works.

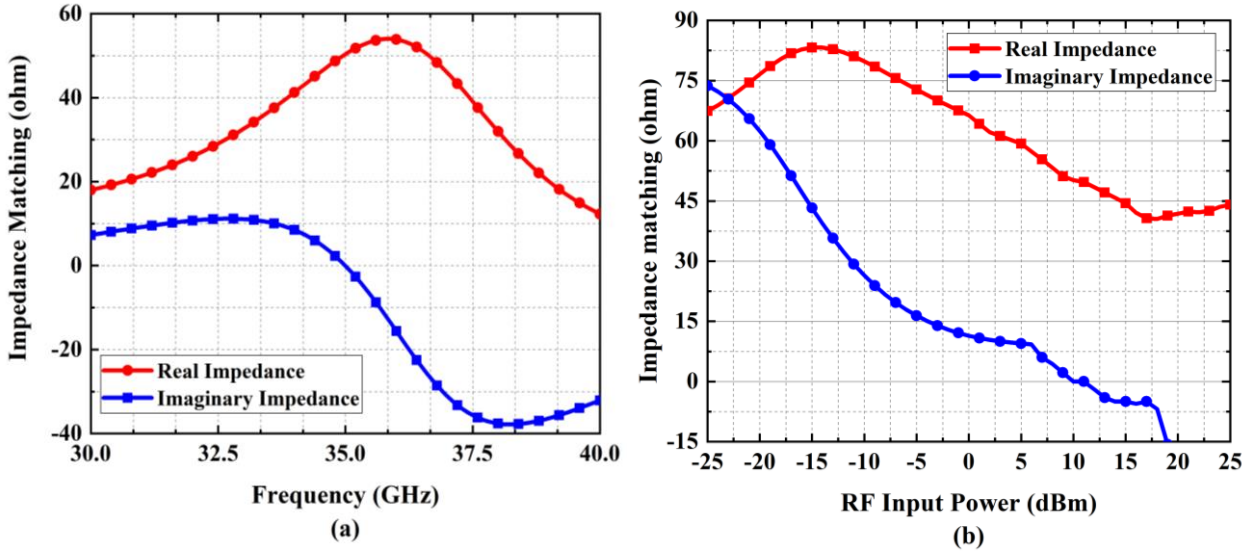

Figure 5.17 Rectifier circuit impedance matching a) Variation with frequency, b) Variation with input power

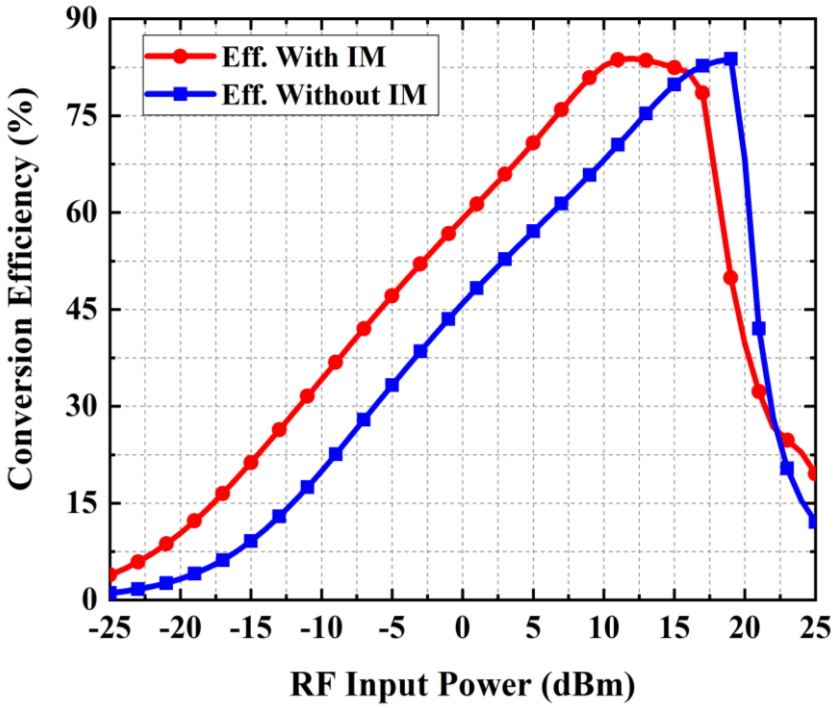

Figure 5.18 Output DC voltage as a function of RF input power

Table 5.2 Efficiency comparison of various rectennas

Source	Frequency (GHz)	Results	Rectifier Element	RF Power Level for Maximum Efficiency (dBm)	Maximum Efficiency (%)
Q. Awais et al, [82]	2.45	Experiment	Schottky HSMS 2850	5	68
Q.Q. Zhang et al, [83]	5.8	Experiment	Schottky BAT15-03W	8.2	69
N. Shinohara et al, [84]	24	Experiment	Schottky MADS-1317	21	54
S. Ladan et al, [78]	24	Simulation	Schottky MA4E1317	12	78
S. Ladan et al, [64]	35	Experiment	Schottky MA4E1317	12	34
A. Mavaddat et al, [85]	35	Experiment	Schottky MA4E1317	8.5	67
Q. Chen et al, [86]	35	Experiment	Schottky Diode	19	68.5
H. Chiou et al, [87]	94	Experiment	0.13-mm CMOS	20	37
This Work	**35**	Simulation	**Schottky MA4E1317**	**9-18**	**80**

5.7.4 Results Large Area Power Collections

This work considers onboard rectenna that could benefit from has mass production, easy interconnections, and integration with power electronics circuitry. The power capacity of a single

rectenna is low; therefore, to fulfill large power demand, there is a requirement for series and parallel combinations. In previous works [90]-[91], It has been shown that series connections offer more power losses than parallel connections, so optimum connection of series /parallel is required for maximum power transfer; otherwise, losses will be high and contribute to heating issues. Also, supplying maximum power for battery charging of UAV is a challenging task. It is due to the energy storage units like rechargeable batteries or supercapacitors do not have the voltage/ current characteristics of a resistor. This problem can be solved by using a cost-effective and efficient Resistance emulation technique as proposed in [92]. First, a module will be developed with optimum rectenna array connection and integrated power circuitry. To determine the optimum module size, power simulation and thermal modeling and simulation will be performed. ADS has an integrated circuit and EM solver (co-simulation) and thermal solver (path-wave) that can be found suitable to determine the optimum module size. The onboard design will be assembled to form a module. Further, these modules combine power and form an assembly to supply the maximum power to the load as shown in Figure 19, where P is the incident RF power on the antennas and rectenna module consists of optimum Series parallel connections with DC combining circuit.

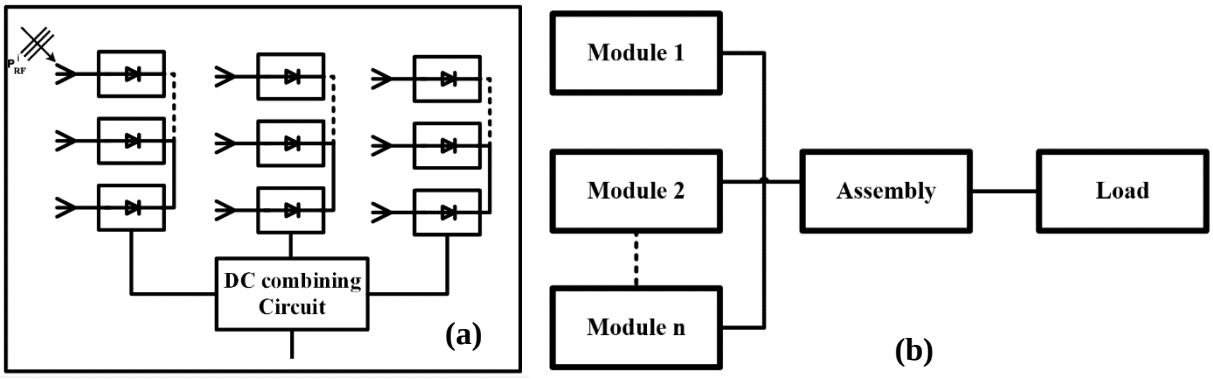

Figure 5.19 Schematics of the investigated rectenna array configurations a) DC combining circuit, b) Power delivery

The designed 4x2 antenna is directly attached to a rectifier circuit in a single rectenna. The effective area of the designed 4x2 antenna is 0.000128 m^2 which can transmit or receive 38.4 mW for RF

power at a density of 300 W/m^2 according to equation 16. A suitable combination of 74000 rectenna elements can effectively feed a 22-kW electrical engine, assuming, a rectenna RF-DC conversion efficiency 80 %, and array efficiency is 85 %.

According to our system described in section 2, an Rx antenna area of 90 m^2 can accommodate 74000 rectenna elements. The UAV is handling high power that is wirelessly transmitted via microwave while maintaining a low operating temperature is proven effective in preventing power loss as well as component degradation. The thermal problem can be countered by applying a suitable cooling method and then the thermal management systems are analyzed in [93].

5.8 Conclusion

The concept of an efficiently transmitting 22 kW of DC power to a UAV using microwave over a distance of 10 km has been presented. The underlying system architecture of UAVs is based on a 35 GHz microwave signal that allows reducing of the antenna size while keeping high transfer efficiency over long distances. An array of microstrip patch antennas is adopted for the transmitting system. It is composed of 4x2 rectangular microstrip patches that have been optimized using a CST tool. The numerically simulated gain, directivity, and efficiency of the proposed 4x2 microstrip patch antenna are 13.4 dBi, 14 dBi, and 85%, respectively. The optimized value of Tx areas and beam efficiency are respectively 108 m^2, and 80 % to transmit microwave power efficiently at a frequency of 35 GHz. Finally, to receive the microwave power, the Rx areas are optimized to 90 m^2 and a rectenna is designed employing the Agilent advanced design system (ADS) software. The proposed rectenna has an efficiency of over 80% for an RF input power range of 9 to 18 dBm and a DC output voltage of 3.5 V for a 10 dBm input power at 35 GHz feeding a load of 1500 Ω.

CHAPTER 6 CONCLUSION AND FUTURE WORKS

6.1 Conclusion

Wireless microwave power transfer has great potential for several fields of application. One of the main applications would be the production of clean energy to meet the future energy demand by solar power satellite concept. WPT can potentially eliminate the utilization of traditional wires and batteries. For example, cell phone and laptop batteries can be charged continuously without a plugging system. In addition, a WPT system can be implemented in a moving fuel-free electric vehicle or a fuel-free airplane. Applications of a fuel-free airplane are increasing because of their versatility. An electric aircraft has drawn attention as a fuel-free airplane. It can be deployed as surveillance monitoring, emergency medical supply to the remote areas, telecommunication or internet supplying platform, weather monitoring, and so on. However, an electric aircraft only run from its battery power, as a result, it has a shorter flight duration. To extend their flight duration and roaming range, WPT would be a promising solution. It has the capability of transferring power up to a long distance. For WPT, we need suitable transmitting and receiving systems. The size of the transmitter and the receiver varies with respect to the distance.

In this work, a 22-kW electrical unmanned aerial vehicle was chosen for the MPT. A distance of 10 km was selected as the transmitting distance. However, the distance can be varied according to the demand and applications. A frequency band of 35 GHz was selected in order to achieve compact transmitting and receiving systems. Based on the above information, the size of the transmitting and receiving systems was calculated. An array of linearly polarised microstrip patch antenna was adopted as the transmitting medium. The simulation result of the microstrip patch antenna array shows that once optimized, the antenna array is linearly polarised. The designed antenna perfectly resonates at 35 GHz frequency, and it has a gain of 13.4 dBi and directivity of 14 dBi. The achieved gain and directivity are higher compared to a single microstrip patch antenna array. The return loss and efficiency of the patch antenna array are -33 dBi and 85 % respectively. All results are indicating that the simulated array is suitable for MPT applications. Thereafter, we have optimized a rectifier system in order to convert the RF energy to DC to run the electrical motor. In this work, we have designed and optimized series and voltage doubler rectifiers. After analyzing the

performance of both rectifiers, we have selected a voltage doubler rectifier for this project. A 10 dBm input power was selected for the rectifier simulation. The final optimized simulation results show that the designed rectifier can achieve more than 80 % of efficiency for an input power ranging from 9 to 18 dBm.

The effective area of the designed 4x2 patch array is 0.000128 m^2. This size of the antenna can transmit a power of 38.4 mW when considering a power density of 300 W/m^2. Therefore, at the transmitter end, 108 m^2 of area are required in order to transfer 32 kW of microwave power over a distance of 10 km. On the other hand, at the receiver end, 90 m^2 of rectenna can accommodate 7 03 125 sets of 4x2 patch antenna array and allow to harvest 27 kW of DC power.

6.2 Future Works

The future work of the thesis could be extended in the following ways,

a. We are working on a long-distance higher energy microwave wireless power transfer in MMW. For demonstration, we can choose a short distance (i.e., 1m) as the first step for point-to-point wireless power transfer. Therefore, we need to design and optimize a transmitting and receiving system. At first, we will design a transmitting antenna array (i.e., 4x2 antenna array) at 35 GHz for fabrication. And then we will design and optimize a rectifier circuit at 35 GHz with a suitable load resistance and connect it to the fabricated antenna array. The combination of an antenna and a rectifier circuit will be working as a receiving antenna. Therefore, we will run a real MPT test for a short distance to verify the received power.

b. If the MPT experiment succeeds for a short distance, then the transmitting distance will be increased in several steps.

REFERENCES

[1] T.F. Villa, F. Gonzalez, B. Miljievic, Z.D. Ristovski, and L. Morawska, “An Overview of Small Unmanned Aerial Vehicles for Air Quality Measurements: Present Applications and Future Prospectives”, *Sensors, Vol. 16, no. 1072, pp. 1-29, Jun 2016.*

[2] Admin, “The good, the bad and the ugly about electric aviation,” *Ecofriend*, 27-Jun-2020. [Online]. Available: https://ecofriend.com/the-good-the-bad-and-the-ugly-about-electric-aviation.html. [Accessed: 21-Oct-2021].

[3] Graham Warwick Graham leads Aviation Week's coverage of technology, G. Warwick, and Graham leads Aviation Week's coverage of technology, “What are the advantages and challenges of electric-powered airliners?,” *Aviation Week Network*, 31-Jul-2020. [Online]. Available: https://aviationweek.com/aerospace/aircraft-propulsion/what-are-advantages-challenges-electric-powered-airliners. [Accessed: 21-Oct-2021].

[4] W.C. Brown, “The history of power transmission by radio waves,” IEEE Trans. Microwave Theory Tech, vol. 32, no. 9, pp. 1230-1242, Sept 1984.

[5] J. Curty, M. Declercq, C. Dehollain and N. Joehl, “Design and optimization of passive UHF RFID systems,” 1st Ed, Springer US, USA, 2006.

[6] W.C. Brown, "'Free-space transmission," *IEEE Spectrum*, vol. 1, no. 10, pp. 86-91, 1964.

[7] W.C. Brown, "'The microwave powered helicopter," *J. Microw. Power*, vol. 1, no. 1, pp. 1-20, 1966.

[8] P.E. Glaser, and W.C. Brown, “An Electrical Propulsion Transportation System for Low-Earth Orbit to Geostationary Orbit Utilizing Beamed microwave power”, *Space Solar Power Review*, vol.4, pp. 119-129, 1983.

[9] J.J. Schlesak, A. Alden, and T. Ohno, “A Microwave Powered High Altitude Platform”, *1988-In international Microwave Symposium Digest, IEEE MTT-S,* New York, NY, USA, pp. 283 – 286, 1988.

[10] H. Matsumoto, N. Kaya, M. Fujita, Y. Fujino, T. Fujiwara, and T. Sato, ‘‘MILAX airplane experiment and model airplane,’’ (in Japanese), in Proc. 11th ISAS Space Energy Symp, pp. 47–52, 1993.

[11] N. Kaya, H, Matsumoto, and R. Akiba, “Rocket Experiment METS Microwave Energy Transmission in Space”, *Journal of Space Power,* vol*, 11*, no. 3 - 4, pp. 267–274, 1992.

[12] N, Shinohara and H. Matsumoto, “Dependence of dc Output of a Rectenna Array on the Method of Interconnection of Its Array Element”, *Electrical Engineering in Japan, Vol, 125, no,* 1, pp. 9–17, 1998.

[13] N. Kaya, S. Ida, Y. Fujino, and M. Fujita, “Transmitting antenna system for airship demonstration (ETHER)”, *Space Energy and Transportation*, Vol. *1, no.* 4, pp. 237–245, 1996.

[14] N. Shinohara and H. Matsumoto “Point to point Microwave power Transfer Experiments” *Scripta Technica, Inc*, vol. 116 B, no 6, pp. 648-653, June 1996.

[15] URSI white paper on solar power satellite (SPS) Systems and Report of the URSI Inter-Commission Working Group on SPS” in URSI inter commission working group on SPS, 2007.

[16] J. Gavan and S. Tapuchi “Microwave Wireless-Power Transmission to High-Altitude-Platform Systems” *The Radio Science Bulletin,* no 334, pp. 25-42, Sept. 2010.

[17] J. Gavan and R. Perez, “Handbook of Electromagnetic Compatibility”, 1st ed, New York, Academic Press, Chapters 19, 20, 1995.

[18] W.C. Brown, **“**Electronic and mechanical improvement of the receiving terminal of a free-space microwave power transmission system”, Raytheon Company, Wayland, MA, Tech. Rep. PT-4964, NASA Rep. CR-135194, Aug. 1977.

[19] W. C. Brown, "A Microwaver Powered, Long Duration, High Altitude Platform," *1986 IEEE MTT-S International Microwave Symposium Digest*, 1986, pp. 507-510.

[20] Y. Aoki, M. Otsuka, T. Idogaki, T. Shibata, and T. Hattori, “Microwave energy transmission system for microrobot” IEICE-Trans.Electr. Vol. E80-c, no. 2, pp. 303-308, Feb. 1997.

[21] C.K. Chin, Quan Xue and Chi Hou Chan, "Design of a 5.8-GHz rectenna incorporating a new patch antenna," in *IEEE Antennas and Wireless Propagation Letters*, vol. 4, pp. 175-178, June 2005.

[22] J. O. McSpadden and K. Chang, "A dual polarized circular patch rectifying antenna at 2.45 GHz for microwave power conversion and detection," *1994 IEEE MTT-S International Microwave Symposium Digest (Cat. No.94CH3389-4)*, 1994, pp. 1749-1752 vol.3.

[23] T. Ito, Y. Fujino, and M. Fujita, “Fundamental experiment of a rectenna array for microwave power reception” IEICE Trans. Commun, Vol. E-76-B, pp. 1508–1513, Dec 1993.

[24] R. J. Gutmann and R. B. Gworek, “Yagi-Uda Receiving Elements in Microwave Power Transmission system Rectennas”, Journal of Microwave Power, Vol. 14, no. 4, pp. 313–320, Jan 1979.

[25] N. Shinohara, S. Kunimi, T. Miura, H. Matsumoto, and T. Fujiwara, “Open experiment of microwave power experiment with automatically target chasing system (japanese)”, IEICE Trans. B-II, Vol. J81-B-II, no. (6), pp. 657-661, Jun 1998.

[26] J. A. Hagerty, N. D. Lopez, B. Popovic and Z. Popovic, "Broadband Rectenna Arrays for Randomly Polarized Incident Waves," *2000 30th European Microwave Conference*, 2000, pp. 1-4.

[27] Y. Fujino and K. Ogimura, “A rectangular parabola rectenna with elliptical beam for sps test satellite experiment”, Proc. of the Institute of Electronics, Information and Communication Engineers, Vol. S29–S20, pp. 1–7, Oct 2004.

[28] T. S. Chu, "An approximate generalization of the Friis transmission formula," in *Proceedings of the IEEE*, vol. 53, no. 3, pp. 296-297, March 1965.

[29] D. C. Hogg, "Fun with the Friis free-space transmission formula," in *IEEE Antennas and Propagation Magazine*, vol. 35, no. 4, pp. 33-35, Aug. 1993.

[30] W. C. Brown, “Beamed Microwave power transmission and its application to space,” *IEEE Trans. Microwave Theory Tech*, vol. 40, no. 6, pp. 1239 – 1250, 1992.

[31] G. Goubau and F. Schwering, "On the Guided Propagation of Electromagnetic Wave Beams," *IRE Transactions on Antennas and Propagation*, vol. 9, no. 3, pp. 248-256, May 1961.

[32] K. A. Dao, and C. D. Nguyen, "Some Theoretical Issues of MPT and Development of 1D Model for Microwave Power Transmission Problem in the Mixed Layers Environment from GEO to the Earth," *International Journal of Modern Communication Technologies & Research (IJMCTR)*, vol. 3, no. 10, pp. 13-19, Oct 2015.

[33] C.A. Balanis, "Antenna Theory: Analysis and Design", 3rd edition, John Wiley, New York, 2005.

[34] W.L. Stutzman, and G.A. Thiele, "Antenna Theory and Design", 3rd Edition, John Wiley & Sons, Hoboken, 2012.

[35] G. Loianno, V. Spurny, J. Thomas, T. Baca, D. Thakur, D. Hert, R. Penicka, T. Krajnik, A, Zhou, A. Cho, M. Saska, and V. Kumar, "Localization, Grasping, and Transportation of Magnetic Objects by a Team of MAVs in Challenging Desert-Like Environments" IEEE Robotics and Automation Letters, vol. 3, no. 3, pp. 1576-1583, Jul 2018.

[36] T. Tomic, K. Schmid, P. Lutz, A. Domel, M. Kassecker, E. Mair, I. Grixa, F. Ruess, M. Suppa, and D. Burschka, "Toward a fully autonomous uav: Research platform for indoor and outdoor urban search and rescue," *IEEE Robotics Automation Magazine*, vol. 19, no. 3, pp. 46–56, Sept 2012

[37] J. Keller, D. Thakur, M. Likhachev, J. Gallier, and V. Kumar, "Coordinated path planning for fixed-wing uas conducting persistent surveillance missions," *IEEE Transactions on Automation Science and Engineering*, vol. 14, no. 1, pp. 17–24, Jan 2017.

[38] S. Weiss, D. Scaramuzza, and R. Siegwart, "Monocular-SLAM-based navigation for autonomous micro helicopters in GPS denied environments," *Journal of Field Robotics*, vol. 28, no. 6, pp. 854–874, 2011.

[39] R. Ritz and R. D'Andrea, "Carrying a flexible payload with multiple flying vehicles," in *2013 IEEE/RSJ International Conference on Intelligent Robots and Systems*, Tokyo, Japan, Nov 2013, pp. 3465–3471.

[40] G. Loianno and V. Kumar, “Cooperative transportation using small quadrotors using monocular vision and inertial sensing,” *IEEE Robotics and Automation Letters*, vol. 3, no. 2, pp. 680–687, April 2018.

[41] M. Bernard, K. Kondak, I. Maza, and A. Ollero, “Autonomous transportation and deployment with aerial robots for search and rescue missions,” *Journal of Field Robotics*, vol. 28, no. 6, pp. 914–931, 2011.

[42] M. Saska, T. Baca, J. Thomas, J. Chudoba, L. Preucil, T. Krajnik, J. Faigl, G. Loianno, and V. Kumar, “System for deployment of groups of unmanned micro aerial vehicles in gps-denied environments using onboard visual relative localization,” *Autonomous Robots*, vol. 41, no. 4, pp. 919–944, Apr 2017.

[43] W. C. Brown, “A survey of the elements of power transmission by microwave beam,” *1961IRE Int. Conv. Rec.*, vol. 9, no. 3, pp. 93-105, 1961.

[44] W. C. Brown, “The combination receiving antenna and rectifier,” *Microwave Power Engineering*, vol. 2, *E. C. Okress, Ed. New York: Academic*, pp. 273-275, 1968.

[45] Y. J. Ren and K. Chang, “5.8-GHz circularly polarized dual-diode rectenna and rectenna array for microwave power transmission,” *IEEE Trans. Microw. Theory Tech.*, vol. 54, no. 4, pp. 1495–1502, Apr. 2006.

[46] B. Strassner and K. Chang, “5.8-GHz circularly polarized dual-rhombic-loop travelling-wave rectifying antenna for low power-density wireless power transmission applications,” *IEEE Trans. Microw. Theory Tech.*, vol. 51, no. 5, pp. 1548-1553, May 2003.

[47] J. Heikkinen and M. Kivikoski, “Low-profile circularly polarized rectifying antenna for wireless power transmission at 5.8 GHz,” *IEEE Microw. Wireless Compon. Lett.*, vol. 14, no. 4, pp. 162–164, Apr. 2004.

[48] Y. J. Ren, M. Y. Li, and K. Chang, "35 GHz rectifying antenna for wireless power transmission," *Electron. Lett*., vol. 43, no. 2, pp. 602- 603, May 2007.

[49] Y. J. Ren and K. Chang, “New 5.8-GHz circularly polarized retrodirective rectenna arrays for wireless power transmission,” *IEEE Trans. Microw. Theory Tech.*, vol. 54, no. 7, pp. 2970–2976, Jul. 2006

[50] Y. H. Suh, and K. Chang, "A high-efficiency dual-frequency rectenna for 2.45- and 5.8-GHz wireless power transmission," *IEEE Trans. Microw. Theory Tech.* vol. 50, no. 7, pp. 1784-1789, July 2002.

[51] J. O. McSpadden, L. Fan, and K. Chang, "Design and experiments of a high-conversion-efficiency 5.8-GHz rectenna," *IEEE Trans. Microw. Theory Tech.*, vol. 46, no. 12, pp. 2053-2060, December 1998.

[52] A. Collado and A. Georgiadis, "24 GHz substrate integrated waveguide (SIW) rectenna for energy harvesting and wireless power transmission," presented at *MTT-S Int. Microw. Symp*. Seattle, USA, 2-7Jun. 2013

[53] S. Ladan and K. Wu, "High efficiency low-power microwave rectifier for wireless energy harvesting," presented at MTT-S Int. Microw. Symp. Seattle, USA, 2-7Jun. 2013.

[54] S. Ladan, S. Hemour and K. Wu, "Towards millimeter-wave high-efficiency rectification for wireless energy harvesting," *in IEEE IWS Int. Wireless. Symp. Dig.*, pp. 1-4, 2013.

[55] H. K. Chiou, and I. Shan Chen, "High-efficiency dual-band on -chip rectenna for 35- and 94-GHz wireless power transmission in O.13-llm CMOS technology," *IEEE Trans. Microw. Theory Tech.*, vol. 58, no. 12, pp. 3598-3606, December 2010.

[56] L. W. Epp, A. R. Khan, H. K. Smith and P. Smith, "A compact dual polarized 8.51-GHz rectenna for high-voltage (50 V) actuator applications," *IEEE Trans. Microw. Theory Tech.*, vol. 48, no. 1, pp. 111-120, January 2000.

[57] Fujino, Y., M. Fujita, N. Kaya, S. Kunimi, M. Ishii, N. Ogihata, N. Kusaka, and S. Ida, “A Dual Polarization Microwave Power Transmission System for Microwave propelled Airship Experiment”, *Proc. of ISAP’96*, Chiba, Japan, Vol. 2, pp. 393-396, 1996.

[58] O. Yuichiro, T. Naohiro, “Study of Electric Aircraft Charged by Beamed Microwave Power”, *IHI Engineering Review*, Vol. 48, No. 2, pp. 29-32, 2015.

[59] D. Belo; D.C. Ribeiro, P. Pinho, and N.B. Carvalho, “A Selective, Tracking, and Power Adaptive Far-Field Wireless Power Transfer System”, *IEEE Trans. Microw. Theory Tech.*, Vol. 67, no. 9, pp. 3856-3866, Sept. 2019.

[60] T.W. Yoo, and K. Chang, “Theoretical and experimental development of 10 and 35 GHz rectennas”, IEEE Trans. Microw. Theory Tech., 40, (6), pp. 1259–1266, 1992.

[61] M. Fingas, C.E. Brown, “Oil Spill Science and Technology” (2nd ed), 2017. [Online]. Available: https://www.sciencedirect.com/topics /engineering/atmospheric-attenuation.

[62] N. Shinohara, Y. Kubo, and H. Tonomura “Wireless charging for electric vehicle with microwaves”, *2013 3rd International Electric Drives Production Conference (EDPC)*, Nuremberg, Germany, 2013.

[63] I. Park, E. Lee, and H. Ku, “Angle Tracking Automatic Beamforming for Microwave Power Transfer Systems” , *2020 IEEE Wireless Power Transfer Conference (WPTC)*, Seoul, South Korea, Nov 2020.

[64] S. Ladan, and K. Wu, “35 GHz Harmonic Harvesting Rectifier for Wireless Power Transmission”, 2014 IEEE MTT-S International Microwave Symposium (IMS2014), Tampa, FL, USA, Jul 2014.

[65] N. Shinohara, “Beam Efficiency of Wireless Power Transmission via Radio Waves from Short Range to Long Range”, *JKIEES*, vol. 10, no.4, pp. 224-230, Dec 2010.

[66] X. Chen, B. Yang, N. Shinohara, and C. Liu, “A High-Efficiency Microwave Power Combining System Based on Frequency-Tuning Injection-Locked Magnetrons”, IEEE Transactions on Electron Devices, vol. 67, no. 10, pp. 4447-4452, Oct 2020.

[67] H. Sun, Y.X. Guo, M. He, and Z. Zhong "Design of a High-Efficiency 2.45-GHz Rectenna for Low-Input-Power Energy Harvesting", *IEEE Antennas and Wireless Propagation Letters*, vol. 11, pp. 929-932, Aug. 2012.

[68] T. Yoo, J. O. McSpadden, and K. Chang, “35 GHz rectenna implemented with a patch and a microstrip dipole antenna,” *IEEE MTT-S Int. Microw. Symp. Dig.*, Albuquerque, NM, USA pp. 345–348. 1992.

[69] J. Akkermans, M. van Beurden, G. Doodeman, and H. Visser, “Analytical models for low-power rectenna design,” *IEEE Antennas Wireless Propag. Lett.*, vol. 4, pp. 187–190, 2005.

[70] Q. He and C. Liu, “An enhanced microwave rectifying circuit using HSMS-282,” *Microw. Opt. Technol. Lett.*, vol. 51, no. 4, pp. 1151–1153, Apr. 2009.

[71] A. J. Cardoso, L. G. de Carli, C. Galup-Montoro, and M. C. Schneider, “Analysis of the rectifier circuit valid down to its low-voltage limit,” *IEEE Trans. Circuits Syst. I, Reg. Papers*, vol. 59, no. 1, pp. 106–112, Jan. 2012.

[72] W. B. Lawrance and W. Mielczarski, “Harmonic current reduction in a three-phase diode bridge rectifier,” *IEEE Trans. Ind. Electron.*, vol. 39, no. 6, pp. 571–576, Dec. 1992.

[73] S.-P. Gao, H. Zhang, T. Ngo, and Y. Guo, “Lookup-table-based automated rectifier synthesis,” *IEEE Transactions on Microwave Theory and Techniques*, pp. 1–1, 2020.

[74] S.-P. Gao, H. Zhang, and Y.-X. Guo, “Analysis of mmwave rectifiers with an accurate rectification model,” *2021 IEEE Wireless Power Transfer Conference (WPTC)*, 2021.

[75] D. A. Fleri and L. D. Cohen, “Nonlinear analysis of the Schottky-barrier mixer diode,” *IEEE Transactions on Microwave Theory and Techniques*, vol. 21, no. 1, pp. 39–43, 1973.

[76] S. Keyrouz, H. J. Visser, and A. G. Tijhuis, “Rectifier analysis for radio frequency energy harvesting and Power Transport,” *2012 42nd European Microwave Conference*, 2012.

[77] H. J. Visser and W. I. S. (O. service), *Approximate antenna analysis for CAD*. John Wiley & Sons Incorporated, 2008.

[78] S. Ladan and K. Wu, “Simultaneous wireless power transmission and data communication”, Ph.D. dissertation, Dept. Elect. Eng., Polytechnique Montreal, Montreal, QC, Canada, 2014.

[79] F. Zhang, X. Liu, F.-Y. Meng et al., “Design of a compact planar rectenna for wireless power transfer in the ISM band,” *International Journal of Antennas and Propagation*, vol. 2014, no. 298127, 1-9, 2014.

[80] V. Kuhn, C. Lahuec, F. Seguin, and C. Person, “A multi-band stacked RF energy harvester with RF-to-DC efficiency up to 84%,” *IEEE Trans. Microw. Theory Tech*, vol. 63, no. 5, pp. 1768–1778, 2015.

[81] S. Ladan, A. Babu, and K. Wu, “A High-Efficiency 24 GHz Rectenna Development Towards Millimeter-Wave Energy Harvesting and Wireless Power Transmission”, *IEEE Transactions on Circuits and Systems,* vol. 61, no. 12, pp. 3358-3366, Dec 2014.

[82] Q. Awais, Y. Jin, H.T. Chattha, M. Jamil, H. Qiang, and B.A. Khawaja, "A compact rectenna system with high conversion efficiency for wireless energy harvesting," *IEEE Access*, vol.6, pp. 35857-35866, 2018.

[83] Q.Q. Zhang, J.H. Ou, Z.Z. Wu, and H.Z. Tan, "Novel microwave rectifier optimizing method and its application in rectenna designs," *IEEE Access*, vol.6, pp. 53557-53565, 2018.

[84] N. Shinohara, K. Nishikawa, T. Seki and K. Hiraga, "Development of 24 GHz rectennas for Fixed Wireless Access," *2011 XXXth URSI General Assembly and Scientific Symposium*, 2011, pp. 1-4.

[85] A. Mavaddat, S. H. M. Armaki and A. R. Erfanian, "Millimeter-Wave Energy Harvesting Using 4x4 Microstrip Patch Antenna Array," *IEEE Antennas and Wireless Propagation Letters*, vol. 14, pp. 515-518, 2015.

[86] Q. Chen, Z. Liu, Y. Cui, H. Cai and X. Chen, "A Metallic Waveguide-Integrated 35-GHz Rectenna With High Conversion Efficiency," *IEEE Microwave and Wireless Components Letters*, vol. 30, no. 8, pp. 821-824, Aug. 2020.

[87] H. Chiou and I. -. Chen, "High-Efficiency Dual-Band On-Chip Rectenna for 35- and 94-GHz Wireless Power Transmission in 0.13-μm CMOS Technology," *IEEE Transactions on Microwave Theory and Techniques*, vol. 58, no. 12, pp. 3598-3606, Dec. 2010.

[88] S. Khang, D. Lee, I. Hwang, T. Yeo and J. Yu, "Microwave Power Transfer with Optimal Number of Rectenna Arrays for Midrange Applications," *IEEE Antennas and Wireless Propagation Letters*, vol. 17, no. 1, pp. 155-159, Jan. 2018.

[89] X. Yi, X. Chen, L. Zhou, S. Hao, B. Zhang and X. Duan, "A Microwave Power Transmission Experiment Based on the Near-Field Focused Transmitter," *IEEE Antennas and Wireless Propagation Letters*, vol. 18, no. 6, pp. 1105-1108, June. 2019.

[90] N. Shinohara and H. Matsumoto, “Experimental study of large rectenna array for microwave energy transmission,” *IEEE Transactions on Microwave Theory and Techniques*, vol. 46, no. 3, pp. 261–268, 1998.

[91] T. Miura, N. Shinohara, and H. Matsumoto, “Experimental study of rectenna connection for Microwave Power Transmission,” *Electronics and Communications in Japan (Part II: Electronics)*, vol. 84, no. 2, pp. 27–36, 2001.

[92] T. Paing, J. Shin, R. Zane, and Z. Popovic, “Resistor emulation approach to low-power RF Energy Harvesting,” *IEEE Transactions on Power Electronics*, vol. 23, no. 3, pp. 1494–1501, 2008.

[93] W. C. Brown, “Ultra Light 2.45 GHz Rectenna and 20 GHz Rectenna,” *Raytheon Co., Rectenna Technology Program*, Waltham, MA, 1987.

APPENDICES

APPENDIX A MICROSTRIP PATCH ANTENNA CALCULATION

The microstrip patch antenna calculation steps are given below,

Step 1: Calculation of the width of the patch, W_P,

$$\boldsymbol{W_P = \frac{C}{2f_0\sqrt{\frac{\varepsilon_r+1}{2}}}} \qquad \textbf{(A1)}$$

where c is the speed of light, f_0, the frequency, and ε_r, the substrate dielectric constant.

Step 2: Calculation of the Effective Dielectric Constant. This is based on the thickness and the dielectric constant of the substrate and the calculated width of the patch antenna,

$$\boldsymbol{\varepsilon_{eff} = \frac{\varepsilon_r+1}{2} + \frac{\varepsilon_r-1}{2}\left[1 + 12\frac{h}{W}\right]^{-1/2}} \qquad \textbf{(A2)}$$

where, $\boldsymbol{\varepsilon_{eff}}$, is the effective dielectric constant, *h*, the thickness of the substrate, and *W*, the width of the substrate.

Step 3: Calculation of the Effective length, $\boldsymbol{L_{eff}}$:

$$\boldsymbol{L_{eff} = \frac{C}{2f_0\sqrt{\varepsilon_{eff}}}} \quad . \qquad \textbf{(A3)}$$

Step 4: Calculation of the length extension, ΔL

$$\boldsymbol{\Delta L = 0.412h\frac{(\epsilon_{eff}+0.3)\left(\frac{W}{h}+0.264\right)}{(\epsilon_{eff}-0.258)\left(\frac{W}{h}+0.8\right)}}, \qquad \textbf{(A4)}$$

Step 5: Calculation of the actual length of the patch, ***Lp***:

$$\boldsymbol{L_P = L_{eff} - \Delta L}\ . \qquad \textbf{(A}_5\textbf{)}$$

Calculate the input impedance

The input impedance is the ratio of the source voltage and the source current. It denoted by $\boldsymbol{Z_{in}}$,

$$\boldsymbol{Z_{in} = \frac{90\varepsilon_r^2}{1-\varepsilon_r^2} * \left(\frac{L_P}{W_P}\right)^2}. \qquad \textbf{(A}_6\textbf{)}$$

If it does not match with the 50-ohm standard microstrip, a quarter wavelength transformer is used to connect them. The characteristic of the transition section should be,

$$\boldsymbol{Z_T = \sqrt{50 * Z_{in}}}\ , \qquad \textbf{(A}_7\textbf{)}$$

where Z_T is the impedance of the transformer.

The width of the transition line/quarter-wave transformer can be determined by

$$\boldsymbol{Z_T = \frac{60}{\sqrt{\varepsilon_r}} \ln\left(\frac{8h}{W_T} + \frac{W_T}{4h}\right)} \qquad \textbf{(A}_8\textbf{)}$$

where, W_T is the width of the transformer.

To obtain the transition line length we need to calculate the relative permittivity $\boldsymbol{\varepsilon_{re}}$ for line which is given by

$$\boldsymbol{\varepsilon_{re} = \frac{\varepsilon_r+1}{2} + \frac{\varepsilon_r-1}{2\sqrt{\left[1+\frac{12h}{W_T}\right]}}}. \qquad \textbf{(A}_9\textbf{)}$$

Hence, the length of the transition (quarter wavelength) line should be

$$\boldsymbol{L_T = \frac{\lambda}{4} = \frac{\lambda_0}{4\sqrt{\varepsilon_{re}}}}. \qquad \textbf{(A}_{10}\textbf{)}$$

Calculate the width of the 50-ohm microstrip feed line

The width of the microstrip feed line, W_f, can be calculated given the characteristic impedance:

$$\boldsymbol{W_f = \frac{8he^A}{e^{2A}-2} \text{ for } W_f \leq 2h} \qquad \textbf{(A}_{11}\textbf{)}$$

$$\boldsymbol{W_f = \frac{2h}{\pi} * \left[B - 1 - \ln(B-1) + \left(\frac{\varepsilon_r - 1}{2\varepsilon_r}\right)\ln(B-1) + 0.39 - \frac{0.61}{\varepsilon_r}\right]} \text{ for } \boldsymbol{W_f < h}$$

$$\boldsymbol{A = \frac{Z_0}{60} * \sqrt{\frac{\varepsilon_r + 1}{2}} + \frac{\varepsilon_r - 1}{\varepsilon_r + 1}\left(0.23 + \frac{0.11}{\varepsilon_r}\right), \quad B = 377\pi/(2Z_0 * \sqrt{\varepsilon_r})} \qquad \textbf{(A}_{12}\textbf{)}$$

where Z_0 is the characteristic impedance.

Hence, the length of the 50-ohm microstrip feed line $\boldsymbol{L_f}$,

$$\boldsymbol{L_f = \frac{\lambda_0}{4\sqrt{\varepsilon_{eff}}}.} \qquad \textbf{(A}_{13}\textbf{)}$$

If the width of the microstrip line is too small to properly make an alternative design to employ an insert feed using the following equation:

$$\boldsymbol{Z_0 = Z_T cos^2\left(\frac{\pi d}{L}\right),} \qquad \textbf{(A}_{14}\textbf{)}$$

$$\boldsymbol{d = \frac{L}{\pi} * cos^{-1}\left(\sqrt{\frac{50}{Z_T}}\right),} \qquad \textbf{(A}_{15}\textbf{)}$$

where d is the insert distance.